Design, Simulation and Optimization of a Biomass-Natural-gas-and-Nuclear to Liquid Fuels and Power Process

Design, Simulation and Optimization of a Biomass-Natural-gas-and-Nuclear to Liquid Fuels and Power Process

By James Alexander Scott, B. Eng. Mgt. (Chemical Engineering and Management)

A Thesis Submitted to the School of Graduate Studies

In Partial Fulfillment of the Requirements

for the Degree

Masters of Applied Science

McMaster University

Master of Applied Science (2016) McMaster University

(Chemical Engineering) Hamilton, Ontario, Canada

TITLE: Design, Simulation and Optimization of a Biomass-Natural-gas-and-Nuclear to Liquid Fuels and Power Process

AUTHOR: James Alexander Scott, B. Eng. Mgt. (Chemical Engineering and Management)

(McMaster University, Hamilton, Ontario, Canada)

SUPERVISOR: Dr. Thomas A. Adams II

NUMBER OF PAGES: xv, 141

Abstract

The unsustainable use of natural resources to power our world has depleted energy stores globally, and evokes a need to explore other environmentally-friendly options. This thesis presents a novel polygeneration design of a woody biomass-natural gas-nuclear energy-to-liquid-fuels and power (BGNTL) process, and assesses its economic and environmental feasibility in the context of Ontario, Canada. To assess the efficacy of nuclear energy in this system, a BGTL (biomass-natural gas to liquid fuels and power) system was compared with the BGNTL system. In both processes, carbon capture sequestration (CCS) was also incorporated. Many different cases of the plant were analyzed, including combinations of steam radiant syngas cooling (RSC), steam methane reforming integrated with the RSC (IR), and the addition or removal of CCS. It was found that for CCS cases, there was a positive relationship between the increase of CO_2 tax and profitability. The optimal design produces only dimethyl ether (DME), uses no nuclear energy, and sends all of the off-gas to the solid-oxide-fuel-cell (SOFC). In the optimal case, the RSC making steam was slightly better than the IR by about 0.6% net-present-value (NPV), and a switch from non-CCS to CCS resulted in a 1% increase in NPV. Minimal DME prices to keep optimal cases profitable were around $798 - $807 for CCS and non-CCS cases, respectively. Overall, it was found that the life cycle CO_2 impact in the optimal case of DME production was much less environmentally damaging compared with traditional diesel production. Specifically, in the CCS case, DME had approximately 100,000 less grams of CO_{2e} / GJ of energy than

a traditional diesel production. In the non-CCS case, the impact was approximately 50,000 less grams of CO_{2e} / GJ of energy.

Acknowledgements

I would like to thank and express my gratitude to my supervisor Dr. Thomas A. Adams II for his support and mentorship throughout my research work, and my undergraduate years.

I would also like to thank the McMaster Advanced Control Consortium, the Department of Chemical Engineering at McMaster University, NSERC, and the Ontario graduate (OGS) program for their financial support throughout my Master's degree.

Special thanks to Jaffer Ghouse, Jake Nease, Chinedu Okoli, and other MACC members for their support and help during my project.

Last but not least, I would like to thank my family and express my love and gratitude to the love of my life Stephanie Wu, and to my parents Allison Scott and Bob Scott for their love and support – I could have not completed this journey without you.

Table of Contents

List of Figures

List of Tables

List of Abbreviations and Symbols

Abbreviation	
ASU	Air Separation Unit
ATR	Auto Thermal Reformer
BGNTL	Biomass, natural gas and nuclear to liquid fuels and power process
BGTL	Biomass and natural gas to liquid fuels and power process
BTL	Biomass to liquid fuels and power process
CanDU	Canada deuterium-uranium
CCS	Carbon Capture and Sequestration
CEPCI	Chemical Engineering Plant Cost Index
CO_{2e}	Carbon dioxide equivalent
CuCl	Copper-Chlorine Cycle
DME	Dimethyl Ether
FT	Fischer-Tropsch
GE	General Electric
GT	Gas Turbine
GTL	Gas to liquids
HHV	Higher heating value
HP	High Pressure
HRSG	Heat Recovery Steam Generation
IR	Internal reformer
LHV	Lower heating value

MeOH	Methanol
MDEA	Methyl-Diethanol Amine
NBS/NRC	National Bureau of Standards/National Research Council
NPV	Net present value
OECD	Organization for Economic Co-operation and Development
PA	Per annum
PR-BM	Peng Robinson with Boston-Matthias
PSO	Particle Swarm Optimization
SCF	Standard cubic feet
SCWR	Super-Critical-Water reactor
SOFC	Solid Oxide Fuel Cell
WGS	Water gas shift

Declaration of Academic Achievement

All work presented in this thesis was performed by myself. Guidance and advice on research direction was provided by Dr. Thomas A. Adams II.

Chapter 1

Introduction

Motivation and Goals

The energy-based economies of developed countries are putting a large strain on the planet's natural resources, particularly on fossil fuels. According to the United Nations, the world's population is expected to grow to around 8.8 billion people by 2035, increasing the world's population by 1.5 billion people from now ("BP p.l.c," 2016). In turn, it is not surprising that the global demand for energy will rise by 1.4% per year (/y), which will be mainly fueled by the fast growth in renewables (6.6% /y) and natural gas (1.8% /y) in the coming years (Figure 1.1.1). However, even with the large growth in renewables, the vast majority of primary energy is still derived from coal (30%), natural gas (24%) and oil

(32%), and will remain relatively high for the foreseeable future. With the increased demand as a result of population and GDP growth, more efficient and environmentally friendly ways of utilizing these natural resources are required.

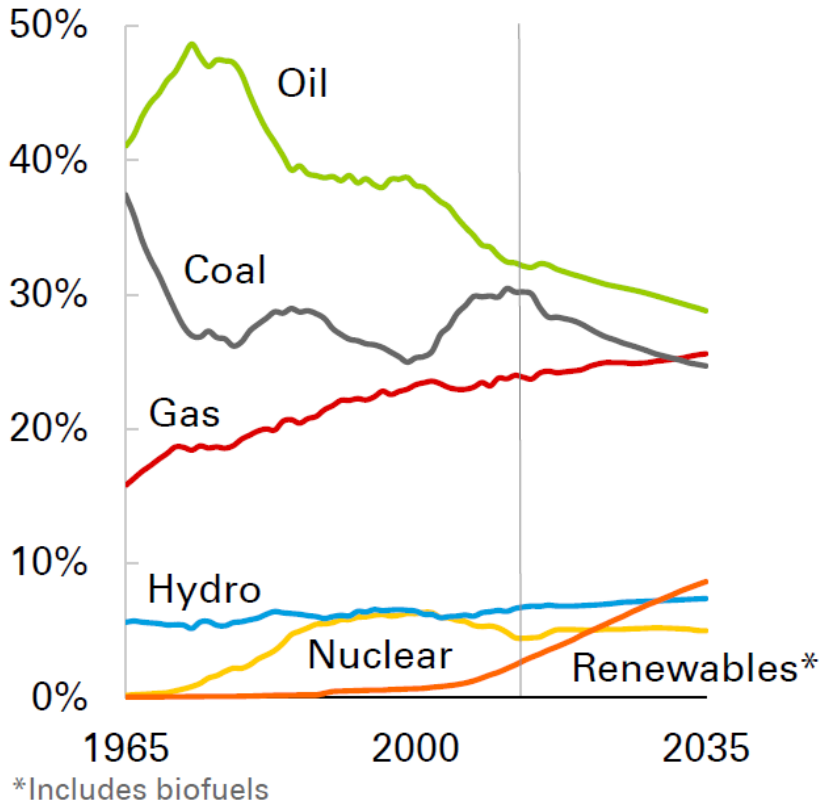

Figure 1.1 Shares of primary energy (reprinted from ("BP p.l.c," 2016)).

Ontario's long term energy power plan is to phase out fossil fuels, primarily coal, from its power portfolio (Government of Ontario, 2016). This effort has mainly been focused on phasing out coal from its energy mix and installing more nuclear, wind, solar, hydro and bio-energy power generation facilities. One unique method of phasing out coal has occurred in Northern Ontario at the Atikokan generating station, where a coal power plant

was retrofitted into a biomass-fueled power facility. The biomass that the facility burns is woody biomass in the form of pellets, which the plant burns in a steam cycle to generate power. This retrofit has made the Atikokan generation station one of the largest biomass plants in North America, providing 205 MW of power ("Ontario's LTEP," 2013). Another coal-fired conversion is also planned for the Thunder Bay generating station, which is scheduled to be operational by 2020. There is a huge potential for Ontario to exploit its woody biomass resources for more efficient and diverse energy needs.

Generation IV nuclear power plants are currently under development by many nations including Canada and Japan. The improvements these generation IV power plants bring with respect to current state-of-the-art nuclear facilities is increased efficiency, safety, and better utilization of nuclear fuel. Currently, Canada is looking at one Gen IV reactor class called the Super Critical Water Reactor (SCWR), specifically the SCW CanDU reactor (Naidin et al., 2009). SCWRs have the potential to be synergistically integrated with other processes for increased efficiency and generation of other products such as hydrogen gas (Greg F. Naterer, Dincer, & Zamfirescu, 2013).

A recent development in integrated fuels and production processes is polygeneration. Polygeneration utilizes various technologies to create conventional energy products and chemicals such as electricity, gasoline, diesel, and methanol from conventional and non-conventional raw material feedstocks such as coal, natural gas, biomass and nuclear power. Polygeneration boasts many advantages over traditional power plant setups including

improved efficiency, the ability to achieve zero CO_2 emissions, and reduced sensitivity to the volatility of market conditions and feedstock prices (Thomas A. Adams & Barton, 2011a; Thomas A Adams & Ghouse, 2015).

To address Ontario's climate change mandate and to exploit Ontario's energy technologies, this study proposes a rigorous steady-state novel process which has been designed for the purpose of utilizing Ontario's woody biomass supply and its nuclear technology to create power, liquid fuels and chemicals with near zero CO_2 emissions.

1.2 Main Contributions

1.2.1 Novel Process Design

This is the first work to develop a novel process that utilizes woody biomass, natural gas and nuclear energy to efficiently produce liquid fuels and power with options for carbon capture and sequestration, called the Biomass-Gas-Nuclear-to-Liquids-and-Power Process (BGNTL). The process design was completed in several different software packages, including Aspen Plus, ProMax, gProms and Matlab. The overall system was implemented in Aspen Plus utilizing reduced order models developed in the other software packages.

1.2.2 Techno-Economic Analysis

Base case economics for the various plant designs were carried out utilizing a net present value approach. Due to uncertainty in the economic parameters of the process, sensitivity

analyses were conducted to show the impact of different parameter changes on the economic viability of the plant. In addition, the impact of CO_2 taxes were analyzed.

1.2.3 Process Optimization

Each case of the process was optimized utilizing a heuristic optimization process called particle swarm optimization and was implemented in Python. The structure of the optimization process is different for each case considered and the optimized results are compared to the base case results.

1.3 Thesis Overview

Chapter 2:

This chapter provides a background and a literature review of relevant topics which relate to this study. Specifically, this section discusses various biomass fuel sources, several novel unit operations such as a gasifier and solid oxide fuel cells (SOFC). These technologies are then linked together within a polygeneration framework, which is thoroughly discussed.

Chapter 3:

This chapter gives an overview of the discussed BGNTL process and the different case studies that were considered in this project. Additionally, this chapter describes the mathematical models and process simulation tools used to model each unit operation in the simulation. In particular, the Aspen simulation, ProMax and gProms models are discussed

in detail. Furthermore, this chapter gives an overview of the optimization framework that was used to determine the best operating conditions for each process case that was considered.

Chapter 4:

This chapter gives an overview of the economic and sensitivity analyses that were undertaken in the work. The environmental impacts of each process was analyzed using a life cycle emissions analysis framework. The chapter also discusses the optimization results with respect to each case.

Chapter 5:

This chapter summarizes the major conclusions and results of the work. In addition, recommendations for future research directions are discussed.

Chapter 2

Background and Literature Review

The purpose of this chapter is to provide background information on some of the topics that will be discussed in the later chapters and to give an overview of past research in this field of study. This work involves the integration of several technologies and feedstocks that has not been performed in previous work. These technologies are gasification, steam methane reforming, water-gas-shift reactors, nuclear power for hydrogen production, solid-oxide-fuel-cells, and polygeneration. A detailed explanation of key technologies will give a better overall context for the reader for the remaining chapters.

2.1 Canadian woody biomass feedstocks

Countries around the world are reconsidering the use of different kinds of biomass as a source of renewable and sustainable energy. Biomass is of particular interest since it is a renewable, abundant and clean resource that is also carbon neutral. In addition, woody biomass is not food competitive.

Canadian studies in this area have shown that there are over 90 million tonnes of residual or waste forestry biomass that is currently available and unused (Levin, Zhu, Beland, Cicek, & Holbein, 2007). This results in about 1.44×10^9 GJ of energy that is currently unexploited. In the literature, there have been studies of utilizing this woody biomass feedstock for power production, hydrogen and methane generation (Levin et al., 2007).

This mismatch between available and exploited fuel availability makes Ontario's woody biomass a perfect feedstock for this study.

2.2 Gasification

2.2.1 Gasifier process overview

Gasification is a process in which some carbonaceous material (biomass, petcoke or coal) is mixed with either air or high purity oxygen, which partially combusts a portion of the feed, gasifying the remaining feed material into synthesis gas or syngas, which is mainly made up of hydrogen (H_2), carbon monoxide (CO), water (H_2O) and carbon dioxide (CO_2) gases. They operate at high temperatures usually around 600 – 1500°C. This syngas is

highly valuable and can be utilized as a feedstock to create products such as methanol, dimethyl ether (DME), gasoline and diesel fuels or electricity. There are three main types of commercial gasifiers. The fixed bed gasifier produces syngas with an exit temperature of 600°C; the fluidized bed gasifier produces temperatures of 1000°C; and the most popular, the entrained flow gasifier, produces temperatures of around 1300°C (Steynberg & Dry, 2004). One popular design of this kind of gasifier is the GE-Texaco gasifier, which has been adopted in this work and other studies (Thomas A. Adams & Barton, 2011a; Ghouse, Seepersad, & Adams, 2015).

The GE-Texaco gasifier considered in this work consists of three major parts: the partial oxidation (POX) zone, the radiant cooling zone and the quench zone. In the POX zone, the material is oxidized with high purity oxygen and the remaining carbonaceous fuel is gasified into high value syngas, with a small amount of inerts. In the radiant cooler phase, the syngas is cooled via a radiant syngas cooler (RSC) and because it is at a very high temperature, the heat can be used for steam generation and natural gas reforming. The next phase is the quenching phase in which the gases blow through a pool of water at the bottom of the reactor which cools the syngas to a usable temperature of about 200°C.

The RSC is of particular interest to this work, since it has the ability to generate high value steam and has the potential for steam natural gas reforming, and has been studied in other works (Thomas A. Adams & Barton, 2011a; Ghouse et al., 2015). The works by Ghouse and Adams is of particular relevance to this study, because one of the objectives is to see

if there is any plant-wide economic benefit of having a steam methane reformer (SMR) embedded in the RSC for high H_2/CO syngas production (H_2/CO > 3), which can be mixed with the low H_2/CO ratio syngas (~0.5-0.6) that exists in the gasifier for liquid fuels production, such as Fischer-Tropsch fuels, methanol and DME.

Entrained flow gasifiers also offer several other benefits that are important to this study. Firstly, entrained flow gasifiers have shown the ability to handle biomass efficiently, with only minor modifications required (Van der Drift et al., 2004). As mentioned before, entrained flow gasifiers are oxygen blown and this leads to several advantages over other kinds of gasifiers. Oxygen blown environments allow for efficient CO_2 separation downstream, and leads to high carbon capture efficiency of 98-99.5% (Thomas A. Adams & Barton, 2010).

2.2.2 Gasification RSC

The entrained flow gasifier has the added benefit of having high value sensible heat that exits the gasifier. This useful heat is normally utilized in the RSC for the purposes of high pressure steam generation. However, research by Adams and Ghouse has shown the applicability of having a RSC that utilizes this high value heat for the purposes of reforming methane with steam (Thomas A. Adams & Barton, 2011a; Ghouse et al., 2015).

For steady-state studies, most state-of-the-art integrated gasification combined cycle technologies (IGCC) and other gasification steady-state plant studies have involved radiant

syngas cooling, but these models were all basic heat exchanger models (Thomas A. Adams & Barton, 2011a; Field & Brasington, 2011). Adams and Barton looked at the applicability of the natural gas radiant cooler utilized as a natural gas steam reformer in previous work, and found that for certain economic conditions, it was a viable option (Thomas A. Adams & Barton, 2011a). However, this study also used a basic approach, utilizing conventional Aspen Plus blocks to model the RSC. Therefore, in this work, the rigorous dynamic model developed by Ghouse and Adams will be adapted for steady-state application, giving the results of this plant-wide study a more realistic result than those found in the literature (Ghouse et al., 2015).

2.3 Methane Reforming

2.3.1 Steam Methane Reforming

Steam methane reforming is a process where a carbonaceous fuel such as natural gas is reacted with steam to form syngas (a mixture of H_2 and CO), usually with the aid of a catalyst (Steynberg & Dry, 2004). The reactions that take place in the SMR are described in equations 2.1 and 2.2.

$$CH_4 + H_2O \rightleftharpoons CO + 3H_2 \quad (2.1)$$

$$CO + H_2O \rightleftharpoons CO_2 + H_2 \quad (2.2)$$

The first reaction, known as the SMR reaction, is largely endothermic while the second reaction, known as the water gas shift (WGS) reaction is mildly exothermic, making the

net of reactions 2.1 and 2.2, endothermic. This means that SMRs require a large external heat source to generate the desired products efficiently. This makes traditional SMR a high CO_2 emissions process, since extra natural gas (or some other fuel) needs to be combusted in order to provide the SMR with the required heat. SMRs usually operate around 700 – 1000°C.

Traditionally, methane (the largest component of natural gas) is reformed to generate hydrogen gas which is then used in various chemical refining applications, such as the catalytic cracker in an oil refinery or in the industrial synthesis of ammonia. However, in recent years, researchers have focused more on utilizing the syngas generated by methane reforming for other applications, such as synthetic fuels production and low quality syngas upgrading (Thomas A. Adams & Barton, 2011a; Thomas A Adams & Ghouse, 2015).

To combat the large CO_2 emissions associated with traditional SMR design, a new technology that utilizes the high value heat from a gasifier's RSC (referred to as "internal" SMR, or internal reformer "IR") has been developed by Adams and Barton and has been successfully implemented in a 2D dynamic model by Ghouse and Adams (Thomas A. Adams & Barton, 2011a; Ghouse et al., 2015). The idea of this internal SMR is that instead of utilizing the heat that would normally be used by the RSC to produce steam, this heat is instead used to reform natural gas, and to produce high H_2 to CO ratio (~3-4) syngas. This can then be directly blended with the gasifier's low H_2 to CO ratio (~0.5-0.7) syngas, which

benefits the entire plant design in certain economic environments (Thomas A. Adams & Barton, 2011a).

2.3.2 Auto-Thermal reforming

Auto-thermal reforming reactors (ATR) utilize oxygen with either steam or CO_2 to produce syngas from methane (Steynberg & Dry, 2004). The reactions that take place in the ATR using CO_2 and steam are shown below in the following reaction systems 2.3 and 2.4, respectively.

$$\begin{aligned} CO_2 + CH_4 &\rightleftharpoons 2H_2 + 2CO \\ CH_4 + 2O_2 &\rightarrow CO_2 + 2H_2O \\ CO + H_2O &\rightleftharpoons CO_2 + H_2 \end{aligned} \tag{2.3}$$

$$\begin{aligned} CH_4 + H_2O &\rightleftharpoons CO + 3H_2 \\ CH_4 + 2O_2 &\rightarrow CO_2 + 2H_2O \\ CO + H_2O &\rightleftharpoons CO_2 + H_2 \end{aligned} \tag{2.4}$$

The methane is partially oxidized within the reactor to reform the remainder of the methane. This is done because the reforming of natural gas is endothermic in both methods (equation 1 of 2.3 and equation 1 of 2.4), meaning that they require heat to proceed forward to the desired products of H_2 and CO. The temperature of ATR reactors can often reach 900-1050°C and operate at pressures between 30-40 bar (Steynberg & Dry, 2004).

Typically, the reaction pathway described by equation 2.4 is favoured over 2.3 because the added steam generates significantly more hydrogen, which yields a higher H_2 to CO ratio. This higher H_2 to CO ratio is desired since the produced syngas is either destined for synthetic fuels processing or hydrogen separation, both of which usually demand a H_2 to CO ratio of at least 1.5 – 2 (Thomas A. Adams & Barton, 2011a; Okoli & Adams, 2014).

Several studies in the literature have shown that including ATRs with steam is beneficial to the overall plant's performance (Thomas A. Adams & Barton, 2011a; Khojasteh Salkuyeh, 2015). The addition of high ratio of H_2/CO syngas to the syngas mix can often benefit process systems that blend low quality syngas (low H_2 to CO ratio), which usually comes from gasification, with the hopes of creating the correct balance of H_2 and CO for the desired application.

2.5 Water Gas Shift Reactors

The WGS reaction, shown in equation 2.2, is a widely used industrial reaction that is employed in the production of many chemical products such as hydrocarbons, methanol and high purity H_2 gas. In synthetic fuels production, such as Fischer-Tropsch (FT) fuel production, WGS reactors are used to balance the H_2/CO ratio, prior to the FT reactor (Steynberg & Dry, 2004).

The WGS forward reaction is thermodynamically favoured at low temperatures, and kinetically favoured at high temperatures (Smith, Loganathan, & Shantha, 2010). Because

of this, industry often utilizes a high temperature shift reactor followed by a low temperature shift reactor, with intercooling in between the two reactors to maintain temperature specifications (Smith et al., 2010). At high temperatures there is a high reaction rate, but because of the thermodynamic limitations of the process, there is relatively low CO conversion. To shift the reaction more towards the right (higher H_2 production), a second lower temperature reactor is used. The high temperature reactor operates around 310-450°C inlet – 550°C outlet, utilizing an iron-oxide/chromium-oxide catalyst, while the low temperature reactor operates around 200-250°C, utilizing a copper-based catalyst (Smith et al., 2010). These industrial reactors can operate up to 80 bars of pressure.

In most industrial practices, the goal is to reduce the CO in the outlet as much as possible, but in some processes, there is a desired H_2 to CO ratio. Many process studies have sought to utilize the water gas shift reactor to "upgrade" a tandem lower quality syngas produced by a gasifier, for use in chemical synthesis (Thomas A. Adams & Barton, 2011a; Clausen, Elmegaard, & Houbak, 2010). This study incorporates the use of the WGS reactor when there is a need for a higher H_2 to CO ratio syngas.

2.6 Nuclear power for hydrogen and oxygen production

There have been many proposed systems to create an integration between nuclear power and efficient hydrogen generation. The main reasons for this are twofold. First, the utilization of nuclear energy for hydrogen and oxygen production makes the system a zero

direct CO_2 emissions process (there are still emissions from fuel purification). The second is that nuclear power plants operate in a steady-state or base-load fashion, meaning that they don't turn down or up too often. This allows for an integrated system to be combined with the nuclear facility to allow for alternative product production while electrical prices are low, and then switching back to mostly electrical generation when electricity prices are high, without changing the operation of the nuclear reactor itself. There have been several concepts that address this topic and are discussed next.

2.6.1 Nuclear-based water electrolysis

The most basic pathway for hydrogen and oxygen production from nuclear power is utilizing the electricity produced by the nuclear plant to split the hydrogen and oxygen in the water molecule, via electrolysis or high temperature electrolysis (Greg F. Naterer et al., 2013). Electrolysis is a means of driving a non-spontaneous chemical reaction with a direct electric current (DC) (Greg F. Naterer et al., 2013). The voltage that is needed for the decomposition of water to hydrogen and oxygen gas is +1.229V. The basic reaction pathway is illustrated below in equation 2.5.

$$H_2O + 2F \rightarrow 0.5O_{2,g} + H_{2,g} \quad (2.5)$$

F represents the Faraday constant (96,490 C/mol) and therefore shows that 2F Coulombs must be provided to form 1 mol of hydrogen and ½ a mol of oxygen gas for each mol of water electrolyzed (Greg F. Naterer et al., 2013). Electrolysis consists of an anode, a

cathode and an electrolyte with the whole apparatus being connected directly to the DC power source.

Studies by Ryland et al. have shown that an advanced CANDU reactor that is coupled with an electrolysis facility can reach 33-34% higher heating value (HHV) thermal efficiency compared with 27% for conventional electrolysis (Ryland, Li, & Sadhankar, 2007).

2.6.2 Thermochemical water decomposition: The Copper-Chlorine cycle

Thermochemical water-splitting cycles are technologies that decompose water into hydrogen and oxygen via a group of chemical reactions. Thermochemical cycles also comprise other chemical compounds such as copper (Cu) and chlorine (Cl), or sulfur (S) and iodine (I). The only consumed material in these processes is water, while hydrogen and oxygen are by-products of the process. All other chemicals involved in these cycles are recycled and used again.

In the literature, there have been over 200 proposed thermochemical hydrogen production methods, that split water into hydrogen and oxygen using clean energy (Wang, Naterer, Gabriel, Gravelsins, & Daggupati, 2010). One of the most promising cycles is the Copper-Chlorine (Cu-Cl) cycle, which was developed at the Ontario Institute of Technology, in collaboration with Atomic Energy of Canada Limited (AECL) (G.F. Naterer et al., 2010; Wang et al., 2010). The Cu-Cl cycle has several variations, one of which is the 5-step cycle, considered in this work. It takes the following form:

Step 1: Hydrogen generation

$$2Cu_{(s)} + 2HCl_{(g)} \rightarrow 2CuCl_{(l)} + H_{2\,(g)} : \text{at } 430 - 475°C \quad (2.6)$$

Step 2: Electrochemical step

$$2CuCl_{(s)} \rightarrow Cu_{(s)} + CuCl_{2\,(aq)} : \text{at ambient temperature} \quad (2.7)$$

Step 3: Flash drying

$$CuCl_{(aq)} \rightarrow CuCl_{(s)} : \text{at } 150°C \quad (2.8)$$

Step 4: HCl production

$$2CuCl_{2\,(s)} + H_2O_{(g)} \rightarrow CuO \cdot CuCl_{2\,(s)} + 2HCl_{(g)} : \text{at } 400°C \quad (2.9)$$

Step 5: Oxygen production

$$CuO \cdot CuCl_{2\,(s)} \rightarrow 2CuCl_{(l)} + 1/2O_{2\,(g)} : \text{at } 500°C \quad (2.10)$$

This reaction network has several benefits. The first is that it operates at relatively low temperatures ($500°C$), and because of this has applicability to be coupled with Canada's generation IV nuclear reactor technology, the Super-Critical-Water-Reactor (SCWR) (Rosen, 2010). In addition, the process has inexpensive reagents, a small amount of solids handling (compared to other thermochemical processes) and each step goes to completion with almost no side reactions. A schematic of the process can be seen below in Figure 2.1.

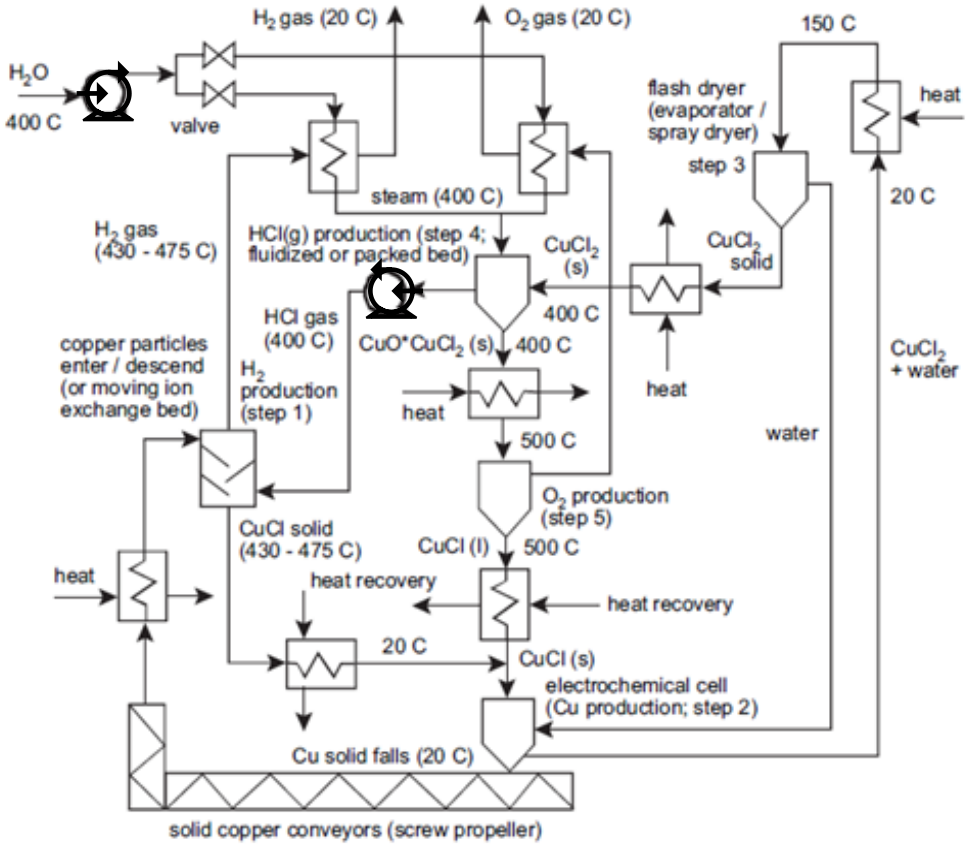

Figure 2.1 Schematic of a 5-step CuCl cycle (reprinted from (Rosen, 2010)).

The co-generation of power, hydrogen and oxygen from a SCWR, via the coupling of nuclear heat and the CuCl cycle, is an exciting combination that has the potential for large synergistic benefits to large scale chemical plants. A simple schematic of the proposed system can be seen below in Figure 2.2.

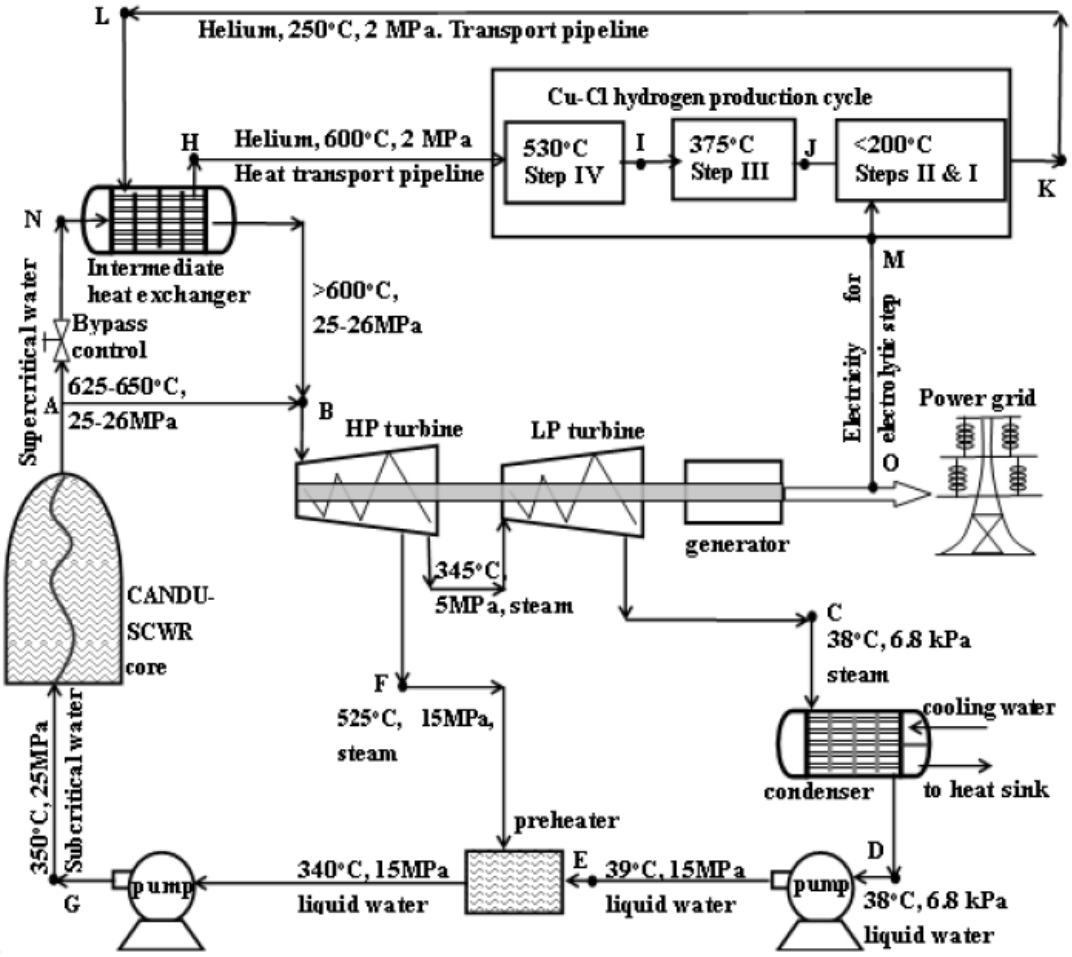

Figure 2.2 SCWR and CuCl cycle integration (reprinted from (Tsvetkov, 2010)).

In the literature, there has been little discussion regarding the potential role that the oxygen gas created by thermochemically splitting water could have on a process that could benefit from both the hydrogen and the oxygen (Rosen, 2010; Wang et al., 2010). If oxygen is a required resource that certain unit operations require (ATR, Gasifier etc.) then there is even more synergy present if this system is coupled with other technologies that could benefit from both oxygen and hydrogen generation.

2.7 Solid-oxide-fuel-cells

A solid-oxide-fuel-cell (SOFC) is an electrochemical device that oxidises a fuel, without the need for combustion (Thomas A. Adams, Nease, Tucker, & Barton, 2013). Oxygen is present in the cathode, usually in air, and fuel is present in the anode. When the ion passes through the solid state conductor, it ends up in the anode side where it can oxidize the fuel, and drive electrons to the load source, creating electrical power. A schematic of the process can be seen in Figure 2.3.

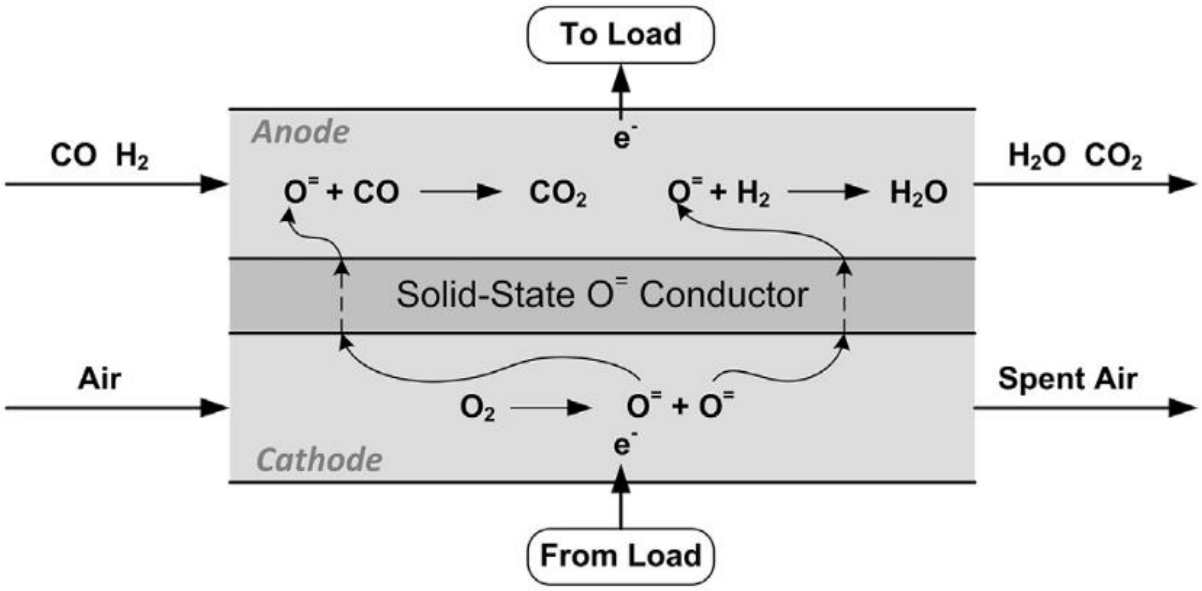

Figure 2.3 Simplified schematic of a SOFC using syngas as its fuel source. Reproduced from (Nease & Adams, 2013).

SOFCs are flexible and can accept a wide variety of fuels such as methanol (Laosiripojana & Assabumrungrat, 2007), natural gas and syngas derived from biomass, coal, and natural gas (Williams, Strakey, & Surdoval, 2005). In addition, because of the solid oxide barrier between the fuel gas and the air, there is no fuel mixing. Thus, the exhaust of the anode

side of the SOFC is nearly all CO_2 and water. This makes CO_2 separation very easy and efficient, and a large absorption plant can be avoided. Moreover, SOFCs can achieve higher electrical efficiencies than a traditional gas turbine system, which would normally be used in state-of-the-art natural gas combined cycle systems (NGCC) (Thomas A. Adams & Barton, 2010; Nease & Adams, 2013).

2.8 Polygeneration

Polygeneration is a term used to describe a process that co-produces at least two products: electricity and at least one other chemical via a thermochemical route that does not rely on petroleum products (Thomas A Adams & Ghouse, 2015). Polygeneration processes are tightly integrated and this integration can benefit the polygeneration process by exploiting synergies, which can lead to a more efficient, environmentally beneficial, and risk-averse process. An in-depth summary of current polygeneration processes has been done by Ghouse and Adams, and has shown that most polygeneration processes are optimally configured to produce a single fuel or chemical along with electricity (Thomas A Adams & Ghouse, 2015).

Fischer-Tropsche (FT) liquids, methanol and dimethyl ether (DME) are common polygeneration co-products that have been studied heavily in the literature (Thomas A. Adams & Barton, 2011a; Clausen, Elmegaard, et al., 2010; Khojasteh Salkuyeh, 2015). These processes are common choices because polygeneration plants often rely on the gasification to generate syngas for co-product production. The FT process converts syngas

to gasoline and diesel precursors, such as naphtha and distillate, utilizing a catalytic reactor vessel and a subsequent separation train (Steynberg & Dry, 2004). The process has been utilized by Sasol in South Africa to produce coal- derived syngas, which is then fed to a slurry phase reactor to generate synthetic gasoline and diesel precursors (Steynberg & Dry, 2004). Methanol and DME are valuable chemical products that are also commonly studied in the literature for their application in polygeneration systems (Thomas A. Adams & Barton, 2011a; Clausen, Elmegaard, et al., 2010).

Nuclear power has recently been used in a study by Salkuyeh and Adams which looked to find synergies between nuclear heat and natural gas reforming in a polygeneration study (Salkuyeh & Adams, 2013). They determined that reforming methane with the heat of an advanced high temperature nuclear reactor, can benefit the system economics and reduce the greenhouse gas emissions from the plant.

Biomass is a promising fuel stock and its potential for gasification and polygeneration has also been studied in the literature (Ahrenfeldt, Thomsen, Henriksen, & Clausen, 2013; Clausen, Elmegaard, et al., 2010; Clausen, Houbak, & Elmegaard, 2010; Van der Drift et al., 2004). With similar syngas outlet conditions, gasified woody biomass behaves similarly to coal when most of the moisture is removed, with coal having a slightly higher H_2 to CO ratio (Van der Drift et al., 2004). Woody biomass has some disadvantages, however, because it has to be harvested in a sustainable manner and it is particularly energy intensive to collect and deliver to the plant, making the price of the biomass usually 3-5

times that of coal (Hewson, Oo, Albion, & Keir, 2011). Some benefits when compared to coal is that biomass syngas is significantly cleaner and there is less sulfur and no mercury present, which make downstream syngas cleaning easier for woody biomass. In addition, coal gasification can be an environmentally viable route with proper CO_2 capturing techniques. However, coal is not very widely accepted politically or socially for new power generation technologies, making the research and investment in biomass power plant technologies more viable for future implementation (Thomas A. Adams & Barton, 2010, 2011a; "Ontario's LTEP," 2013)

The novel design and technoeconomic analysis of a polygeneration plant will be the main focus of this study. The proposed feedstocks will be biomass, natural gas and nuclear energy, the selection of which is motivated by the goals of this study to design a process that is energy efficient and environmentally friendly, and particularly beneficial and applicable to Ontario, Canada. Only Ruth et al has proposed the integration of biomass with nuclear energy but no technical process studies have been done and no proposed system has considered the use of the CuCl cycle for integration in a polygeneration process (Ruth et al., 2014).

Chapter 3

Process Description and Modeling Methodology

The purpose of this chapter is to give an overview of the proposed novel Biomass-Gas-Nuclear-to-liquids process and the 8 different case studies that will be included in the work. In addition, this chapter gives a detailed summary of the modeling framework used in this proposed study. The specific unit operations that were used in Aspen Plus, gProms and ProMax will be discussed.

3.1 Introduction and process structure

In previous work, polygeneration plants have been shown to utilize biomass, coal and natural gas very effectively (Thomas A Adams & Ghouse, 2015). In this work, a polygeneration process that utilizes woody biomass, natural gas and nuclear power for polygeneration of chemicals is proposed. The process is called the biomass-gas-nuclear-to-liquids process or BGNTL, and no other process like it is known in the literature. The full process structure that is considered in this work is outlined in Figure 3.1 below.

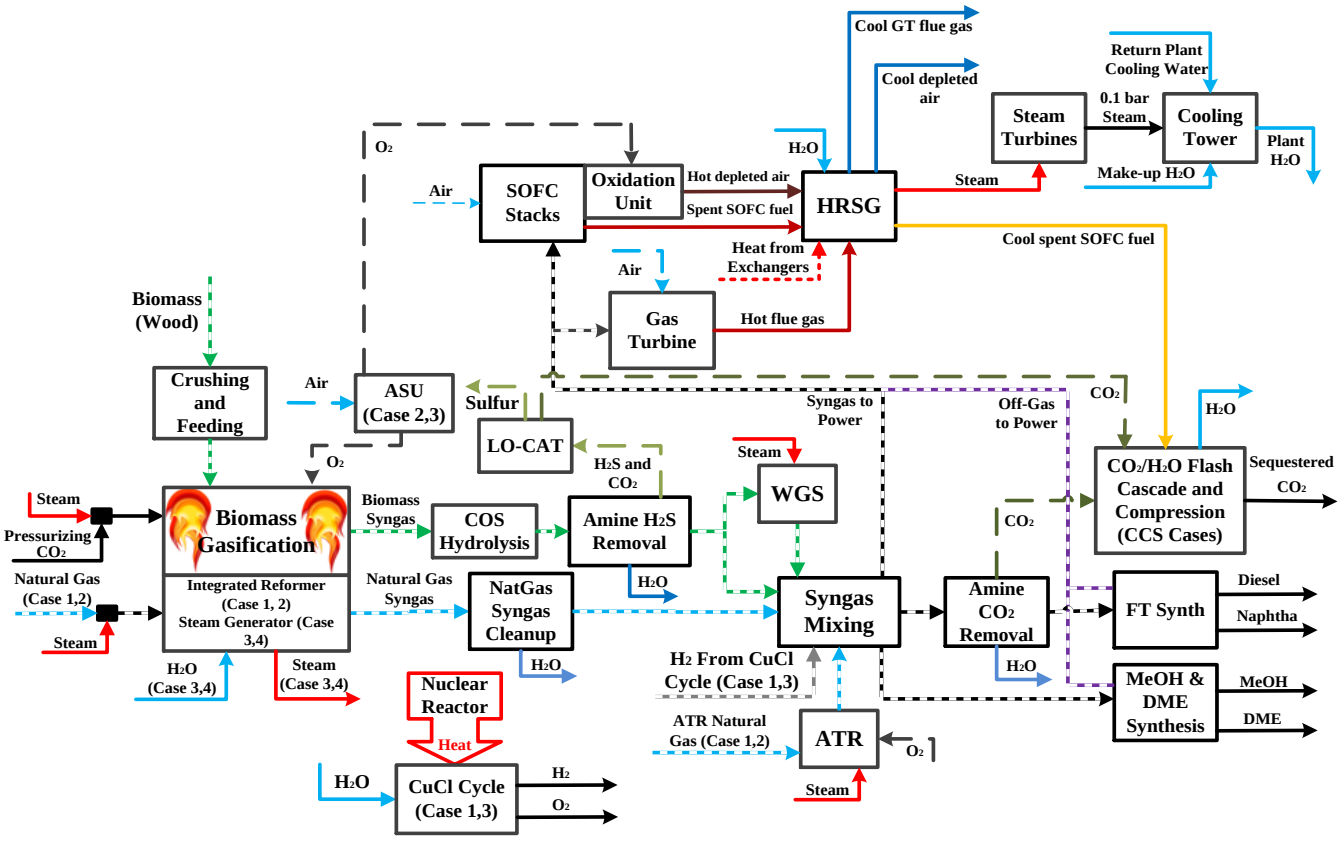

Figure 3.1 BGNTL process structure.

The process begins with biomass crushing and feeding to the gasifier. In addition to the woody biomass being fed to the gasifier, carbon dioxide, steam and oxygen are fed to the gasifier to facilitate syngas production and feeding. Partial oxidation then occurs in the gasifier, and the heat is transferred to the integrated reformer (IR), which is composed of the SMR and the RSC. The IR utilizes this heat to reform the natural gas into syngas. After this step occurs, the syngas is quenched using process water, to around 200°C so that it can be utilized for further processing. After the gasifier, the biomass syngas is then sent to be processed in the COS reactor and then to the acid gas removal section. The purpose of these two sections is to remove all of the sulfur that is naturally present in wood, leaving clean or sweet syngas that is mostly made up of CO and H_2 gas. After this section, the syngas is mixed with natural gas generated syngas from the RSC, ATR syngas, shifted syngas from the WGS and hydrogen gas generated by the CuCl cycle. The availabilities of these mixing materials depends on the process case, which will be discussed later in this chapter.

After the syngas is mixed, it is destined for one of three places. It is either mixed to 2.01 H_2/CO ratio and sent to either of the Methanol / DME section or the FT section, or it is mixed in a non-specific H_2/CO ratio and sent to the power generation system – either to the gas turbine (GT) or the SOFC system for power generation. The final products of the process are Diesel, Naphtha, DME, Methanol and Electricity.

In addition to these processes, there is also a heat recovery and steam generation section that generates power through a steam cycle from waste heat of the BGNTL process.

Finally, there is a CO_2 compression section for carbon capture and storage plant design cases.

3.2 Process Cases

The process cases that were considered in this study are summarized below in Table 3.1.

Table 3.1 Process cases considered in this work.

Case	Case Name	Biomass?	Natural gas?	Nuclear?	RSC+SMR?	CCS?
1.1	BGNTL-CCS-IR	✓	✓	✓	✓	✓
1.2	BGNTL-**wo**CCS-IR	✓	✓	✓	✓	–
1.3	BGNTL-CCS-Steam RSC	✓	✓	✓	–	✓
1.4	BGNTL-**wo**CCS-Steam RSC	✓	✓	✓	–	–
2.1	BGTL-CCS-IR	✓	✓	–	✓	✓
2.2	BGTL-**wo**CCS-IR	✓	✓	–	✓	–
2.3	BGTL-CCS-Steam RSC	✓	✓	–	–	✓
2.4	BGTL-**wo**CCS-Steam RSC	✓	✓	–	–	–

3.3 Process modeling strategy and basis

The BGNTL process (and its other predecessor cases) discussed in chapter 3 was modeled utilizing a variety of process simulation tools including Aspen Plus v8.8, Matlab, ProMax and gProms. These tools, and how they were implemented in the overall model, will be discussed in this section. In addition, the overall flowsheet was implemented with the Peng-Robinson equation of state with the Boston-Mathias modification (PR-BM), with the following exceptions: (1) The TSWEET property package in ProMax was used to model the acid gas and CO_2 removal steps, (2) NBC/NRC steam tables were used to model pure water streams, (3) in the CO_2 removal section, PSRK was used to model the CO_2 and water equilibrium that exists at high pressures (Thomas A. Adams & Barton, 2010). These equations of state best represent the real world process.

The simulation basis of this process was set at 1500 MW of thermal energy input by higher heating value (HHV), which included the total input of wood, natural gas, nuclear energy. This plant was designed such that all utility needs were produced on site, with no utilities imported, with the exception of water.

3.3.1 Process feedstock

The biomass that was assumed to be used in this plant was cedar wood chips as received, with an 8% moisture content. The composition of biomass used in this study can be seen below in Table 3.2.

Table 3.2 Properties of the biomass (cedar) used in this study (Hewson et al., 2011).

Proximate Analysis (wt%)		**Ultimate Analysis (wt% Dry)**		**HHV (kj/kg)**	**LHV (kj/kg)**
Fixed Carbon	58.16	Carbon	48.62	19804.82	18790
Volatile matter	39.94	Hydrogen	5.991		
Ash	1.90	Nitrogen	0.478		
Moisture	8	Sulfur	0.005		
		Oxygen	43.006		
		Chlorine	0.209		

In addition, the average ash molecular weight and the amount of iron oxide present in the cedar wood is also modeled and shown below in Table 3.3.

Table 3.3 Properties of cedar wood ash used in this study ("Phyllis2 - ECN Phyllis classification," n.d.).

Wood parameter	Value
Average molecular weight of ash (AMWA)	0.06515 [kg/mol]
Mol fraction of Fe_2O_3 in ash	2.613%

The natural gas composition that was used in this study is shown below in Table 3.4.

Table 3.4 Properties of natural gas used in this study (Salkuyeh & Adams, 2013).

Component – molar %					
$CH_4 - 93.9$	$C_2H_6 - 3.2$	$C_3H_8 - 0.7$	$n - Butane - 0.4$	$CO_2 - 1$	$N_2 - 0.8$

3.3.2 Gasification model

The modeled gasifier was a biomass, steam, pressurizing CO_2 and oxygen fed entrained flow gasifier. The system was modeled as a 0-D system in Aspen Plus, which considered the three stages of the gasifier: biomass decomposition, gasification and cooling.

The radiant cooler and the quench system is also modeled in this section using various heater blocks and flash tanks. The model was based partially off of the work of Field et al. and Adams et al. (Thomas A. Adams & Barton, 2010; Field & Brasington, 2011). The decomposition step utilized the ultimate, proximate and sulfonate analysis from Table 3.3 and broke the biomass into solid C and S elements as well as water, H_2, and Cl_2 gases. The decomposition reactor was modeled as a RYield block in Aspen Plus. The gasification step was modeled as an equilibrium reactor within Aspen Plus - this section is where the required oxygen, high pressure steam (HPS) and pressurizing CO_2 was added to the reactor, and brought to chemical equilibrium via the following reactions described in equation set 3.1 (Thomas A. Adams & Barton, 2010).

$$\begin{gathered} H_2O + CO \rightleftharpoons CO_2 + H_2 \\ C + 0.5O_2 \rightleftharpoons CO \\ C + O_2 \rightleftharpoons CO_2 \\ N_2 + 3H_2 \rightleftharpoons 2NH_3 \\ CH_4 + H_2O \rightleftharpoons CO + 3H_2 \\ S + H_2 \rightleftharpoons H_2S \end{gathered} \tag{3.1}$$

$$CO + S \rightleftharpoons COS$$

$$Cl_2 + H_2 \rightleftharpoons 2HCl$$

There were two gasifier modes considered in this work. In the first, the radiant syngas cooler was used to reform natural gas via steam methane reforming, while the second case used the radiant cooler as a steam generator, being fed with boiler feed water. The flow diagrams of the IR case and the steam generator RSC case cases can be seen below in Figure 3.2 and Figure 3.3, respectively.

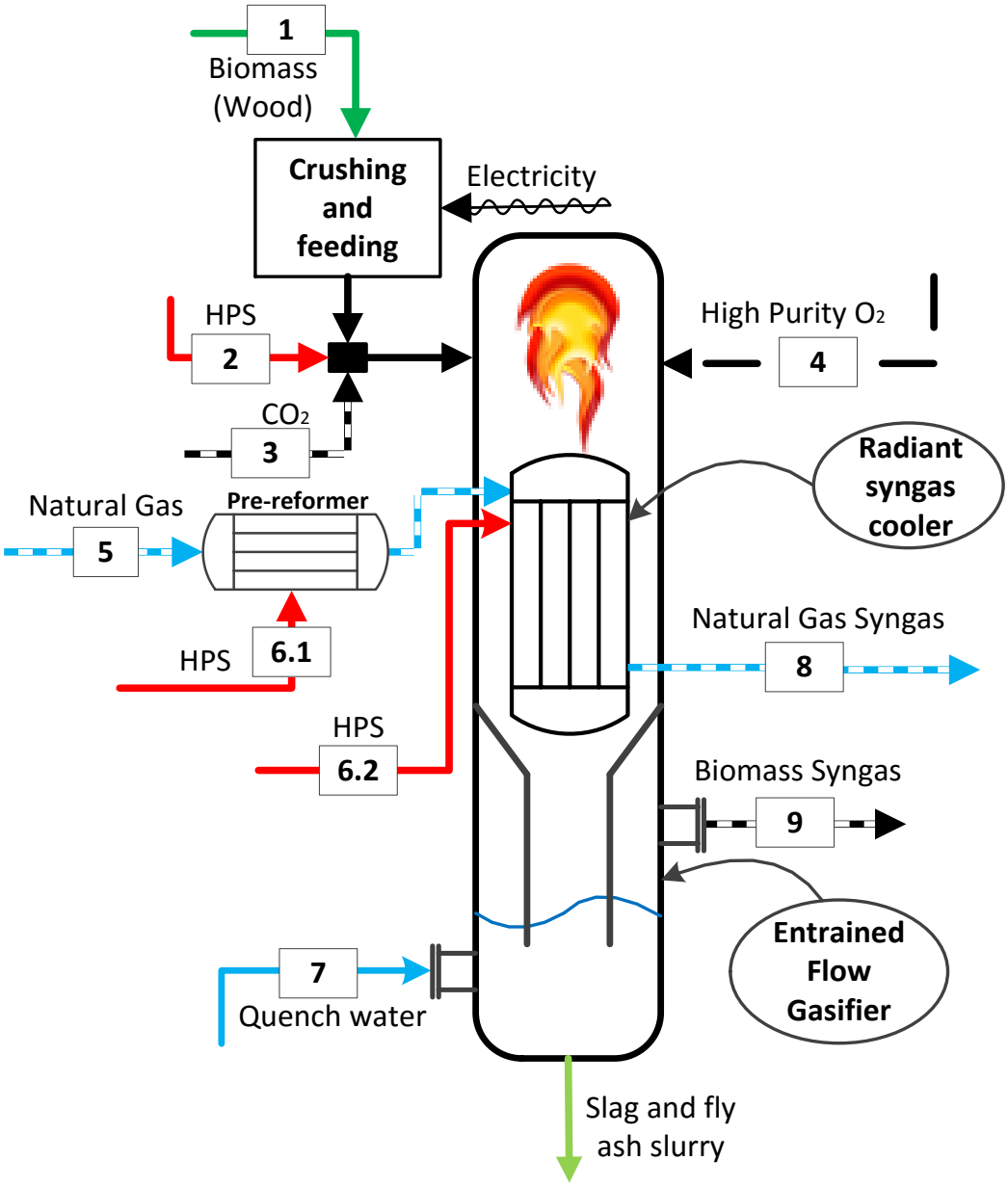

Figure 3.2 Gasifier flow diagram with IR, simplified from Aspen Plus model.

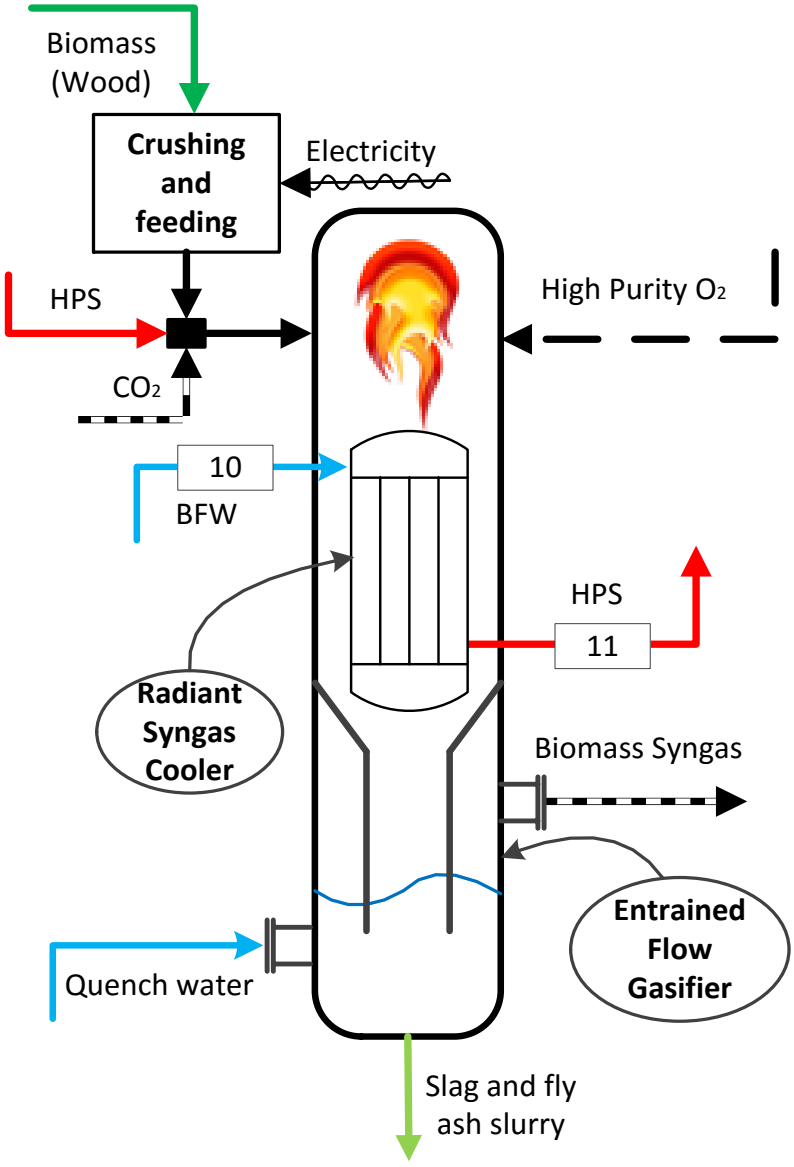

Figure 3.3 Gasifier flow diagram with steam generating RSC, simplified from Aspen Plus model.

To accompany the gasifier drawings, the stream properties indicated by the stream ID's in Figure 3.2 and Figure 3.3 are summarized in Table 3.5 below.

Table 3.5 Sample stream conditions for gasifier operation at 100% throughput.

Stream ID	1*	2	3	4	5	6.1	6.2	7	8	9	10	11
T (°C)	20	500	30	160	30	500	500	31	808	200	100	500
P (bar)	1.05	50	46	47	30	50	50	45	24	43.3	52	50
Flow rate (kmol/hr)	100,000	161	273	1548	674	354	2471	5636	4625	9329	2741	2741
Vapour fraction	0	1	1	1	1	1	1	0	1	1	0	1
Mol fraction (%)												
Wood	100											
H_2									39	17		
CO									9	32		
CO_2			100		1.0	100	100		3.5	11		
H_2O		100						100	45.5	40	100	100
Ar				0.3						0.05		
O_2				99.5								
N_2				0.2	0.8				0.1	0.2		
NH_3										7.5 ppm		
COS										0.02		
H_2S										0.3		
HCl										0.06		
CH_4					93.9				2.9	55 ppm		
C_2H_6					3.2							
C_3H_8					0.7							
C_4H_{10}					0.4							

* Flow units in kg/hr

Biomass is required to be of very small size prior to entering a gasifier, to achieve optimal mixing while gasifying (Van der Drift et al., 2004). To achieve this, additional crushing of the biomass is required to get the biomass to have a particle diameter of no more than 1mm. Therefore, a crushing power of $0.02\ kW_e/kW_{th,HHV\ wood}$ is required to crush the biomass to the required size (Van der Drift et al., 2004).

The feed to the gasifier was the same scale in all cases except the biomass only cases. The base feed rate of wood to the gasifier was 100 tonnes per hour, at 8% moisture (Table 3.2). In addition, high pressure steam at a rate of 2.8% of the biomass feed mass was added along with 12% by weight pressurizing CO_2 (Clausen, Elmegaard, et al., 2010). CO_2 is used as a

pressurizing agent, which moves the biomass material into the gasifier, which operates at 45 bar. Pressurizing agents like N_2 have been used in the past on coal fed gasifiers, but increased system efficiencies are seen when pressurizing with CO_2 (Van der Drift et al., 2004), and the presence of N_2 can negatively affect downstream reaction efficiencies. In addition, CO_2 and steam help with supressing soot formation during gasification (Van der Drift et al., 2004). The effects of the low levels of ash that exist in biomass and the need for ash recycle is neglected in this work (Clausen, Elmegaard, et al., 2010). The temperature of the gasifier was controlled to 1300°C by the amount of added oxygen. It is also assumed that there is 100% carbon conversion of the gasified biomass and that 2.7% of the heat generated by the gasifier is lost to the surroundings (Clausen, Elmegaard, et al., 2010). Finally, quench water is added to the gasifier to cool the syngas to 200°C, prior to downstream processing.

3.3.3 Radiant syngas cooler

There were two RSC modes considered in this work, namely a RSC that acts as a steam generator and a RSC that operates as a SMR (IR).

3.3.3.1 Radiant syngas cooler – steam generator

The RSC steam generator was modeled as a simple heater block and generated high pressure steam for use across the plant. This process is shown in Figure 3.3, with stream conditions outlined in Table 3.5.

3.3.3.2 Radiant syngas cooler – SMR

The model of the IR was based on the same integrated model developed by Ghouse and Adams (Ghouse et al., 2015). This model integrated a SMR within the RSC of a coal fed entrained flow gasifier. The model developed was a non-linear two-dimensional heterogeneous model that was implemented into gProms; an overview of the model is shown in Figure 3.4. The model was a set of partial differential algebraic equations, and was solved using a finite difference method; for further details, please refer to (Thomas A Adams & Ghouse, 2015; Ghouse & Adams, 2013). The goal in this project was to create a reduced order steady-state model (ROSSM) of this highly non-linear process that could be implemented within the Aspen Plus framework.

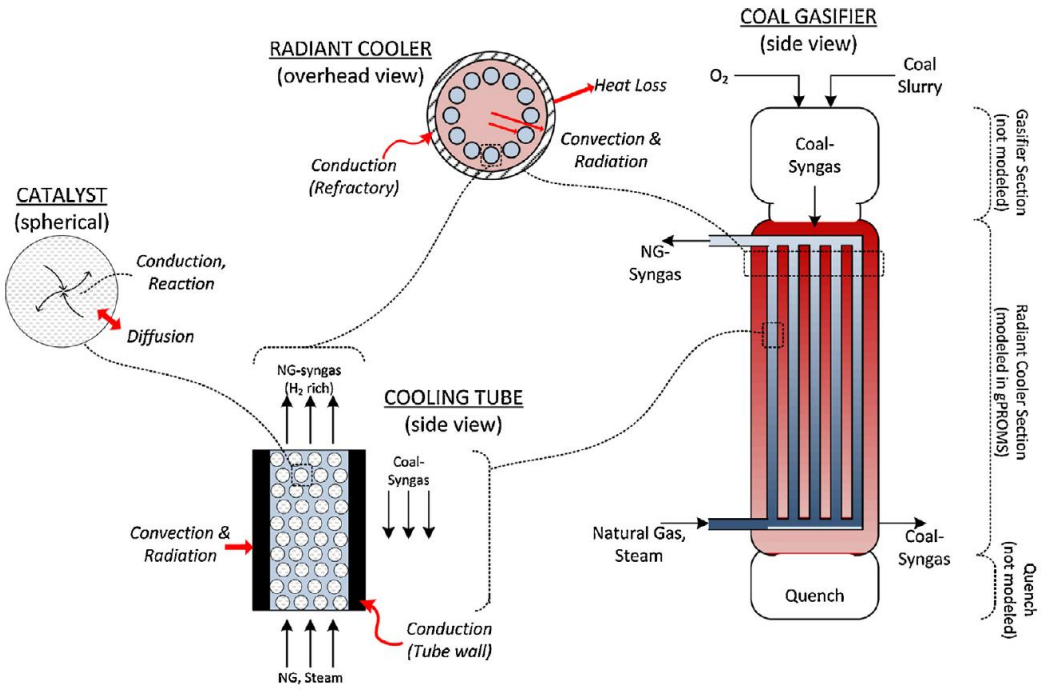

Figure 3.4 RSC integrated with a SMR reprinted from (Seepersad, Ghouse, & Adams, 2015).

However, prior to the ROSSM, the natural gas was sent through a pre-reformer, modeled as an equilibrium, adiabatic reactor in Aspen Plus. This was implemented because the model developed by Adams and Ghouse did not consider the presence of ethane, propane or n-butane, which was considered in the natural gas composition, outlined in Table 3.4. Equation set 3.2 shows the reactions that take place in the pre-reformer and it was assumed that equations 1-3 in 3.2 go to 100% completion. High pressure steam was added to the reformer at a rate of 52.5% of the incoming natural gas flow rate (Thomas A. Adams & Barton, 2011a).

$$
\begin{aligned}
C_2H_6 + 2H_2O &\rightarrow 2CO + 5H_2 \\
C_3H_8 + 3H_2O &\rightarrow 3CO + 7H_2 \\
n - C_4H_{10} + 4H_2O &\rightarrow 4CO + 9H_2 \\
CH_4 + H_2O &\rightleftharpoons CO + 3H_2 \\
CO + H_2O &\rightleftharpoons CO_2 + H_2
\end{aligned}
\tag{3.2}
$$

The development of the ROSSM started with developing a size requirement for the RSC. The syngas composition, flowrate, temperatures and pressures developed in Table 3.5 were the specifications fed to the inlet of the gasifier. The size of the RSC was selected to be approximately 20 meters long with a 4.5 meter diameter holding 137 tubes (8 cm diameter). The inputs to the model were the natural gas flow rate and the molar steam to carbon ratio (CH_4/H_2O), referred to as X and Y, respectively. The outputs of the model were the required radiant cooler duty (Z_1), the CH_4 conversion (Z_2), the H_2O conversion (Z_3), the

gas exit temperature (Z_4), and the reactor pressure drop (Z_5). The summary of the inputs and outputs are summarized below in Table 3.6.

Table 3.6 ROSSM inputs, outputs and search space parameters.

Model inputs	**Units**	**Model Outputs**	**Units**
$X -$ Natural gas flow rate	(kmol/hr)	$Z_1 -$ Required radiant cooler duty	(MW)
$Y -$ Steam to carbon ratio	unitless	$Z_2 - CH_4$ conversion	(%)
		$Z_3 - H_2O$ conversion	(%)
		$Z_4 -$ Reactor exit temperature	(°K)
		$Z_5 -$ Reactor pressure drop	(bar)
Upper and lower bounds on model inputs			
$X_{low} = 506.9$			
$X_{high} = 753.5$			
$Y_{low} = 2.6$			
$Y_{high} = 4$			

The upper and lower bounds on the input parameters outlined in Table 3.6 were put in place because the model developed by Ghouse and Adams has specific limitations on the tube wall, catalyst and refractory temperatures in the RSC. The search space that was chosen allows for safe operation within the different configurations possible in the 2 dimensional sample space (Ghouse et al., 2015).

The next step in the model development was generating data. This was done by running 80 simulations varying X and Y within the search space, utilizing a latent hypercube design – generated with the `lhsdesign` function in Matlab. A latent hypercube design allows for no two X and Y search variables to be explored twice, allowing for thorough exploration of the search space. The rigorous simulation was modeled in gProms and the outputs were sent to Matlab via the gOMatlab interface. If a simulation failed, its data was flagged and

thrown out during data reconciliation. Some reasons for failure of the gProms included poor initial guesses, and numerical errors during simulation.

The various model structures that were considered to build the ROSSM can be seen in equations 3.3 – 3.5.

$$Z = a_1 + a_2\frac{X}{\overline{X}} + a_3\frac{Y}{\overline{Y}} \tag{3.3}$$

$$Z = a_1 + a_2\frac{X}{\overline{X}} + a_3\frac{Y}{\overline{Y}} + a_4\left(\frac{X}{\overline{X}}\right)^2 + a_5\left(\frac{Y}{\overline{Y}}\right)^2 + a_6\left(\frac{X}{\overline{X}}\right)\left(\frac{Y}{\overline{Y}}\right) \tag{3.4}$$

$$Z = a_1 + a_2\frac{X}{\overline{X}} + a_3\frac{Y}{\overline{Y}} + a_4\left(\frac{X}{\overline{X}}\right)^2 + a_5\left(\frac{Y}{\overline{Y}}\right)^2 + a_6\left(\frac{X}{\overline{X}}\right)^3 + a_7\left(\frac{Y}{\overline{Y}}\right)^3 + a_8\left(\frac{X}{\overline{X}}\right)\left(\frac{Y}{\overline{Y}}\right) \tag{3.5}$$

To determine the best model to use, 60 of the simulation runs were used to build the training model and 20 points were used to generate the testing data set. The resulting R^2_{train} and R^2_{test} were then analyzed to determine the best model to use. The results can be seen below in Table 3.7.

Table 3.7 Candidate model structures for ROSSM.

Model Structure	**Average R^2_{train}**	**Average R^2_{test}**	**Average Max Err (%)**
Equation 3.3	0.988	0.978	0.842
Equation 3.4	1	0.998	0.074
Equation 3.5	1	0.997	0.072

The linear equation set 3.3 had the lowest R^2_{train} and R^2_{test} and was not used in the final implementation. The quadratic and cubic sets of equations 3.4 and 3.5 both had very good performance, with the quadratic set being slightly better indicating that the cubic structure had some slight overfitting. Moreover, the cubic coefficients a_6 and a_7 were small. Therefore, structure 3.4 was ultimately chosen. The resulting coefficients of equation 3.4 are shown in Table 3.8.

Table 3.8 Model coefficients for ROSSM using equation structure 4.4.

Output variable	Units	Coefficients	R^2_{train}	R^2_{test}	Max Err (%)
Z_1	MW	$a_1 = 5.726, a_2 = 32.529, a_3 = 10.417$ $a_4 = -9.871, a_5 = -2.601, a_6 = 2.336$	1	1	0.04
Z_2	%	$a_1 = 1.068, a_2 = -0.679, a_3 = 0.257$ $a_4 = 0.144, a_5 = -0.062, a_6 = 0.030$	1	0.99	0.14
Z_3	%	$a_1 = 0.864, a_2 = -0.231, a_3 = -0.571$ $a_4 = 0.027, a_5 = 0.145, a_6 = 0.096$	1	1	0.15
Z_4	°K	$a_1 = 1512, a_2 = -362.9, a_3 = -86.85$ $a_4 = 110.4, a_5 = 28.44, a_6 = -72.49$	1	1	0.03
Z_5	bar	$a_1 = -14.815, a_2 = 21.06, a_3 = 17.68$ $a_4 = -7.113, a_5 = -4.098, a_6 = -18.06$	1	0.998	0.01
Average input variables					
$\bar{X} = 637.329$	$\bar{Y} = 3.293$				

The model was implemented in Aspen Plus as an RStoic reactor with the SMR equations outlined in equations 2.1 and 2.2. In terms of actual implementation in Aspen Plus, the first step was to set the heat duty to the SMR via the RSC from the gasifier block; this assigned a value in MW to Z_1. In addition, a conservative value of 80% methane conversion for Z_2 was chosen, as this value is a normal expected methane conversion value in a SMR (Ghouse et al., 2015). Once these two values were selected, the degrees of freedom of the two equations become zero and X (required steam to carbon ratio) and Y (natural gas flow rate)

can be solved for. These values were then sent to the remaining equations (Z_3 – Z_5) and these values were then implemented into ROSSM, to give the outputs of the ROSSM reactor. An overview of the pre-reformer and the ROSSM process can be seen in Figure 3.5.

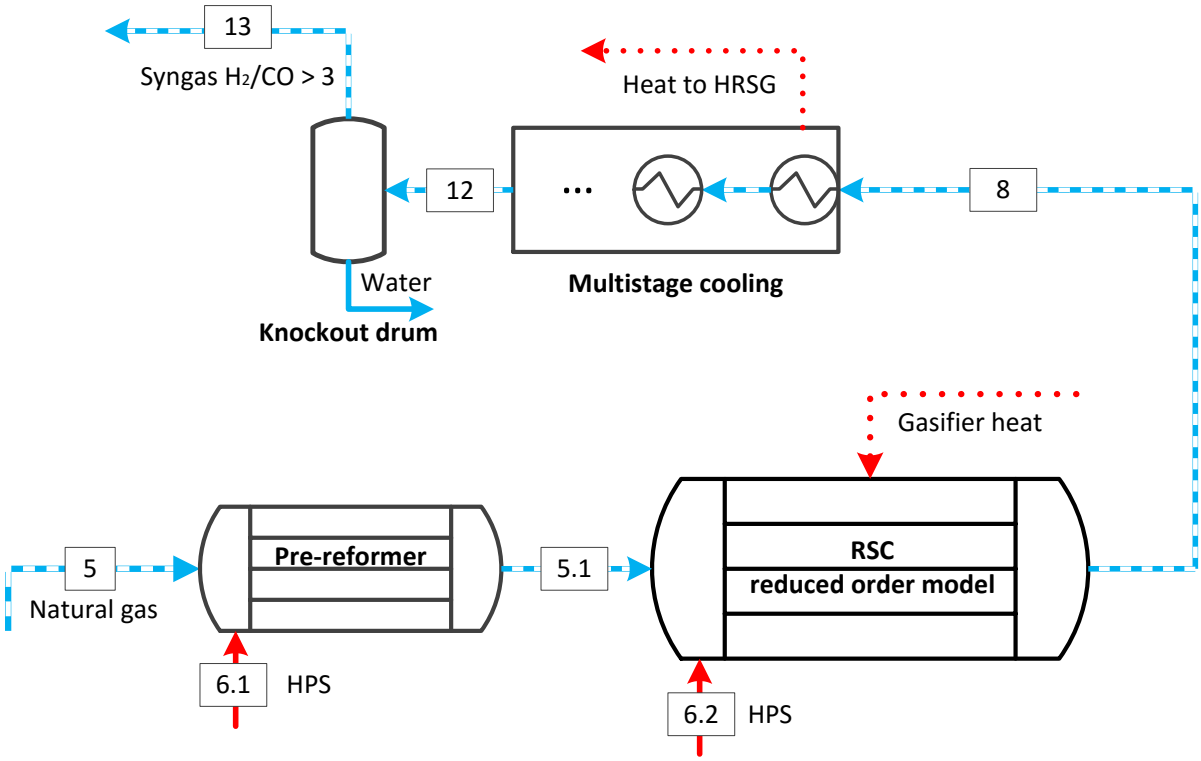

Figure 3.5 IR implementation with stream IDs, as modeled in Aspen Plus.

Sample values for stream IDs for Figure 3.5 in can be seen in Table 3.9.

Table 3.9 Sample stream conditions for Figure 3.5.

Stream ID	5.1	6.1	6.2	12	13
T (°C)	325	500	500	40	40
P (bar)	29.4	50	50	18	17.8
Flow rate (kmol/hr)	756	354	2471	4625	2530
Vapour fraction	1	1	1	0.55	1
Mol fraction (%)					
H_2	2			39.1	71.4
CO	64 ppm			8.8	16.1
CO_2	2			3.5	6.4
H_2O	30.7	100	100	45.5	0.4
Ar					
O_2					
N_2	0.5			0.1	0.2
NH_3					
COS					
H_2S					
HCl					
CH_4	64.8			3	5.5
C_2H_6					
C_3H_8					
C_4H_{10}					

3.3.4 Air separation unit

The air separation unit (ASU) is not modeled in this study. The processes that require oxygen receive it at 99.5% O_2 purity and the economics that keep track of the sizing of the required plant and the power it would consume to provide the power are discussed in the economics section (Clausen, Elmegaard, et al., 2010). In addition, N_2 is available to the gas turbine in an amount proportional to the O_2 fed to the system from the ASU.

3.3.5 Acid gas removal

3.3.5.1 COS reactor

After the gasifier, a hydrolysis reactor reacts COS with water, generating H_2S, which is easier to remove than COS from syngas, making downstream sulfur removal more cost

efficient (Thomas A. Adams & Barton, 2011b). The reactions that take place in the COS reactor are shown as equation 3.6. The reactor was modeled as an adiabatic RStoic reactor in Aspen Plus and 100% conversion of COS is assumed in the COS reactor.

$$\begin{gathered} \mathrm{COS} + \mathrm{H_2O} \rightarrow \mathrm{H_2S} + \mathrm{CO_2} \\ \mathrm{H_2O} + \mathrm{CO} \rightleftharpoons \mathrm{CO_2} + \mathrm{H_2} \end{gathered} \tag{3.6}$$

The COS reactor is shown in Figure 3.6.

3.3.5.2 Acid gas removal

Whether it is sent to electricity or fuels production, H_2S needs to be removed from the syngas since it can harm catalysts and downstream equipment. The most popular method to remove H_2S from syngas is to use a solvent-based method where the gas is passed through the liquid and the solvent selectively absorbs certain components. For this application, Methyldiethanolamine (MDEA) was chosen for this task of removing the H_2S from the syngas – other solvents such as DEA, Selexol or Rectisol may be preferred but are not considered in this work (T. A. Adams, Salkuyeh, & Nease, 2014). In addition to having a high affinity for H_2S, MDEA also has a high affinity for CO_2 and removes both simultaneously since both CO_2 and H_2S are soluble in MDEA and have the following electrolytic reactions: 3.7 for CO_2 and 3.8 for H_2S, respectively (T. A. Adams et al., 2014).

$$\begin{gathered} \mathrm{MDEA-H^+ + H_2O \rightleftharpoons MDEA + H_3O^+} \\ \mathrm{2H_2O \rightleftharpoons OH^- + H_3O^+} \\ \mathrm{CO_2 + 2H_2O \rightleftharpoons HCO_3^- + H_3O^+} \\ \mathrm{HCO_3^- + H_2O \rightleftharpoons CO_3^{=} + H_3O^+} \end{gathered} \tag{3.7}$$

$$\begin{gathered} \mathrm{H_2S + H_2O \rightleftharpoons H_3O^+ + HS^-} \\ \mathrm{HS^- + H_2O \rightleftharpoons H_3O^+ + S^{=}} \end{gathered} \tag{3.8}$$

There are specific challenges in modeling this system in Aspen Plus. Namely, the use of the ElecNRTL property package has substantial convergence problems, and would often crash due to the small amount of electrochemical species that are apparent in the system, when flow rates were changed. To overcome this challenge, ProMax, another software environment that can effectively simulate acid gas removal, was used. ProMax is another flow sheet simulation software that has a very realistic property package for acid gas removal applications called TSWEET, utilizing the Peng Robinson equation of state (T. A. Adams et al., 2014; Burr & Lyddon, 2008; Warudkar, Cox, Wong, & Hirasaki, 2013). To implement the ProMax model in Aspen Plus, a reduced order model of the ProMax process was created for Aspen Plus implementation. A schematic of the acid gas removal section developed in ProMax is shown in Figure 3.6. The process begins by absorbing the H_2S and CO_2 in the absorption column at high pressure. Then, the H_2S rich solvent is sent to a low pressure stripper column, which essentially flashes off the captured H_2S and CO_2 products. The lean solvent is then recycled back to the absorber column to repeat the process. Make-

up solvent (MDEA) and water are added to the system as some is lost in the sweet syngas stream and acid gas stream.

The absorption column operates at high pressure (7 ideal stages (21 actual trays) – 42.4 bar top, 42.75 bar bottom), while the stripper column operates at a relatively low pressure (10 ideal stages (30 actual trays) - 2.6 bar top, 3 bar bottom) (Mackenzie, Prambil, Daniels, & Bullin, 1987). In addition, low pressure steam is used to heat the bottom of the column and cooling water is used in all of the cooling blocks in Figure 3.6. In addition, a sweet syngas outlet specification was set in the ProMax model that set the amount of H_2S in the sweet syngas to be no more than 0.01 molar %. The model used ProMax TSWEET kinetics.

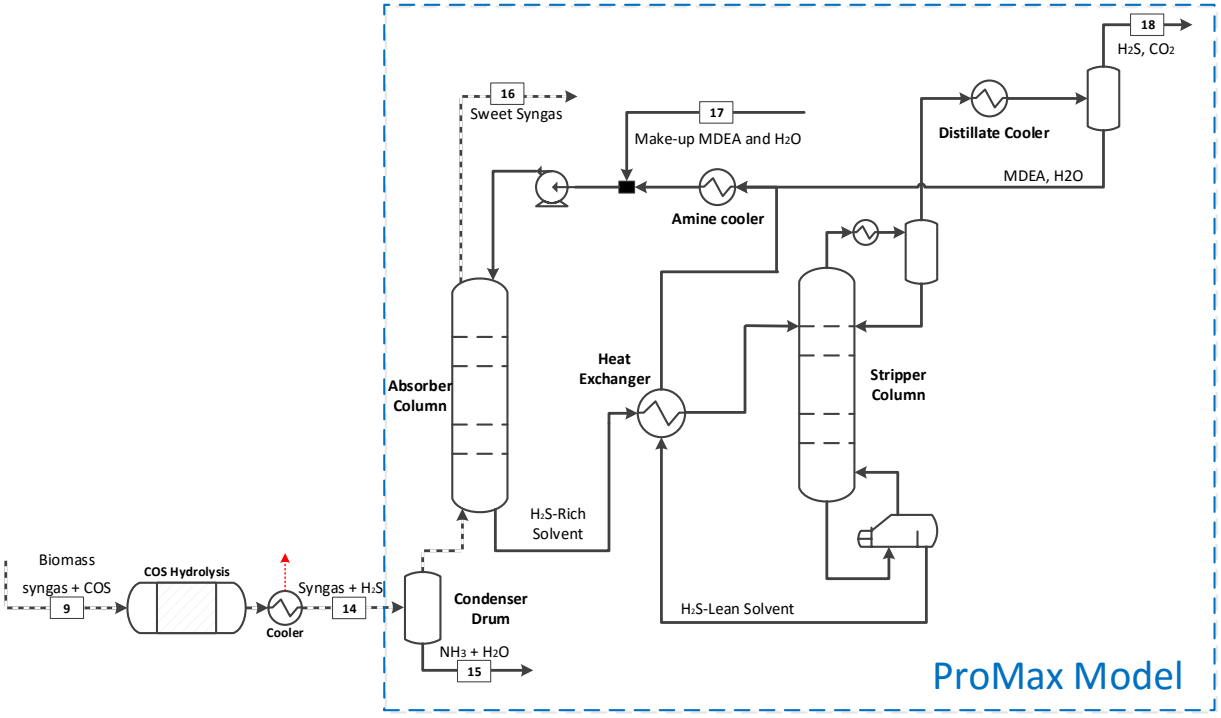

Figure 3.6 Acid gas removal section with stream IDs, as modeled in ProMax [blue]. Aspen Plus model not shown.

Because of the design specification of the system, the only dependent variables that were identified were the inlet molar flowrates of H_2S (X_{AGR}) and CO_2 (Y_{AGR}). The model structure of the acid gas ProMax model (AGPM) was selected to be linear, because fitting higher order models saw minimal improvement. The structure of the H_2S capture model is shown below as equation 3.9.

$$z_{AGR} = a_1 + a_2 \frac{X_{AGR}}{\overline{X}_{AGR}} + a_3 \frac{Y_{AGR}}{\overline{Y}_{AGR}} \tag{3.9}$$

To build the model outlined in equation 3.9, 50 simulation runs were done in ProMax varying the inlet conditions of stream 14 outlined in Figure 3.6 with different compositions of CO_2 and H_2S. 37 of the 50 data points were used as training data, and the remaining 13 data points were used as testing data. The model's output variables included the make-up water and amine feeds and the heat duties on all of the operating units in the process including the stripper columns, reboiler, and condenser duties. The results of the AGPM can be seen in Table 3.10.

Table 3.10 Reduced order model coefficients for the AGPM.

Input variable								
X_{AGR} - Inlet H_2S (kmol/hr)	$\bar{X}_{AGR} = 31.1061$		$X_{AGR,min} = 23.3296 - X_{AGR,max} = 38.8826$					
Y_{AGR} - Inlet CO_2 (kmol/hr)	$\bar{Y}_{AGR} = 994.0321$		$Y_{AGR,min} = 745.5241 - Y_{AGR,max} = 1242.5401$					
Output variable	**Description**	**Units**	a_1	a_2	a_3	R^2_{train}	R^2_{test}	**Max Err (%)**
$z_{AGR,1}$	MDEA make-up	(kmol/hr)	-0.0013	0.0155	7.324×10^{-4}	0.977	0.983	2.25
$z_{AGR,2}$	H2O make-up	(kmol/hr)	-2.638	32.29	13	1	1	0.104
$z_{AGR,3}$	Pump power	kW	-3.969	256.5	-56	1	1	0.054
$z_{AGR,4}$	Reboiler Duty	kW	283.1	1.638×10^4	1792	1	1	0.05
$z_{AGR,5}$	Condenser Duty	kW	-33.37	1024	488	1	1	0.053
$z_{AGR,6}$	Distillate Cooler	kW	-79.93	34.32	3968	1	1	0.054
$z_{AGR,7}$	Amine Cooler	kW	-74.48	74.09	7040	1	1	0.05

The models built for the AGPM were implemented in Aspen Plus as calculator blocks. Sample output data for the acid gas removal section is outlined in Table 3.11.

Table 3.11 Sample stream conditions for Figure 3.6.

Stream ID	14	15	16	17	18
T (°C)	40	40	74	83	43.1
P (bar)	42.75	42.7	42.4	40	2.6
Flow rate (kmol/hr)	9329	3749	5393	83.37	369
Vapour fraction	0.61	0	1	0	0.99
Mol fraction (%)					
H_2	17.1	0.02	30.1		0.2
CO	31.9	0.03	56.1		0.3
CO_2	10.8	0.4	12.6		88.6
H_2O	39.5	99.3	0.07	99.98	3
Ar	0.05	0.7 ppm	0.09		6.4 ppm
O_2					
N_2	0.2	1 ppm	0.3		13 ppm
NH_3	7.5 ppm	18.6 ppm			
COS					
H_2S	0.3	0.02	0.01		7.8
HCl	0.06	0.1			
CH_4	55 ppm	0.7 ppm	97 ppm		1.6 ppm
MDEA			2.5 ppm	0.02	2.3 ppm

The AGPMs were implemented into Aspen Plus with separator and heater blocks. After the H_2S separation train, the remaining gas containing most of the H_2S is sent to a LO-

CAT® system which uses a catalyst to oxidize the H_2S into solid sulfur (Okoli & Adams, 2014). This system is not modeled as a reaction system but it is accounted for in the economics section. In addition, cleaning of the sour water is taken into account in the economics section.

3.3.6 Syngas mixing section

The syngas mixing section is the area that mixes the syngas to a desired specification or sends it to the SOFC for power generation. Additional unit operations that are present in this section are the WGS reactor and the ATR reactor, which are discussed next.

3.3.6.1 Water gas shift reactor

The purpose of the water gas shift reactor (WGSR) section is to upgrade syngas coming from the biomass gasifier which has a low H_2 / CO ratio to a higher ratio of 2.01, since this syngas is destined for methanol and Fischer-Tropsch chemical production (Thomas A. Adams & Barton, 2011a). The WGSR was modeled as a set of plug flow reactors (RPlug) in Aspen Plus. The sequencing of reactors exploits the fast kinetics of the first two reactors, but utilizes the favourable low temperature equilibrium of the reaction system at the end. The low temperature reactor exploits the equilibrium moving more towards the products, namely hydrogen gas. The amount of steam that was added to the start of the first reactor was a design specification to meet a syngas H_2 to CO ratio of 2.01 at the exit of the last reactor. A schematic of the WGSR section is shown below in Figure 3.7 with sample stream

conditions in Table 3.12. Note that the flow rate of this section varies widely between simulation cases.

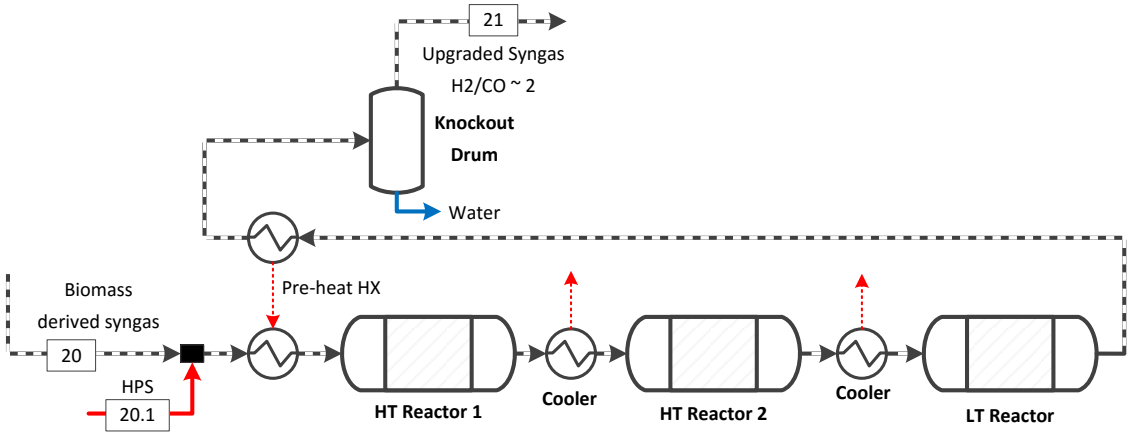

Figure 3.7 WGS reactor section, as modeled in Aspen Plus.

Table 3.12. Sample stream conditions for Figure 3.7.

Stream ID	20	20.1	21
T (°C)	74	500	100
P (bar)	42.4	50	39.1
Flow rate (kmol/hr)	980	347	1281
Vapour fraction	1	1	1
Mol fraction (%)			
H_2	30		44.1
CO	56		22
CO_2	13		31
H_2O	0.7	100	3
Ar	0.1		0.07
O_2			
N_2	0.3		0.3
NH_3			
COS			
H_2S	0.01		76 ppm
HCl			
CH_4	97 ppm		74 ppm
MDEA	2.5 ppm		1.9 ppm

The high temperature kinetic power-law equations are represented below as equation set 3.10. The high temperature reaction takes place between 300 and 450°C over a Fe_2O_3/ Cr_2O_3/CuO catalyst (Adams II & Barton, 2009).

$$-r_{CO} = d_{cat}(1-\theta)F_{press}\left(1.69\times10^{6}\frac{mol}{g\cdot hr\cdot atm}\right)\exp\left(\frac{-88000\frac{J}{mol}}{RT}\right)$$

$$\times y_{CO}^{0.9}y_{H_2O}^{0.31}y_{CO_2}^{-0.156}y_{H_2}^{-0.05}\left(1-\frac{y_{CO_2}y_{H_2}}{K_{eq}y_{CO}y_{H_2O}}\right)$$

$$\ln(K_{eq}) = \frac{4577.8}{T(°K)} - 4.33$$

$$F_{press} = P^{0.5-P/500} \qquad (3.10)$$

$$\theta = 0.5 \text{ (void fraction)}$$

$$d_{cat} = 2476\frac{kg}{m^3}$$

The low temperature kinetic power-law equations are represented below as equation set 3.11. The low temperature reaction occurs over a $Cu/ZnO/Al_2O_3$ catalyst between 120 and 300°C (Adams II & Barton, 2009).

$$-r_{CO} = d_{cat}(1-\theta)F_{press}\left(2.96\times10^{5}\frac{mol}{g\cdot hr\cdot atm}\right)\exp\left(\frac{-47400\frac{J}{mol}}{RT}\right)$$
$$\times\left(y_{CO}y_{H_2O}-\frac{y_{CO_2}y_{H_2}}{K_{eq}}\right)$$
$$\ln(K_{eq}) = \frac{4577.8}{T(°K)} - 4.33 \qquad (3.11)$$
$$F_{press} = P^{0.5-P/500}$$
$$\theta = 0.5 \text{ (void fraction)}$$
$$d_{cat} = 5904\frac{kg}{m^3}$$

3.3.6.2 Auto-thermal reforming section

The purpose of the aerothermal reforming (ATR) section is to provide syngas derived from natural gas, steam and oxygen for power or syngas upgrading for fuels and chemical production. The equations for ATR are represented in equation set 2.4, and are used in this section. A flow diagram of the ATR section is shown below in Figure 3.8.

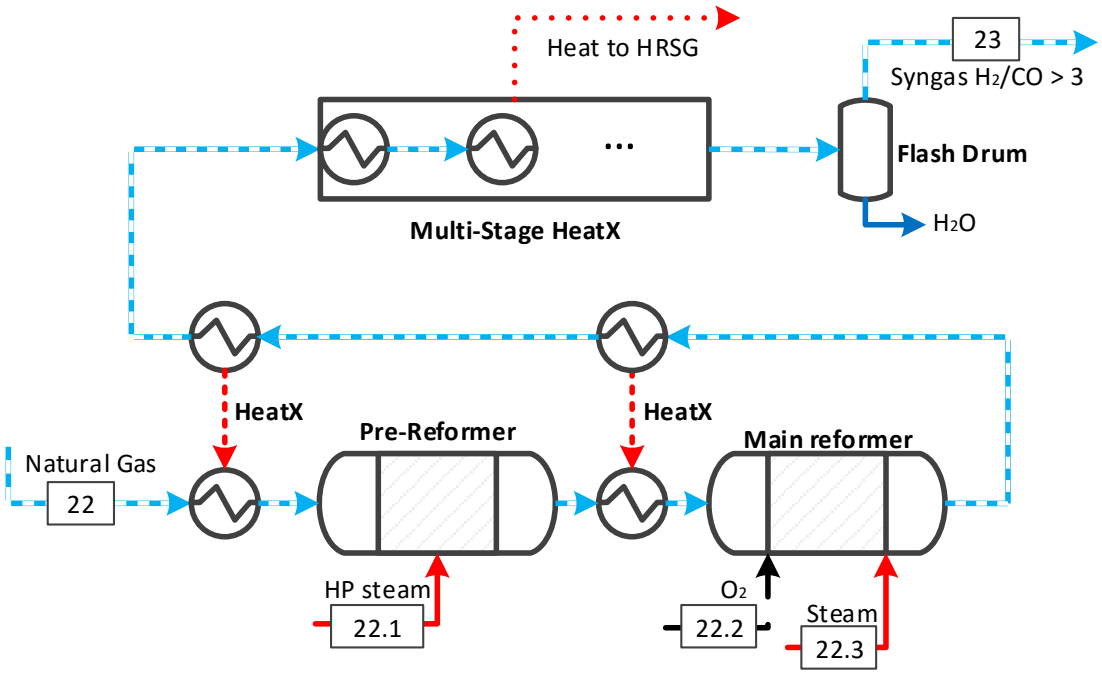

Figure 3.8 Flow diagram for ATR section, as modeled in Aspen Plus.

The pre-reformer and the main reformer were modeled as adiabatic equilibrium reactors in Aspen Plus. The reactors operated at 30 bars of pressure due to the availability of natural gas at this pressure and the need for high pressure syngas downstream. The pressure drop of the pre-reformer was 0.4 bar and the pressure drop of the main reformer was 0.6 bar (Adams II & Barton, 2010). The purpose of the first reformer is to pre-reform the syngas and totally reform the largest hydrocarbons (C_2 – C_4), while the purpose of the second reformer is to oxidize a portion of the methane in the natural gas to provide the heat to drive the endothermic methane steam reforming reaction. The amount of high pressure steam that was added to each reformer is based off the work by Adams and Barton (Thomas A. Adams & Barton, 2011a). The amount of oxygen added to the system was controlled so

that the outlet temperature of the main reformer was 950°C. The pre-reformer inlet was preheated to 500°C and the main reformer inlet was preheated to 840°C. Sample stream conditions for this section can be seen below in Table 3.13.

Table 3.13 Sample stream conditions for Figure 3.8

Stream ID	22	22.1	22.2	22.3	23
T (°C)	30	500	102	500	40
P (bar)	30	50	29.5	50	27.7
Flow rate (kmol/hr)	2500	1313	1336	3589	8218
Vapour fraction	1	1	1	1	1
Mol fraction (%)					
H_2					67.5
CO					20.9
CO_2	1				10
H_2O		100		100	0.3
Ar			0.3		0.05
O_2			99.5		
N_2	0.8		0.2		0.3
NH_3					
COS					
H_2S					
HCl					
CH_4	93.9				1
C_2H_6	3.2				
C_3H_8	0.7				
C_4H_{10}	0.4				

3.3.6.3 Nuclear reactor and Cu-Cl modeling

The complexities of the nuclear reactor and CuCl cycle were not taken into account in this study, but has been extensively modeled in previous works using Aspen Plus (Ferrandon et al., 2008; G.F. Naterer et al., 2011; Wang et al., 2010). Instead, a RYield reactor in Aspen Plus was used to dissociate hydrogen and oxygen from an inlet water stream. It was assumed that the CuCl cycle acts as a stand-alone external utility, and the BGNTL process purchases the hydrogen and oxygen for a fee on a \$/kg H_2 basis, which will be discussed in the economics section. Based on the work by Ferrandon et al., it was assumed that it

took 145MJ_{therm} and 60.7MJ_{elec} to generate 1 kg of hydrogen (Ferrandon et al., 2008). However, assuming the thermal efficiency of the SCRW is 50%, a total of 266MJ_{therm} from a nuclear power plant is required to generate 1 kg of H_2 in this process (Naidin et al., 2009).

The hydrogen from the CuCl cycle is destined for either one of two places. It is either sent to the FT section for hydrocracking, or it is blended with the other syngas mixtures. The oxygen generated by the CuCl cycle is used to displace the oxygen generated by the ASU, making its size and energy consumption smaller. The outlet conditions of the O_2 and H_2 from the CuCl cycle are assumed to be 20°C and 10 bar (Rosen, 2010). The CuCl cycle is shown in Figure 3.9.

3.3.6.4 Syngas mixing section overview

The outline of the syngas mixing section can be seen below in Figure 3.9.

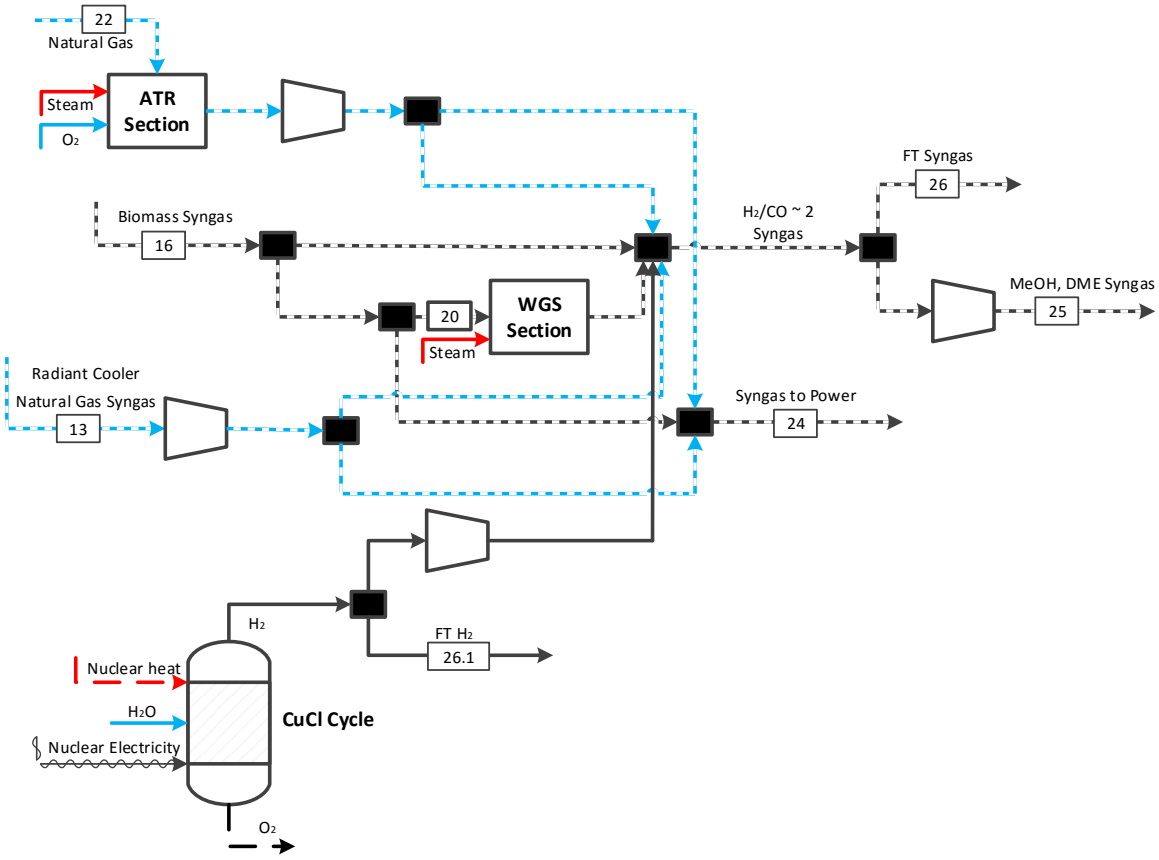

Figure 3.9 Syngas mixing section, simplified from Aspen Plus model.

Two streams are formed, with one destined for power in the gas turbine or SOFC and the other destined for fuels, either FT liquids or methanol and DME synthesis. The fuels syngas needs to be mixed to a H_2/CO ratio of 2, which feeds the FT and methanol reactors. Table 3.14 shows sample stream results for the syngas mixing section – note that this section greatly changes between cases.

Table 3.14 Sample stream conditions for Figure 3.9

Stream ID	24	25	26	26.1
T (°C)	80	112	79	20
P (bar)	27.6	52	39.1	10
Flow rate (kmol/hr)	2139	12040	3010	170
Vapour fraction	1	1	1	1
Mol fraction (%)				
H_2	63.6	57.8	57.8	1
CO	24.5	28.8	28.8	
CO_2	10	11.2	11.2	
H_2O	0.3	0.6	0.6	
Ar	0.05	0.05	0.05	
O_2				
N_2	0.3	0.3	0.3	
NH_3				
COS				
H_2S		34 ppm	34 ppm	
HCl				
CH_4	0.1	1	1	
MDEA	0.3 ppm	0.8 ppm	0.8 ppm	

3.3.7 Power production - Solid-Oxide-Fuel-Cell and gas turbine modeling

3.3.7.1 Solid-Oxide-Fuel-Cell

The SOFCs produce power through the following reaction pathways, shown as equations 3.12, 3.13 and 3.14 (Adams II & Barton, 2010):

$$H_2 + O^{2-} \rightarrow H_2O + 2e^- \quad \text{(anode)} \tag{3.12}$$

$$CO + O^{2-} \rightarrow CO_2 + 2e^- \quad \text{(anode)} \tag{3.13}$$

$$O_2 + 4e^- \rightarrow 2O^{2-} \quad \text{(cathode)} \tag{3.14}$$

The SOFC model was adapted from previous work by Adams and Barton, where further details of the process are explained (Thomas A. Adams & Barton, 2010; Adams II &

Barton, 2010). The main contribution of the SOFC in the plant is that it generates heat and power very efficiently from the incoming syngas feed. An overview of an individual module is shown below in Figure 3.10.

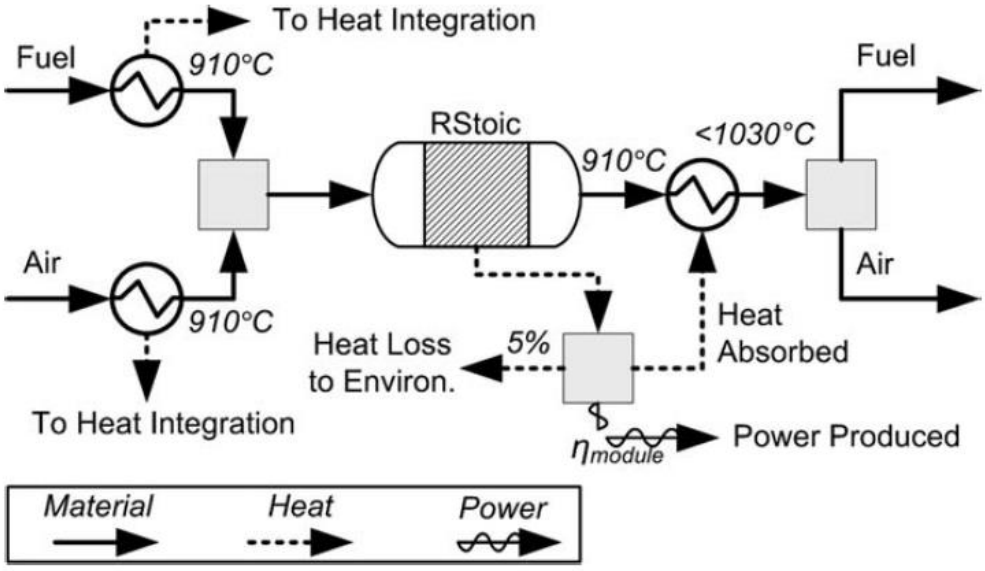

Figure 3.10 Flow diagram for a single SOFC module model (reproduced from (Thomas A. Adams & Barton, 2010))

A SOFC module was modeled as an RStoic reactor with mixing and heater blocks and cooling blocks – there were 7 modules stacked together to create the SOFC stack. Fuel utilization, or the extent of the consumption of H_2 and CO, was set at 86% (Nease & Adams, 2014). The achieved voltage of the process was assumed to be 0.69V, for pressures of 10 bar and above (Thomas A. Adams & Barton, 2010). The process had a DC to AC conversion efficiency assumed to be 96% and 5% of the energy is radiated to the environment as lost heat (Thomas A. Adams & Barton, 2010). After the SOFC stack, the hot spent air is expanded through expansion turbines for power and the spent fuel is further

oxidized to get the last remaining energy value from the fuel gas. Both the spent air and fuel are then sent to the heat recovery and steam generation (HRSG) section. From the HRSG section, the spent fuel, which is now mostly carbon dioxide and water, has the water condensed out through cascading flash drums and the remaining CO_2 is sent to sequestration. Figure 3.11 shows the process flow diagram of the SOFC system modeled in this work.

3.3.7.2 Gas Turbine modeling

The gas turbine in this work was modeled using RGibbs and compressors/turbine blocks in Aspen Plus. The gas turbine was set to operate at 21 bar and 9% excess O_2 (in the form of air) was added to the gas turbine for combustion. A portion of this air stream was split and sent to mix with the combusted fuel to maintain a safe operating outlet combustion temperature (Thomas A. Adams & Barton, 2011a; Clausen, Elmegaard, et al., 2010). In addition, N_2 was mixed from the ASU to dilute the incoming fuel stream and to achieve a lower heating value of 4.81MJ/Nm^3 (Thomas A. Adams & Barton, 2011a). The electrical conversion was also assumed to be 100% efficient for the gas turbine (Clausen, Elmegaard, et al., 2010). The spent fuel is then sent to the HRSG section for heat recovery. Figure 3.11 shows the GT in conjunction with the SOFC, completing the power generation section with sample stream results for the section in Table 3.15.

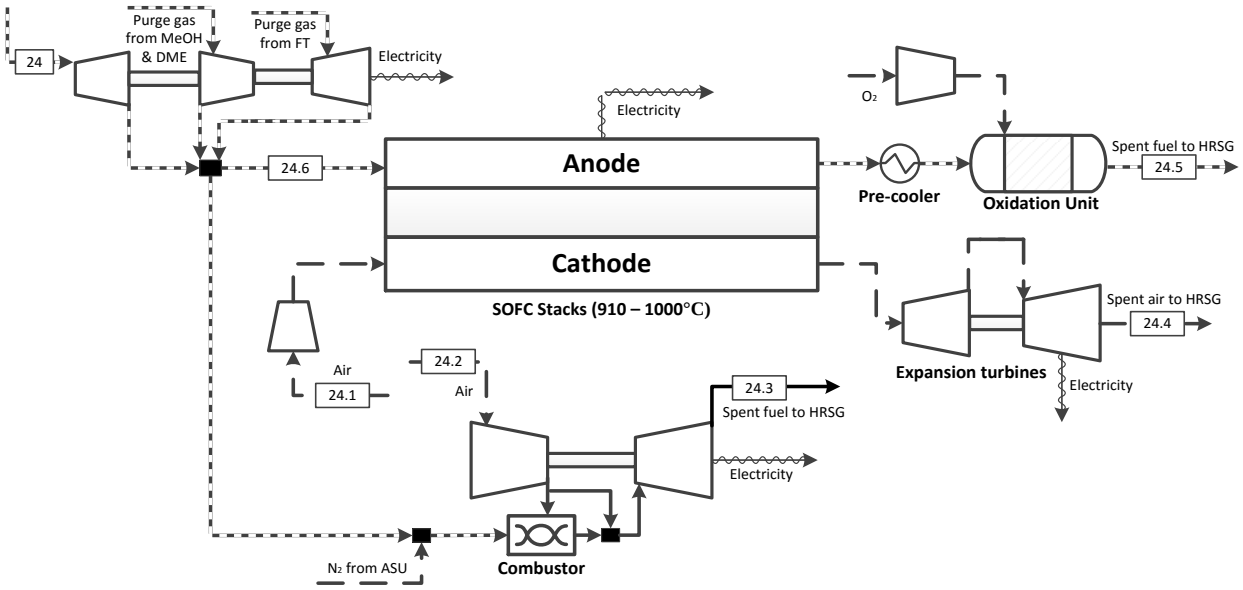

Figure 3.11 Power generation section, simplified from Aspen Plus model.

Table 3.15 Sample stream conditions for Figure 3.11.

Stream ID	24.1	24.2	24.3	24.4	24.5	24.6
T (°C)	15	15	524	519	987	37
P (bar)	1.01	1.01	1.05	1.1	17.6	21
Flow rate (kmol/hr)	5329	8508	13629	4400	3360	3133
Vapour fraction	1	1	1	1	1	1
Mol fraction (%)						
H_2			1.8		0.07	47.8
CO			4.2		0.03	21.1
CO_2	0.03	0.03	7.6	0.03	47.6	26.5
H_2O	1.1	1.1	11.5	1.3	51.1	0.2
Ar	0.9	0.9	0.7	1.1	0.2	0.2
O_2	20.8	20.8	6.5	4	0.2	
N_2	77.2	77.2	67	93.5	0.7	0.7
NH_3						
COS						
H_2S			11 ppm		64 ppm	69 ppm
HCl						
CH_4					0.03	3
SO_2			4.7 ppm			
MDEA					0.09 ppm	0.09 ppm
CH_3OH						0.6
C_2H_6O						3.7 ppm
$C_2H_4O_2$						0.04

3.3.8 Carbon dioxide removal

Similar to the acid gas removal (AGR) section, this section focuses on utilizing the same amine (MDEA) to capture CO_2 prior to it being sent to the FT section. This step is needed because inerts in the syngas feed such as CO_2, argon and N_2 need to be removed prior to FT synthesis, which can only handle at most 5% inerts in the feed. CO_2 is captured in this step because the other inert chemicals are much harder to remove. CO_2 is captured using MDEA in a very similar setup as the AGR section. In addition, the remaining H_2S left in the syngas will also be absorbed along with the CO_2. Equation sets 3.5 and 3.6 detail the reactions that occur in this section.

Because of the difficulties in modeling this system in Aspen Plus (as mentioned in the AGR section), this process was also modeled in ProMax, utilizing the TSWEET kinetics property package. The CO_2 removal process has a very similar structure to that of the AGR removal process, with a contacting absorption column and regenerative stripper column. The absorption column operates at high pressure (15 ideal stages (45 actual stages) – 38 bar top, 39 bar bottom), while the stripper column operates at a relatively low pressure (10 ideal stages (30 actual stages) – 1.8 bar top, 2 bar bottom). In addition, low pressure steam is used to heat the bottom of the column and cooling water is used in all of the cooling blocks. Figure 3.12 below shows a schematic of the CO_2 removal process.

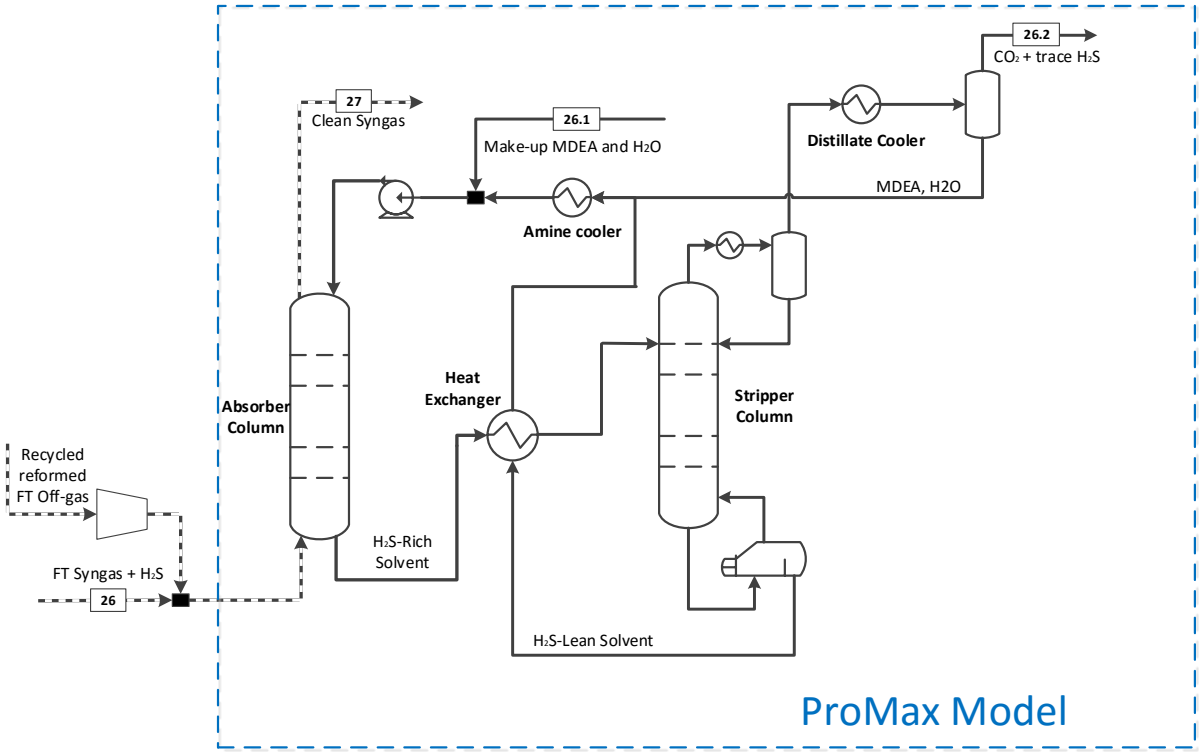

Figure 3.12 CO_2 removal process, as modeled in ProMax [blue]. Aspen Plus model not shown.

The CO_2 reduced order model (CROM) (equation 3.15) that was used in this section takes a linear form, due to little gains being achieved with higher order models. The ProMax model was run with different CO_2 concentrations in the feed gas 75 times, with 55 of these data points used for training and the remaining 20 for testing the model. The CROMs' output variables (Z_{CO_2}) were the same as the ones considered in the AGR section. These models were implemented in Aspen Plus as calculator blocks, similar to the AGR section. The CROM coefficients can be seen below in Table 3.16.

$$z_{CO_2} = a_1 + a_2 \frac{X_{CO_2}}{\bar{X}_{CO_2}} \tag{3.15}$$

Table 3.16 Reduced order model coefficients for the CROM.

Input variable							
X_{CO_2} - Inlet CO_2 (kmol/hr)		$\bar{X}_{CO_2} = 827.47$		$X_{CO_2,min} = 620.6025$ $X_{CO_2,max} = 1033.75$			
Output variable	**Description**	**Units**	a_1	a_2	R^2_{train}	R^2_{test}	**Max Err (%)**
$z_{CO_2,1}$	MDEA make-up	(kmol/hr)	5.595×10^{-4}	6.709×10^{-3}	0.843	0.812	5
$z_{CO_2,2}$	H_2O make-up	(kmol/hr)	-1.235	40.92	0.963	0.900	5
$z_{CO_2,3}$	Pump power	kW	3.099	425	1	0.997	0.7
$z_{CO_2,4}$	Reboiler Duty	kW	-117.9	-15950	1	0.998	0.6
$z_{CO_2,5}$	Condenser Duty	kW	0.581	128.9	1	0.999	0.4
$z_{CO_2,6}$	Distillate Cooler	kW	14.64	3220	1	0.999	0.4
$z_{CO_2,7}$	Amine Cooler	kW	-74.48	7040	1	0.991	1.1

Sample stream data for the CO_2 removal section can be seen below in Table 3.17.

Table 3.17 Sample stream conditions for Figure 3.12.

Stream ID	26.1	26.2	27
T (°C)	46	47.7	50.2
P (bar)	38	1.6	38
Flow rate (kmol/hr)	18.3	301	2750
Vapour fraction	0	0.97	1
Mol fraction (%)			
H_2		0.6	64
CO		0.3	32
CO_2		90.3	2.5
H_2O	99.98	9	0.2
Ar		6.6 ppm	0.06
O_2			
N_2		19 ppm	0.3
NH_3			
COS			
H_2S		0.03	0.6 ppm
HCl			
CH_4		0.04	1.4
MDEA	0.02	5.1 ppm	0.1 ppm

3.3.9 Fischer Tropsch

The FT section is shown in Figure 3.13. Upstream syngas with a H_2/CO ratio of 2 is sent to the FT reactor where it is pre-heated to 240°C and reacted at 36 bar to generate hydrocarbons numbered n = 1 to 60, depending on equation 3.16 (Thomas A. Adams & Barton, 2011a):

$$nCO + (2n + 1)H_2 \rightarrow C_nH_{2n+2} + nH_2O \quad (3.16)$$

A cobalt catalyst is used in this reaction section, which promotes higher molecular weights; however, for this catalyst to be effective, it requires inert concentrations of less than 5 mol%, which is achieved by removing CO_2 in the prior section (Hamelinck, Faaij, Denuil, & Boerrigter, 2004). Based on the work by Adams and Barton, the product mixture contains (in mol%): CH_4 at 5%, C_2H_4 at 0.05%, CO_2, C_2H_6, C_3H_8, C_4H_{10} at 1%, and C_3H_6 and C_4H_8 at 2% (Thomas A. Adams & Barton, 2011a). The remaining hydrocarbons considered in this work (n = 5 to 60) are assumed to follow the distribution described in the following Anderson-Schulz-Flory equation (3.17).

$$x_n = (1 - \alpha)\alpha^{n-1} \quad (3.17)$$

x_n represents the mol fraction of the outlet of the FT reactor, as a mol fraction of straight chained hydrocarbons of carbon length n with the value of α set to 0.92 and CO conversion of 65% (Thomas A. Adams & Barton, 2011a).

Once the FT products exit the reactor, they are subsequently cooled by two 3-phase flash tanks, which separate water destined for water treatment into two groups - the lights (naphtha (C_5 - C_{11}) - gasoline precursor) and heavies (diesel or distillate: C_{12} – C_{20}). These are sent to the refinery column, while off-gasses are sent to an ATR (which operates at 950°C and at an exit CO/H_2 ratio of 2) in the FT section for reforming. The off-gasses are then either recycled back to the CO_2 removal section or sent to power generation. The light and heavy components then enter the refinery column which is modeled in Aspen Plus using the PetroFrac block. The column has 20 stages with a top pressure of 2.7 bar and a bottom pressure of 3.4 bar. The reboiler operates at 430°C and the condenser operates at 38°C. In addition, the following ASTM design specification for the tower was used: 95% vol: gasoline 170°C and diesel 340°C.

After the refinery column, the heavier hydrocarbons are sent to the hydrocracker where the carbon chains are broken into smaller chains for fuels production. Hydrogen is added to the hydrocracker either by pressure-swing absorption, where a portion of the FT feed has its hydrogen stripped from it for use in the hydrocracker as indicated in Figure 3.13, or by H_2 generated in the CuCl cycle. It was assumed that hydrocracking of the large molecules resulted in an even split, represented by equation 3.18.

$$C_{2n}H_{4n+2} + H_2 \rightarrow 2C_nH_{2n+2} \quad (3.18)$$

It was also assumed that carbon numbers above 23 are completely cracked to smaller chains. The hydrocracker uses a stoichiometric amount of H_2 as per equation 3.18, so that the cracking of the large hydrocarbons go to completion.

The effluent of the hydrocracker is separated using a simple separator block in Aspen Plus, and was assumed to completely recover C_5 - C_{11} destined for naphtha and C_{12} and larger to diesel. For the purposes of analysis in this work, it is assumed that the naphtha and distillate products represent gasoline and diesel for selling prices for future parts of this study.

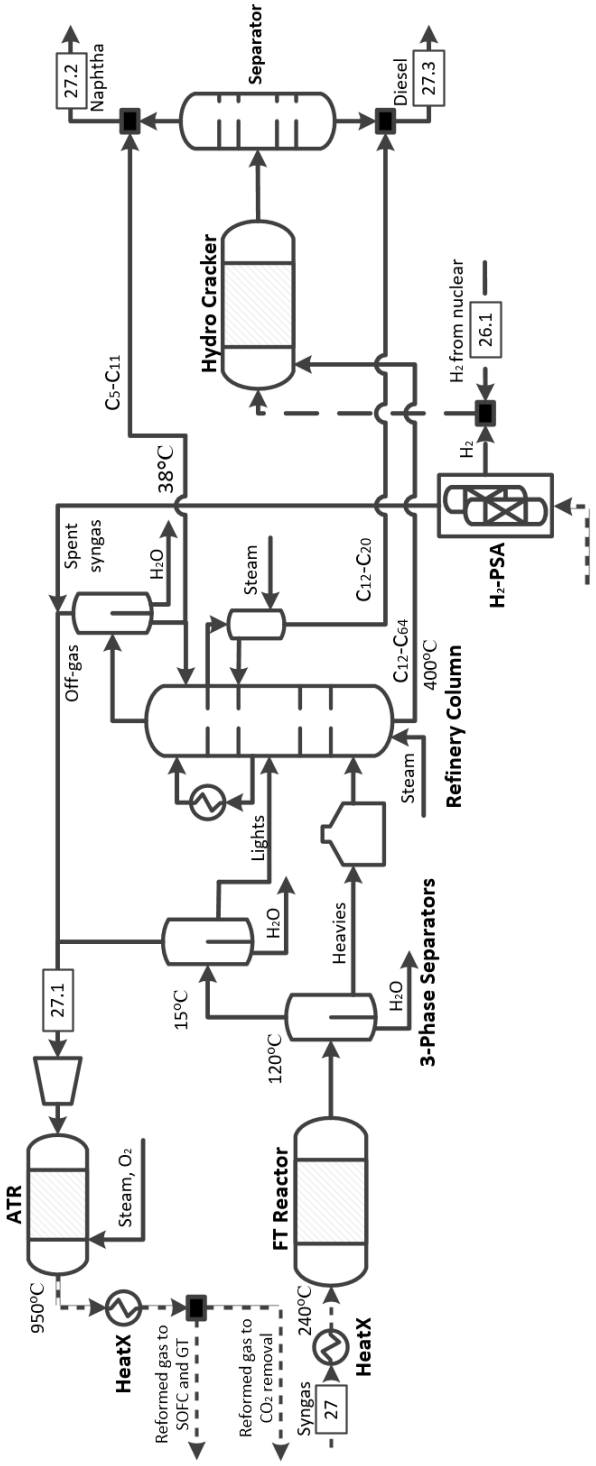

Figure 3.13 FT synthesis section. Flow diagram as modeled in Aspen Plus.

Sample stream conditions for the FT section are shown in Table 3.18.

Table 3.18 Sample stream conditions for Figure 3.13

Stream ID	27.1	27.2	27.3
T (°C)	43	88.9	200
P (bar)	39.8	2.8	3
Flow rate (kmol/hr)	1199	18.28	23.6
Vapour fraction	1	0	0
Mol fraction (%)			
H_2	60.6	0.04	
CO	25.5	0.05	
CO_2	6.1	0.4	
H_2O	0.06		
Ar	0.1	5.4 ppm	
O_2			
N_2	0.7	12 ppm	
NH_3			
COS			
H_2S	1.3 ppm	4.3 ppm	
HCl			
CH_4	5.5	0.05	
MDEA		390 ppm	0.03
$C_2 - C_5$	1	5	0.4 ppm
$C_6 - C_{11}$	0.1	94.4	9.4
$C_{12} - C_{20}$	0.3 ppm	40 ppm	90.5
$C_{20} +$			

3.3.10 Methanol and DME synthesis

The methanol and DME section is shown in Figure 3.14. This section produces methanol and DME from $H_2/CO = 2$ syngas with two separate reaction pathways. The first step in this process is methanol synthesis which reacts with syngas in the reaction pathway described by equation set 3.19.

$$CO_2 + 3H_2 \leftrightarrow CH_3OH + H_2O \ (1)$$
$$CO_2 + H_2 \leftrightarrow CO + H_2O \ (2) \qquad (3.19)$$

The methanol reaction and the water gas shift reaction (3.19) occur over a $Cu/ZnO/Al_2O_3$ catalyst with the following Langmuri Hinshelwood Hougen Watson (LHHW) kinetics (equation set 3.20) (Bussche & Froment, 1996; Salkuyeh & Adams, 2014).

$$r_{3.19\,(1)} = \frac{k_{11} p_{CO_2} p_{H_2} \left[1 - \frac{1}{K_{3.19\,(1)}} \left(\frac{p_{H_2O} p_{CH_3OH}}{p_{H_2}^3 p_{CO_2}}\right)\right]}{\left(1 + K_1 \frac{p_{H_2O}}{p_{H_2}} + K_2 \sqrt{p_{H_2}} + K_3 p_{H_2O}\right)^3} \left[\frac{kmol}{kg_{cat}\, s}\right]$$

$$r_{3.19\,(2)} = \frac{k_{12} p_{CO_2} \left[1 - \frac{1}{K_{3.19\,(2)}} \left(\frac{p_{H_2O} p_{CO}}{p_{CO_2} p_{H_2}}\right)\right]}{\left(1 + K_1 \frac{p_{H_2O}}{p_{H_2}} + K_2 \sqrt{p_{H_2}} + K_3 p_{H_2O}\right)} \left[\frac{kmol}{kg_{cat}\, s}\right]$$

$$K_1 = 3453.38$$

$$K_2 = 0.499 \exp\left(\frac{17197 \frac{kJ}{kmol}}{RT(°K)}\right)$$

$$K_3 = 6.62 \times 10^{-11} \exp\left(\frac{124119 \frac{kJ}{kmol}}{RT(°K)}\right) \qquad (3.20)$$

$$k_{11} = 1.07 \exp\left(\frac{36696 \frac{kJ}{kmol}}{RT(°K)}\right)$$

$$k_{12} = 1.22 \times 10^{10} \exp\left(\frac{-94765 \frac{kJ}{kmol}}{RT(°K)}\right)$$

$$\ln\left(K_{3.19\,(1)}\right) = \frac{3066}{T(°K)} - 10.592$$

$$\ln\left(K_{3.19\,(2)}\right) = \frac{2073}{T(°K)} - 2.029$$

The methanol reactor operates at 240°C and has a pre-heat step after the methanol exits the reactor. The reactor was modeled as an RPlug model in Aspen Plus, utilizing the kinetics in equation 3.20. In addition to reactions in reaction set 3.19 occurring, there are also two side reactions that occur, which are represented by equations 3.20 and 3.21. The formation of ethanol (3.20) occurs at 3% and methyl formate (3.21) occurs at 0.3mol% and 0.08mol% of methanol, respectively (Thomas A. Adams & Barton, 2011a).

$$2CH_3OH \rightarrow C_2H_5OH + H_2O \quad (3.20)$$

$$CH_3OH + CO \rightarrow HCOOCH_3 \quad (3.21)$$

The unreacted syngas is then cooled down to 35°C and is flashed in a flash drum (mostly unreacted gases such as N_2, CO and H_2). The off gas is either recycled back to the start of the reactor or sent to the power generating section. After the liquid methanol exits the first drum, it is flashed in a methanol recovery unit, which acts as a second light gas removing column. This column was modeled using a RadFrac block in Aspen Plus with 20 equilibrium stages using the NRTL-RK property method. The off gases of the methanol recovery column are then sent to the power generating section.

The methanol purification column then purifies the incoming methanol to 99.5% mol purity, with the bottom of the column being mostly water. This column was modeled as a RadFrac column using 40 equilibrium stages and the NRTL-RK property package. After

the methanol purification column, a portion of the methanol is split for sale and the remainder is sent to DME synthesis.

The portion of the methanol that is sent to DME synthesis is first pressurized to 56 bar and sent to a single pass DME reactor operating at 280°C and 56 bar (Clausen, Elmegaard, et al., 2010). Reaction 3.22 takes place in the DME reactor over a $\gamma - Al_2O_3$ catalyst, represented in reaction set 3.23 (Bercic & Levec, 1993; Salkuyeh & Adams, 2014).

$$2CH_3OH \leftrightarrow CH_3OCH_3 + H_2O \tag{3.22}$$

$$r_{CH_3OCH_3} = \frac{k_{13}K_4^2\left[C_{CH_3OH}^2 - \left(\frac{1}{K_{eq,3}}\right)C_{H_2O}C_{CH_3OCH_3}\right]}{\left(1 + 2\sqrt{K_4 C_{CH_3OH}} + K_5 C_{H_2O}\right)^4}\left[\frac{kmol}{kg_{cat}\,s}\right]$$

$$K_4 = 5.39 \times 10^{-4}\exp\left(\frac{8487}{T(°K)}\right)$$

$$K_5 = 8.47 \times 10^{-2}\exp\left(\frac{5070}{T(°K)}\right) \tag{3.23}$$

$$k_{13} = 5.35 \times 10^{13}\exp\left(\frac{-17280}{T(°K)}\right)$$

$$\ln\left(K_{CH_3OCH_3}\right) = \frac{2835.2}{T(°K)} + 1.675\ln(T(°K)) - 2.39 \times 10^{-4}T(°K) - 0.21 \times 10^{-6}T(°K)^2 - 13.36$$

DME is then recovered in the DME purification column, which is modeled as a RadFrac column with 30 equilibrium stages, utilizing the NRTL-RK package. The DME is purified to 99.5mol% at the top of the column and the bottom of the column is recycled back to the methanol purification column.

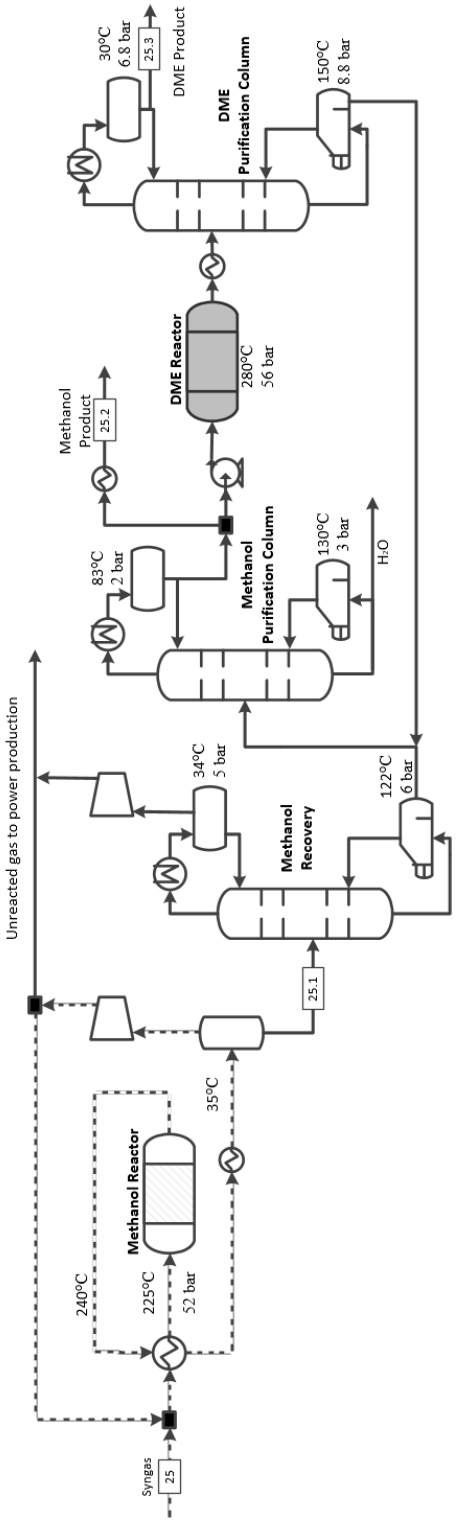

Figure 3.14 Methanol and DME synthesis section, as modeled in Aspen Plus.

Sample stream values for the methanol and DME section are shown in Table 3.19.

Table 3.19 Sample stream conditions for Figure 3.14.

Stream ID	25.1	25.2	25.3
T (°C)	35	40	30
P (bar)	50.4	1	6.8
Flow rate (kmol/hr)	3361	160	1305
Vapour fraction	0	0	0
Mol fraction (%)			
H_2	0.2		
CO	0.2		
CO_2	8.5		
H_2O	6.7	65 ppm	
Ar	45 ppm		
O_2			
N_2	0.01		
NH_3			
COS			
H_2S	70 ppm		
HCl			
CH_4	0.2		
MDEA	3 ppm		
CH_3OH	84.1	99.5	0.49
CH_3OCH_3			99.5
C_2H_5OH	0.1	0.4	0.2 ppm
$HCOOCH_3$	0.07	0.2 ppm	0.5 ppm

3.3.11 Heat recovery and steam generation

The purpose of the heat recovery and steam generation (HRSG) section is to take waste heat from the plant and generate various pressures of steam for additional power production and steam supply demands across the plant. There are three levels of steam used in this work: High Pressure (HP) (500°C, 50bar), Medium Pressure (MP) (300°C, 20bar), and Low Pressure (LP) (180°C, 5bar) steam. Various parts of the process utilize these different levels of steam, and steam demand outlets are made for each steam pressure based on plant demands. Temperature approaches of $\Delta T_{min} = 10℃$ are used when constructing the various heat exchangers across the plant (Seider, Seader, Lewin, & Widagdo, 2008). The excess steam that is not consumed by the plant is sent through 3 steam turbines, which

generate additional power for the plant. In addition, boiler feed water heating and deaerating are taken into consideration when modeling the HRSG plant. The heat recovery section is shown in Figure 3.15.

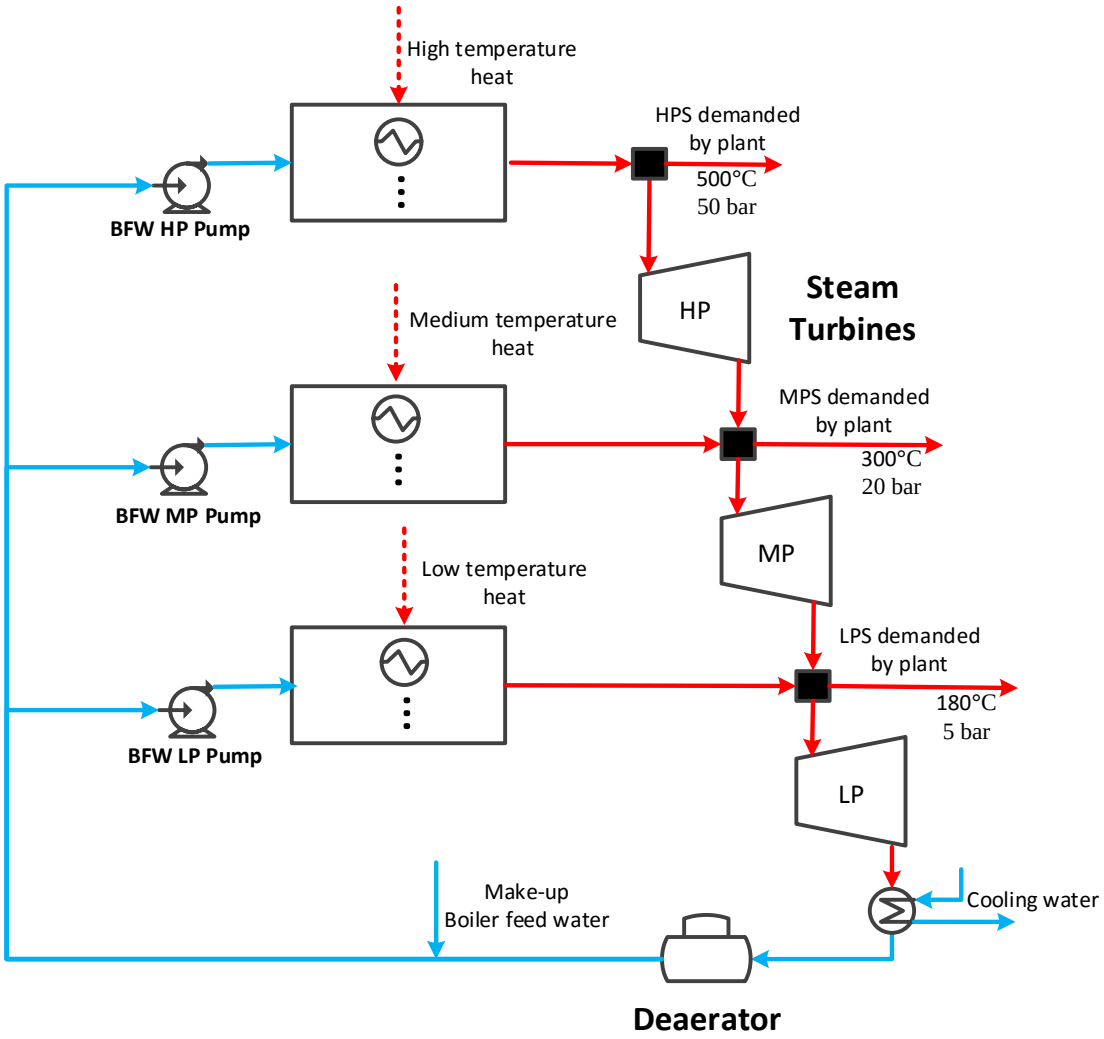

Figure 3.15 HRSG section, simplified from Aspen Plus model.

3.3.12 CO_2 Compression and Sequestration

This section focuses on compressing CO_2 from various parts of the plant and sequestering it at 153 bars of pressure. This stage is particularly energy intensive as there are multiple cooling steps involved and large power demands from the multiple compressors that are involved. For this reason, this section is omitted for non-CCS cases.

This section is modeled using the PSRK equation of state as it more accurately models the equilibrium of water and CO_2 in the liquid and gas phases at the relevant pressures of interest (Thomas A. Adams & Barton, 2010). The acid gas CO_2 has been cleaned of all H_2S in a Lo-Cat process, which strips the rest of the sulfur out of the stream, leaving mainly CO_2 (Okoli & Adams, 2014). The SOFC spent fuel is at sufficient pressure already and it is sent directly to the second stage of compression. Figure 3.16 shows the CO_2 compression processes with sample stream conditions in Table 3.20.

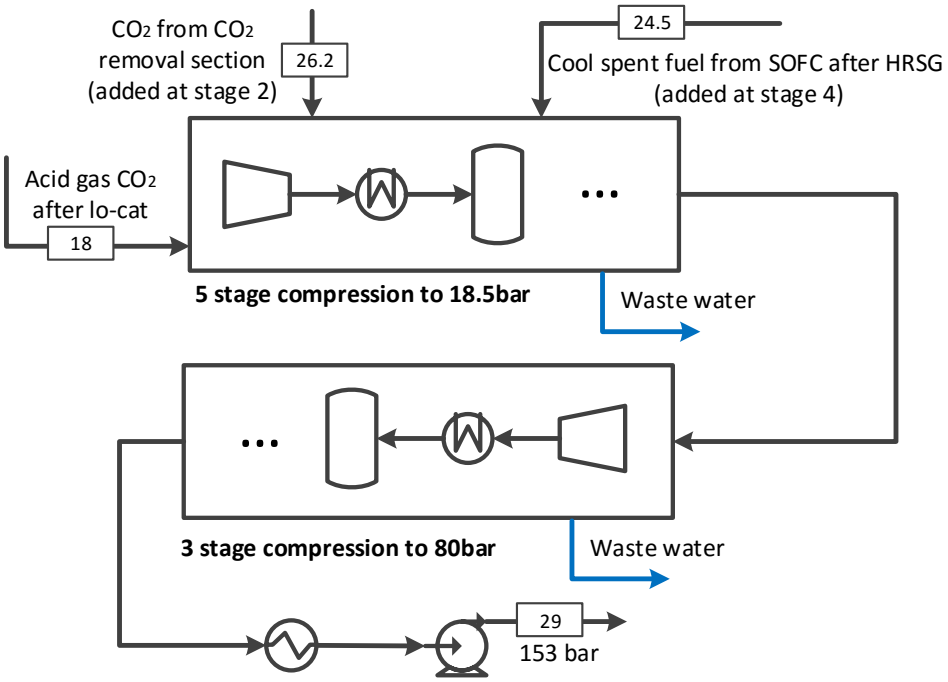

Figure 3.16 CO_2 compression section, simplified from Aspen Plus model.

Table 3.20 Sample stream conditions for Figure 3.16

Stream ID	28
T (°C)	56
P (bar)	153
Flow rate (kmol/hr)	2337
Vapour fraction	0
Mol fraction (%)	
H_2	0.07
CO	0.1
CO_2	97.9
H_2O	0.08
Ar	0.03
O_2	0.4
N_2	1
NH_3	
COS	
H_2S	100 ppm
HCl	
CH_4	0.04
MDEA	0.7 ppm
CH_3OH	7.7 ppm
CH_3OCH_3	
C_2H_5OH	4.4 ppm
$HCOOCH_3$	0.02

3.3.13 Cooling tower section

The cooling water section was modeled in this work as a two-stage equilibrium RadFrac column in Aspen Plus (Queiroz, Rodrigues, Matos, & Martins, 2012). External air was blown through the tower to remove the heat of the incoming return cooling water (~50°C) from the plant. Figure 3.17 shows the cooling tower section.

Some of the water escapes as water vapour through the top of the tower; as such, makeup cooling water is added to the plant return water, which is around 30°C. The incoming air is assumed to be 20°C. In addition to the cooling tower, there are other utilities that require extra cooling, so chilled water is used for these streams. The cooling water streams were modeled as utility streams with temperature inlet and outlet of 7°C – 32°C (Seider et al., 2008).

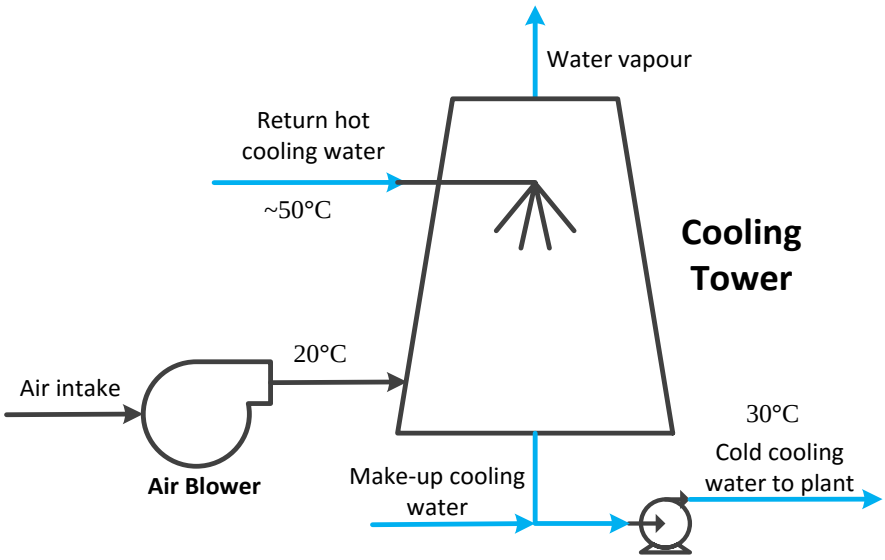

Figure 3.17 Cooling tower section, simplified from Aspen Plus model.

3.3.14 Plant equipment

Equipment such as gas turbines, steam turbines, compressors and expanders modeled in Aspen Plus had specifications which are outlined in Table 3.21.

Table 3.21 Plant equipment specifications.

Equipment	$\eta_{Isentropic}$	$\eta_{polytropic}$	$\eta_{Mechanical}$	Ref
Plant Compressors		0.85	0.94	(Clausen, Elmegaard, et al., 2010)
Gas turbine	0.898		0.988	(Salkuyeh & Adams, 2014)
Expanders	0.898		0.988	(Salkuyeh & Adams, 2014)
Steam turbines	0.875		0.983	(Salkuyeh & Adams, 2014)
Pumps			0.8	

Chapter 4

Economics and Optimization

The purpose of this chapter is to first describe the economic analysis procedure used in the work and to present the base case simulation results of each process case studied. These results will then be compared with the optimized results for each case and discussed.

4.1 Economics

4.1.1 Economic Parameters

The main economic parameters used in this work are shown in Table 4.1.

Table 4.1 Economic parameters assumed for base case analysis.

Raw material		Value	Units ($CDN)	Reference
	Woody biomass	100	$/tonne	(Hewson et al., 2011)
	Natural gas	0.0957	$/std m^3	("Natural Gas Rate Updates," n.d.)
	Nuclear H_2 gas	2.1	$/kg	(Wang et al., 2010)
Product prices				
	Wholesale gasoline	0.618	$/L	(N. R. C. Government of Canada, n.d.-a)
	Wholesale diesel	0.617	$/L	(N. R. C. Government of Canada, n.d.-b)
	Methanol	346	$/tonne	("Pricing | Methanex Corporation," 2016)
	DME	1300	$/tonne	("Dimethyl Ether Prices - Alibaba.com," n.d.)
	Electricity	0.083	$/kWh	(*IESO Backgrounder on BPRIA*, 2015)
Plant utilities				
	Chilled water	5.20	$/GJ	(Seider et al., 2008)
	Cooling water	0.03	$/m^3	(Seider et al., 2008)
	Process water	0.26	$/m^3	(Seider et al., 2008)
	Boiler feed water	0.65	$/m^3	(Seider et al., 2008)
	Water treatment	1.26	$/m^3	(Seider et al., 2008)
	Lo-Cat chemicals	758.06	$/tonne sulfur	(Okoli & Adams, 2014)
	MDEA solvent	2.73	$/kg	("Export Data and Price of mdea Zauba," n.d.)
	Cost to transport and sequester CO_2	10	$/tonne	(Thomas A. Adams & Barton, 2011a)
Economic assumptions				
	Corporate tax rate	38	%	(C. R. A. Government of Canada, 2005)
	Capital depreciation rate (Declining balance)	30	%	(C. R. A. Government of Canada, 2004)
	Capacity factor	85	%	(Adams II & Barton, 2010)
	Operating hours	8000	Hours/year	
	Debt percentage	50	%	(Adams II & Barton, 2010)
	Debt interest rate	9.5	%	(Adams II & Barton, 2010)
	Debt lifetime	30	Years	(Adams II & Barton, 2010)
	Plant lifetime	30	Years	(Adams II & Barton, 2010)
	Working capital	15	% of FCI	(Peters & Timmerhaus, 1991)
	Indirect costs	20	% of direct costs	(Peters & Timmerhaus, 1991)
	Equity return rate	20	%	(Adams II & Barton, 2010)
	Inflation rate	1.13	%	("Historic inflation Canada – historic CPI inflation Canada," n.d.)
	CO_2 tax rate	25	$/tonne	

In addition to the costs above, labour, maintenance, operating overhead, property taxes and insurance, and general expenses were calculated using the methods outlined by Seider (Seider et al., 2008).

4.1.2 Capital costs

All capital costs for this work take into account the CEPCI for the year in which the equipment was specified ($CEPCI_{base\ year}$), the base cost B_0, the base scaling factor C_0, the exponential scaling factor n, and the installation factor f, as shown in equation 4.1. In addition, it was assumed that all prices in the literature, unless specifically stated, are in $USD. Therefore, these were converted to $CAD using the exchange rate 1.30000 CAD = USD ("XE currency converter," 2016).

$$Installed_{cost} = B_0 \times \left(\frac{C}{C_0}\right)^n \times f \times \left(\frac{CEPCI_{2015}}{CEPCI_{base\ year}}\right) \quad (4.1)$$

The capital costs for this work are summarized in Table 4.2.

Table 4.2 Capital cost data in $CDN.

Equipment	Base Cost ($MM)	Base scaling factor	Units of Base	Scale factor	Installation factor	Base year	Reference
Air separation unit[b]	183	52	(kg O_2/s)	0.5	1	2007	(Clausen, Elmegaard, et al., 2010)
Gasifier island	156.07	730	LHV sent to gasifier	0.7	1	2006	(Villanueva Perales, Reyes Valle, Ollero, & Gómez-Barea, 2011)
COS removal	3.84	1	Kmol/hr COS fed	0.65	1	2012	(Khojasteh Salkuyeh, 2015)
AGR Removal	37.44	2.48	Kmol/s of feed	0.63	1.55	2007	(Clausen, Elmegaard, et al., 2010)
Internal Reformer (IR)	Assumed to be 10% of the gasifier capital cost						
Water Gas shift reactor	11.73	8819	Kmol/hr of CO + H_2	0.65	1.81	2002	(Hamelinck et al., 2004)
Autothermal reformer	38.87	365	Million scf/day of feed gas	0.67	1.32	2007	(Kreutz, Larson, Liu, & Williams, 2008)
CO_2 removal section	56.39	327	CO_2 removed in tons / hour	0.67	1	2002	(Larson & Tingjin, 2003)
CO_2 compression	12.38	13	MW of compressor power	0.62	1.32	2007	(Clausen, Elmegaard, et al., 2010)
FT reactor	13.65	2.52	Million scf/hr of feed gas	0.72	1.52	2003	(Larson, Jin, & Celik, 2005)
Pressures swing absorption column	7.10	0.294	Purge gas flow kmol/s	0.74	1.52	2003	(Larson et al., 2005)
Pressure swing absorption purge compressor	4.83	10	MWe compressor power	0.67	1.52	2003	(Larson et al., 2005)
Pressure swing absorption CO_2 rich compressor	4.83	10	MWe compressor power	0.67	1.52	2003	(Larson et al., 2005)
FT hydrocarbon recovery unit	0.73	14.44	Thousands lbs/hr feed	0.7	1.52	2003	(Larson et al., 2005)
FT Hydro treater	9.37	8.984	Feed in thousands of pounds / hr	0.7	1.52	2003	(Larson et al., 2005)
FT Autothermal reformer	38.87	365	Million scf/day of feed gas	0.67	1.32	2007	(Kreutz et al., 2008)
Methanol reactor	106.3	10.81	Syngas fed in kmol/s	0.65	1	2002	(Larson & Tingjin, 2003)
Methanol separation	2.24	4.66	Methanol production in kg/s	0.291	1	2002	(Larson & Tingjin, 2003)
DME reactor	20.5	2.91	Feed rate of MeOH to DME reactor	0.65	1.52	2003	(Larson et al., 2005)
DME separation	27.7	6.75	DME produced in kg/s	0.65	1.52	2003	(Larson et al., 2005)

SOFC stacks[a]	$500/kW installed every 10 years						(Nease & Adams, 2014)
Plant Compressors	8.19	10	MW of compressor power	0.67	1.32	2007	(Clausen, Elmegaard, et al., 2010)
SOFC expansions turbines	5.72	10.3	MW of power generated	0.7	2	2002	(Hamelinck et al., 2004)
HRSG – Steam turbines and condenser	86.71	275	MW of power generated	0.67	1.16	2007	(Clausen, Elmegaard, et al., 2010)
HRSG – Heat exchangers	53.56	355	Total heat exchanger duty MWth	0.67	1.16	2003	(Larson et al., 2005)
Cooling plant	2.21	3.3	Total power to cooling fan	0.7	1.32	2007	(Clausen, Elmegaard, et al., 2010)
Gas turbine	95.16	266	Total GT power MWe	0.75	1.27	2007	(Clausen, Elmegaard, et al., 2010)

Note[a]: The SOFC cost is paid three times throughout the plant lifetime as their expected lifetime of operation is only 10 years (Thomas A. Adams & Barton, 2011b)
Note[b]: The ASU was assumed to have a power consumption of 1 MWe/(kg O_2/s) (Clausen, Elmegaard, et al., 2010)

4.1.3 Environmental and CO_2 tax considerations

This study assumes a base CO_{2e} (CO_2 equivalent) tax of $25/tonne, applied to the net emissions of the entire supply chain. This tax rate is similar to that observed in Alberta, Canada, which is increasing from $20/tonne to $30/tonne within the next year ("Carbon levy and rebates," 2016). The reasoning behind the inclusion of a carbon tax is that even if emission taxes are only applied to the source of direct emissions, the costs of any taxes applied to upstream process steps would invariably be passed down to the consumer anyway, i.e. the polygeneration facility. For example, if there is negative cradle-to-plant-exit CO_{2e} emissions (equation 4.4) then the net CO_{2e} tax could be negative, and the company would actually receive money, such as in a cap-and-trade system in which the company could sell their carbon credits in the open market for $25/tonne. The considered upstream emissions sources are described in Table 4.3.

Table 4.3 Upstream CO_{2e} plant emissions.

Upstream emission source	Value	Units	Reference
Life cycle emissions of woody biomass harvesting and transportation to plant-gate-entrance (LCWe)	0.133	Tonnes of CO_{2e} / tonne of biomass	(Zhang et al., 2010)
Well-to-plant-gate-entrance emissions for Natural gas (LCNGe)	7.2	g CO_{2e}/MJth	(ICF Consulting Canada, 2012)
Earth-to-plant-gate-entrance emissions of nuclear power for Ontario (LCNe)	3.2	g CO_{2e}/kWhr	(Lenzen, 2008)

Equation 4.2 represents the direct CO_{2e} emissions of the plant, which include emissions from the gas turbine, the SOFC, the CO_2 removal section, and the sour gas removal section. If CCS is enabled, then the CO_{2e} emissions from the SOFC, the CO_2 removal section, and the sour gas removal section are avoided and are not directly emitted. The amount of CO_2 sent to the gasifier is subtracted from this amount. If no CO_2 at high purity is available for gasifier injection, it is assumed to be purchasable at the rate of $25/tonne.

Direct CO_{2e} emissions = CO_{2e} emitted from gas turbine + CO_{2e} emitted from SOFC + CO_{2e} emitted from CO_2 removal section + CO_{2e} emitted from acid gas removal section - CO_2 recycled to the gasifier for feed pressurization (4.2)

Equation 4.3 represents the cradle-to-plant-gate CO_{2e} emissions taking into account a credit for using biomass in the form of equivalent biomass CO_2. Biomass as CO_2 is calculated by calculating an atom balance; that is, the total molecular carbon in the incoming biomass stream is converted to an equivalent molecular weight of CO_2 (Mass of biomass carbon * (44.01 g/mol CO_2)/(12.01 g/mol C) = Mass of biomass carbon*3.664). The biomass as CO_2 value assumes that all of the carbon in the biomass feed originated in the air. In addition,

equation 4.3 uses the life cycle CO_{2e} emissions of woody biomass to plant-gate-entrance (LCWe), the well-to-plant-gate-entrance CO_{2e} emissions for natural gas (LCNGe), and the earth-to-plant-gate-entrance CO_{2e} emissions of nuclear power for Ontario (LCNe) found in Table 4.3.

$$\text{Cradle-to-plant-gate } CO_{2e} \text{ emissions} = LCWe + LCNGe + LCNe - \text{Biomass as } CO_2 \quad (4.3)$$

Equation 4.4 represents the cradle-to-plant-exit CO_{2e} atmospheric emissions that will be charged or credited to the plant.

$$\text{Cradle-to-plant-exit } CO_{2e} \text{ atmospheric emissions} = \text{Direct } CO_{2e} \text{ emissions} + \text{Cradle-to-plant-gate } CO_{2e} \text{ emissions} \quad (4.4)$$

In addition, end use CO_{2e} emissions (plant-exit-to-grave emissions) were calculated, but no carbon taxes associated with these emissions were considered because it was assumed they would be paid by the end user and not otherwise affect the economic analysis from the perspective of the polygeneration facility operator. This means that the environmental emissions costs of using fuel or chemicals generated in the plant are passed on to the end user. It was also assumed that the end use of each chemical generated in the plant was for combustion purposes i.e. that all carbon atoms eventually end up as CO_2 emitted to the atmosphere. The end use plant-to-grave CO_{2e} emissions are summarized in equation 4.5 and Table 4.4.

Plant-exit-to-grave CO_{2e} emissions = Fuel distribution + Fuel dispensing + combustion (4.5)

Table 4.4 End use CO_{2e} emissions for the plants fuel products.

Plant to grave emissions source	Value	Units	Reference
Fuel dispensing of gasoline and diesel (also assumed for DME and Methanol)	138	g CO_{2e}/GJ	(S&T Consultants Inc., 2007)
Fuel distribution and storage of gasoline and diesel (also assumed for DME and Methanol)	575	g CO_{2e}/GJ	(S&T Consultants Inc., 2007)
Plant-to-grave emissions of gasoline	19.64	lbs CO_{2e}/gallon	("U.S. Energy Information Administration (EIA)," 2016)
Plant-to-grave emissions of diesel	22.38	lbs CO_{2e}/gallon	("U.S. Energy Information Administration (EIA)," 2016)
Plant-to-grave emissions of methanol	1.37	kg CO_{2e}/kg	Assumed to fully combust
Plant-to-grave emissions of DME	1.91	kg CO_{2e}/kg	Assumed to fully combust

Equation 4.6 below describes the cradle-to-grave CO_{2e} emissions of the process. This number represents the total emissions from upstream raw material extraction, synthesis and final product use of the BGNTL process and its products.

Cradle-to-grave CO_{2e} emissions = Cradle-to-plant-exit CO_{2e} atmospheric emissions + Plant-exit-to-grave CO_{2e} emissions (4.6)

Figure 4.1 shows a visual representation of equations 4.4 and 4.5, with dashed lines indicating CO_{2e} emission boundaries. The total Cradle-to-grave CO_{2e} emissions of the BGNTL process is described by combining the two dashed areas seen in Figure 4.1.

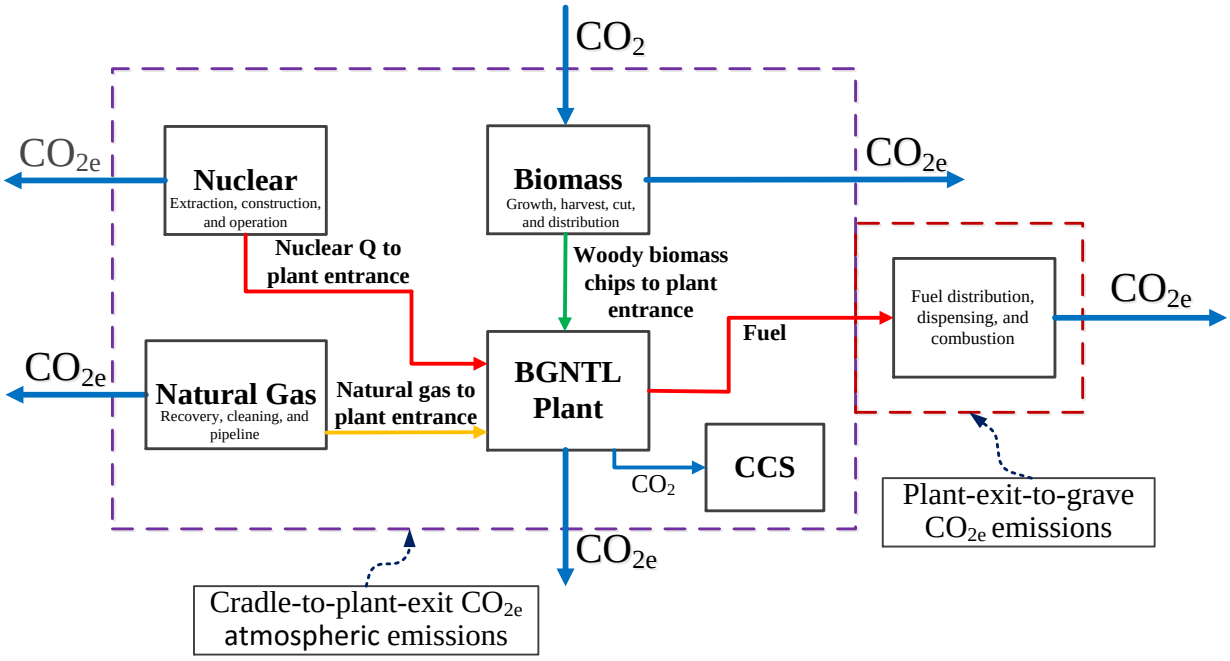

Figure 4.1 CO_{2e} emissions flowsheet, visually representing equations 4.4 and 4.5.

4.1.4 Economic Net-Present-Value outline

The economic viability of each plant case was determined using the net-present-value approach (NPV). This approach uses a discount rate or equity rate of return (20% in this study) to determine the present value of future costs and sales. The NPV calculation is the summation of present and future values all discounted back to the present, based on the equity return rate represented by equation 4.7.

$$NPV = \sum_{n=1}^{30} \frac{\text{Net cash flow}}{(1+\text{Equity rate of return})^n} \quad (4.7)$$

The net yearly cash flow has several components which are described below in equation 4.8. Equation 4.8 also includes the equity portion of the capital investment in the first period of operation.

$$\text{Net cash flow} = \text{Gross income} - \text{Income tax paid} \quad (4.8)$$

The capital depreciation rate is based on a declining balance approach using a 30% rate (C. R. A. Government of Canada, 2004). It was also assumed that during the first period of operation, only 50% of the book value is able to be depreciated (C. R. A. Government of Canada, 2004). In addition, it was assumed that if the current year had a negative taxable income, the company would not pay tax in that period and the negative taxable income is carried forward to future periods (C. R. A. Government of Canada, 2004). The equations for gross income and taxable income are shown in equations 4.9 and 4.10, respectively. These assumptions are true for a Canadian context, but do not hold in an American context.

$$\text{Gross Income} = \text{Revenue} - \text{Expenses} - \text{Loan payment} \quad (4.9)$$

$$\text{Taxable Income} = \text{Gross income} - \text{Depreciation} - \text{Loan interest paid} \quad (4.10)$$

It was assumed that the plant starts up in 2016 with the entire capital investment spent in the first period of operation, starting in period 1.

4.2 Thermal efficiency (HHV) analysis

The thermal efficiency of the plant was calculated using the HHV% methodology calculated in equation 4.11. This value will be used later in the work to assess different plant configurations.

$$\text{Thermal efficiency \% (HHV)} = \frac{\text{HHV}_{\text{fuels}} + \text{Net electricity generated}}{\text{HHV}_{\text{Biomass}} + \text{HHV}_{\text{Natural gas}} + \text{Q}_{\text{Nuclear energy}}} \quad (4.11)$$

4.3 Base-Case Economic Results

4.3.1 BGNTL economic results

The economic summary for the base case BGNTL process is summarized in Table 4.5. The base case had a roughly even distribution of the fuels and most of the syngas was destined for fuels production.

Table 4.5 Economic results for 4 select cases of the BGNTL process (all amounts in $CAD).

Scenario	BGNTL	BGNTL	BGNTL	BGNTL
CCS enabled?	yes	yes	no	no
RSC Steam or IR?	IR	Steam	IR	Steam
% of output as electricity	22.7	23.5	27.5	21.6
Capital cost by section ($1000s)				
Air separation unit	$149,792	$157,230	$150,587	$149,662
Gasifier Island	$137,529	$137,529	$137,529	$137,529
COS removal	$5,643	$5,643	$5,643	$5,643
Acid gas removal	$63,233	$63,233	$63,233	$63,233
SMR upgrade for radiant syngas cooler	$13,753	$0	$13,753	$0
Water gas shift	$8,665	$9,581	$9,300	$10,078
Syngas mixing autothermal reformer	$11,571	$13,637	$12,148	$13,643
CO_2 removal	$13,103	$13,883	$12,640	$18,037
CO_2 compression	$15,253	$15,987	$0	$0
FT synthesis, separation, and PSA section	$56,988	$55,698	$47,705	$70,261
FT autothermal reformer	$9,705	$9,453	$8,262	$11,782
Methanol synthesis	$109,571	$102,330	$128,686	$105,697
Methanol separation	$4,841	$4,805	$4,812	$4,600
DME synthesis	$15,071	$14,283	$14,324	$13,446
DME separation	$81,971	$77,684	$77,906	$73,132
SOFC stack	$291,877	$307,948	$213,126	$70,590
Steam turbines and condenser	$38,476	$42,806	$37,281	$35,158
Gas compressors	$42,139	$43,335	$35,647	$21,862
Expansion turbine cost	$52,632	$54,453	$42,829	$19,289
Gas turbine	$27,565	$21,661	$61,492	$74,679
HRSG heat exchangers	$107,502	$112,108	$109,630	$102,205
Cooling tower	$2,874	$3,016	$2,916	$2,606
Indirect Cost	$163,872	$163,232	$161,133	$147,087
Fixed Capital investment	$184,356	$183,635	$181,274	$165,473
Total capital investment	$1,607,978	$1,613,171	$1,531,854	$1,315,689
Cost breakdown at 85% Capacity ($1000s)				
Total labour cost (per year)	$12,144	$12,144	$12,144	$12,144
Total maintenance cost (per year)	$84,804	$84,472	$83,386	$76,118
Operating overhead (per year)	$13,004	$12,963	$12,829	$11,928
Property tax (per year)	$16,387	$16,323	$16,113	$14,709
General expenses (per year)	$51,494	$49,565	$50,099	$47,126
Solvents, water, catalysts, and sequestration costs (per year)	$26,254	$27,017	$11,584	$11,235
Total fuel cost (per year)	$125,249	$125,962	$123,377	$125,962
Sales breakdown at 85% Capacity ($1000s)				
Methanol sales (per year)	$17,429	$25,471	$25,588	$14,624
DME sales (per year)	$362,893	$334,113	$335,581	$304,472
Gasoline sales (per year)	$22,147	$21,606	$17,305	$29,897
Diesel Sales (per year)	$44,221	$43,043	$34,536	$59,613
Electricity sales (per year)	$92,513	$94,776	$111,588	$84,857
CO_2 credit (per year)	$21,412	$22.300	-$6,225	-$3,303
Gross earnings (per year)	$159,422	$141,285	$138,185	$122,361
Average annual income tax (per year)	$92,766	$87,416	$89,305	$79,613
Net Present Value	**$116,245**	**$25,549**	**$48,803**	**$40,006**

The selected case studies shown in Table 4.5 have the following energy balance and carbon emissions data, outlined in Table 4.6.

Table 4.6 Selected mass and energy flows of cases outlined in Table 4.5.

Scenario	BGNTL	BGNTL	BGNTL	BGNTL
CCS enabled?	yes	yes	No	No
RSC Steam or IR?	IR	steam	IR	steam
% of output as electricity	22.7	23.5	27.5	21.6
Thermal input (MW HHV)				
Biomass	550	550	550	550
Natural gas	833	855	887	855
Nuclear energy	117	95	62	95
Total thermal input	1500	1500	1500	1500
Thermal output (MW HHV)				
Net-Power	164	168	198	150
Total HHV of all liquid fuels	558	547	520	545
Plant thermal efficiency % (HHV)	48.1	47.7	47.9	46.3
Carbon data (tonnes/year)				
Cradle-to-plant-gate CO_{2e} emissions	-1,033,463	-1,033,705	-1,034,058	-1,033,705
Direct CO_{2e} emissions	176,999	141,708	500,977	710,420
Cradle-to-plant-exit CO_{2e} emissions	-856,464	-891,997	249,008	132,138
Plant-exit-to-grave CO_{2e} emissions	879,510	861,922	810,652	880,201
Cradle-to-grave CO_{2e} emissions	23,046	-30,075	1,059,660	1,012,339
Carbon to energy output ratios				
$\frac{\text{Cradle-to-plant-exit } CO_{2e} \text{ emissions (grams)}}{\text{GJ of energy output}}$	-41,189	-43,318	12,042	6,602
$\frac{\text{Cradle-to-grave } CO_{2e} \text{ emissions (grams)}}{\text{GJ of energy output}}$	1,108	-1,461	51,245	50,576

Table 4.6 shows that when CCS is included, the cradle-to-plant-exit CO_{2e} emissions are negative, giving the cases with CCS extra income in the form of selling the CO_{2e} for carbon tax credits. In addition, the cradle-to-grave CO_{2e} emissions of the BGNTL processes with CCS have far less CO_{2e} emissions than the non-CCS cases.

4.3.2 BGNTL sensitivity analysis

Figure 4.2 shows the effect of the H_2 price on the base case BGNTL NPV. Although the thermal input of H_2 made up a very small fraction in each of the base cases outlined in Table 4.6, it still showed significant impact in profitability.

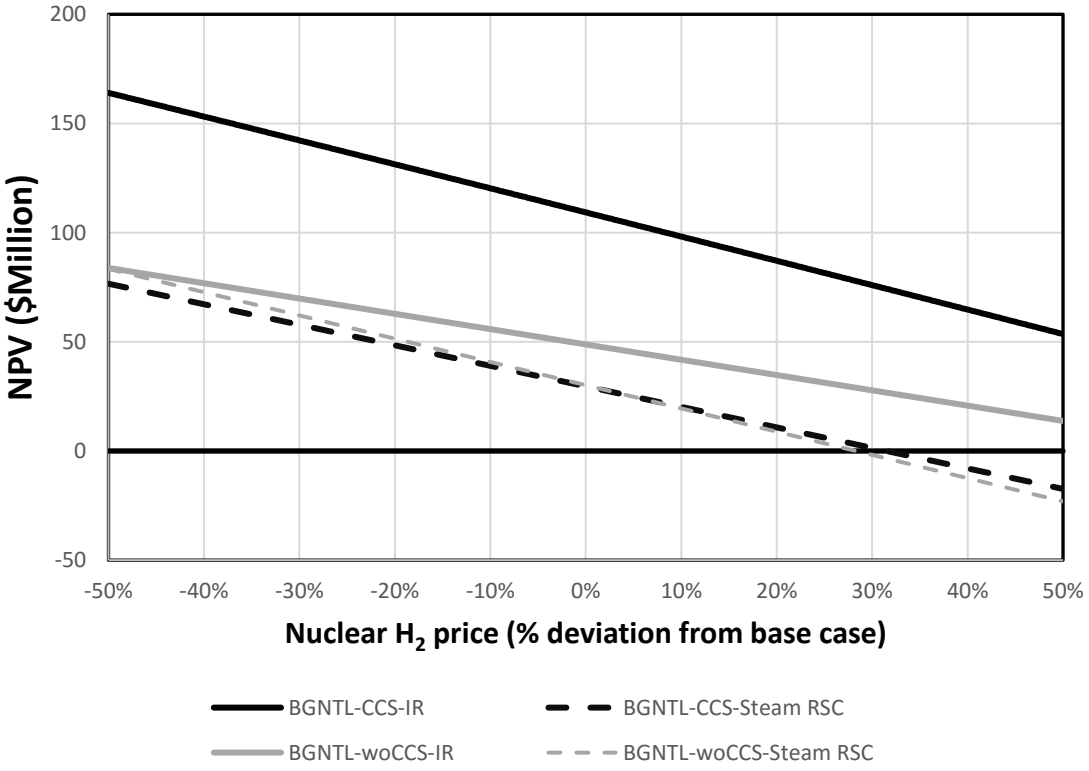

Figure 4.2 Effect of the nuclear hydrogen price on the NPV of each BGNTL base case. All other parameters in this sensitivity analysis were held constant at the base case prices, outlined in Table 4.1.

Figure 4.3 below shows the effect of the CO_2 tax on the NPV of the plant. The effect of carbon tax on non-CCS cases was found to be fairly minimal due to the biomass usage credit that each plant received. It can be seen that for a price increase of 5% ($26/tonne) and a decrease of 46% ($14/tonne) in the base CO_2 tax price, for the steam RSC and the IR case, respectively, it becomes equally profitable to have CCS or non-CCS enabled, making these two prices crossover points. For prices above these rates, there is a positive trend with increasing CO_2 tax shown by the black lines in Figure 4.3. So for an economic environment of high CO_2 taxes, having carbon capture and sequestration drastically improves the overall plant economics.

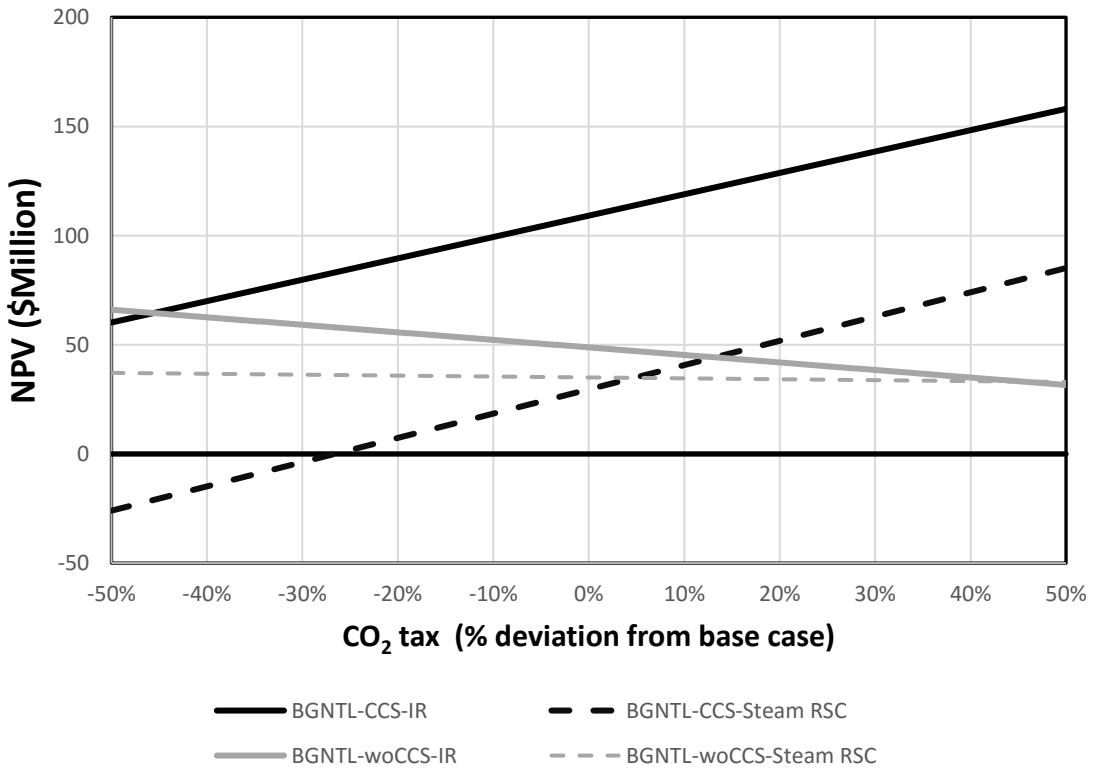

Figure 4.3 Effect of the CO_2 tax price on the NPV of each BGNTL base case. All other parameters in this sensitivity analysis were held constant at the base case prices, outlined in Table 4.1.

Figure 4.4 shows the impact of the DME prices on the overall plant performance of each BGNTL base case. DME was the main fuel produced in each base case and shows a very sensitive trend with respect to the NPV of the plant, with small changes resulting in drastic increases or decreases in the BGNTL's NPV. It should also be noted that each case is roughly affected to the same degree by the change in DME price.

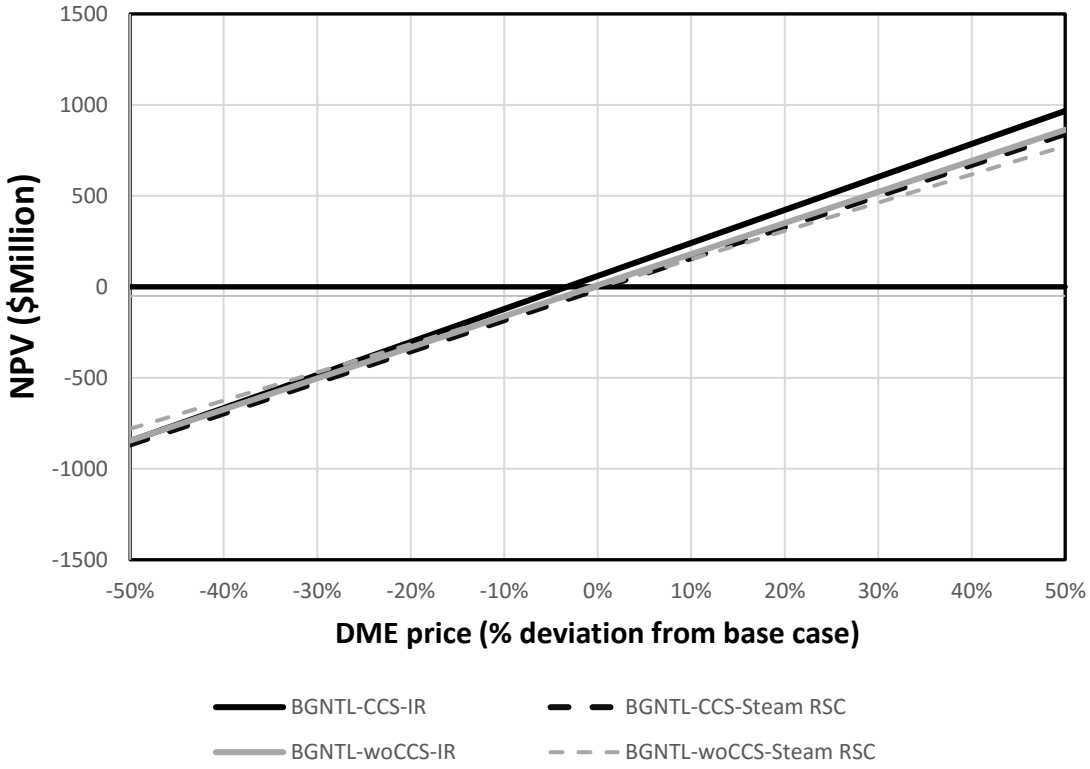

Figure 4.4 Effect of the DME price on the NPV of each BGNTL base case. All other parameters in this sensitivity analysis were held constant at the base case prices, outlined in Table 4.1.

Figure 4.5 shows the effect of the woody biomass price on the NPV of the process. It can be seen that the profitability of the base case process is very susceptible to price fluctuations in the woody biomass price, with a strong negative trend. For price increases in woody biomass of 10-30%, the BGNTL becomes unprofitable.

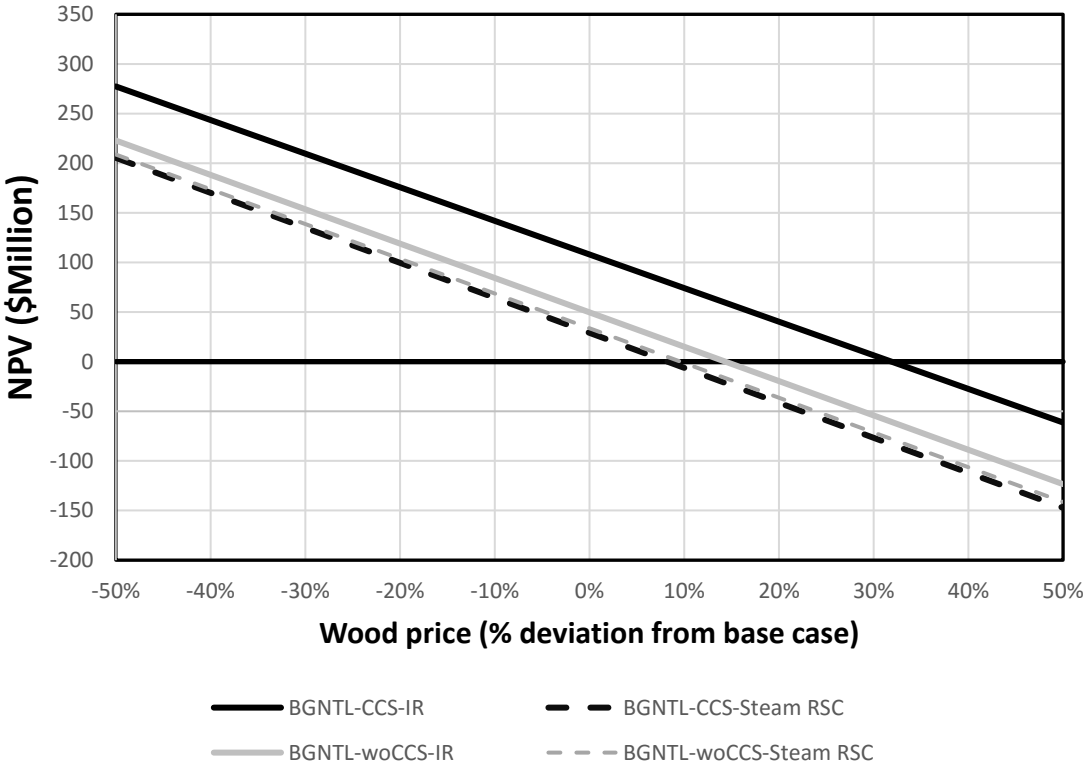

Figure 4.5 Effect of the wood biomass price on the NPV of each BGNTL base case. All other parameters in this sensitivity analysis were held constant at the base case prices, outlined in Table 4.1.

Figure 4.6 below shows the effect of the electricity price on the NPV of the BGNTL cases. Even with only roughly 20% electricity output for each of the BGNTL base cases, it still remains a very relevant parameter. For electricity price decreases of around 10-20%, the BGNTL becomes unprofitable.

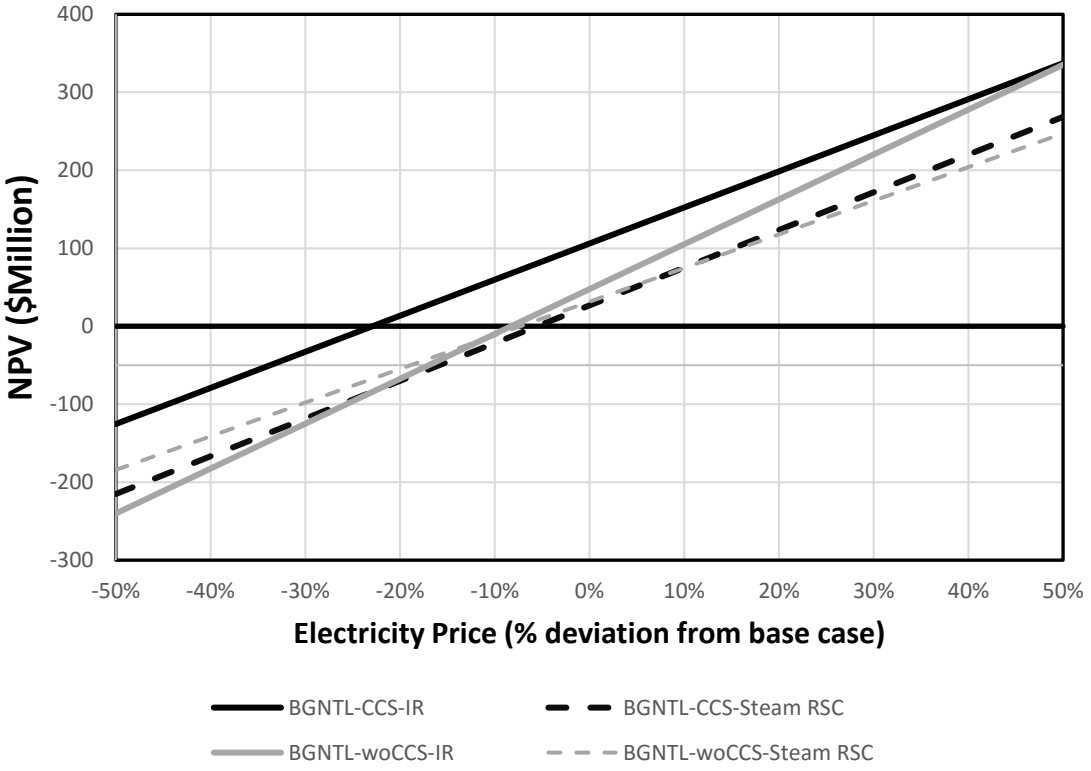

Figure 4.6 Effect of the electricity price on the NPV of each BGNTL base case. All other parameters in this sensitivity analysis were held constant at the base case prices, outlined in Table 4.1.

The BGNTL process case studies show some promise for further study. The base case results show that there is a positive correlation between CO_2 taxes and profitability of the proposed BGNTL process, making this a viable option for future energy projects encountering anticipated future CO_2 emission taxes in Ontario.

4.3.3 BGNTL effects of CuCl oxygen on economics

The CuCl cycle, as discussed in previous sections, has the additional benefit of adding oxygen to the plant, which can help relieve the demands of the ASU – decreasing its capital and operating costs. A value of $0.023/kg was calculated, which represents the added benefit of the additional oxygen alongside the hydrogen gas. The operational cost decrease and the change in the size of the required ASU results in a positive NPV change of around $10 million with respect to a process case that does not use the oxygen.

4.3.4 BGTL economic results

The economic summary for the base case BGTL process is summarized in Table 4.7. The base case had a roughly even distribution of the fuels and most of the syngas was destined for fuels production, similar to the BGNTL case.

Table 4.7 Economic results for 4 select cases of the BGTL process (all amounts in $CAD).

Scenario	BGTL	BGTL	BGTL	BGTL
CCS enabled?	Yes	yes	no	no
RSC Steam or IR?	IR	Steam	IR	Steam
% of output as electricity	23.4	21.5	24.3	26.6
Capital cost by section ($1000s)				
Air separation unit	$164,965	$167,196	$160,835	$165,625
Gasifier Island	$137,529	$137,529	$137,529	$137,529
COS removal	$5,643	$5,643	$5,643	$5,643
Acid gas removal	$63,233	$63,233	$63,233	$63,233
SMR upgrade for radiant syngas cooler	$13,753	$0	$13,753	$0
Water gas shift	$9,357	$10,085	$9,304	$10,085
Syngas mixing autothermal reformer	$12,845	$14,638	$12,846	$14,638
CO_2 removal	$17,362	$15,545	$15,701	$16,694
CO_2 compression	$16,496	$16,153	$0	$0
FT synthesis, separation, and PSA section	$73,750	$62,231	$66,591	$67,017
FT autothermal reformer	$11,203	$9,484	$10,113	$10,166
Methanol synthesis	$108,475	$138,954	$111,973	$107,748
Methanol separation	$4,784	$4,950	$4,836	$4,749
DME synthesis	$14,677	$14,673	$13,930	$14,436
DME separation	$79,825	$79,808	$75,765	$78,518
SOFC stack	$314,997	$291,974	$239,955	$243,978
Steam turbines and condenser	$40,536	$41,319	$37,465	$42,390
Gas compressors	$45,207	$42,982	$39,159	$38,834
Expansion turbine cost	$55,511	$52,837	$46,075	$46,702
Gas turbine	$29,089	$27,280	$49,884	$49,664
HRSG heat exchangers	$120,881	$117,754	$115,098	$119,827
Cooling tower	$2,934	$3,064	$2,827	$3,106
Indirect Cost	$174,316	$172,720	$165,007	$165,835
Fixed Capital investment	$196,105	$194,311	$185,633	$186,564
Total capital investment	$1,713,470	$1,684,363	$1,583,155	$1,592,979
Cost breakdown at 85% Capacity ($1000s)				
Total labour cost (per year)	$12,144	$12,144	$12,144	$12,144
Total maintenance cost (per year)	$90,208	$89,383	$85,391	$85,820
Operating overhead (per year)	$13,674	$13,572	$13,077	$13,130
Property tax (per year)	$17,432	$17,272	$16,501	$16,584
General expenses (per year)	$51,017	$50,903	$49,736	$50,403
Solvents, water, catalysts, and sequestration costs (per year)	$28,034	$27,818	$11,650	$11,879
Total fuel cost (per year)	$122,711	$122,711	$122,711	$122,712
Sales breakdown at 85% Capacity ($1000s)				
Methanol sales (per year)	$16,733	$37,602	$34,708	$16,313
DME sales (per year)	$348,386	$348,266	$321,497	$339,648
Gasoline sales (per year)	$24,280	$19,270	$21,168	$21,394
Diesel Sales (per year)	$48,590	$38,460	$42,278	$42,700
Electricity sales (per year)	$96,224	$89,414	$101,139	$107,723
CO_2 credit (per year)	$21,148	$20,881	-$7,377	-$8,769
Gross earnings (per year)	$143,704	$144,353	$129,849	$133,620
Average annual income tax (per year)	$94,585	$94,505	$88,021	$91,190
Net Present Value	**$46,621**	**$58,728**	**$28,689**	**$37,328**

The selected case studies shown in Table 4.7, have the following energy balance and carbon emissions data, outlined in Table 4.8. The results in Table 4.8 are similar to the results that were found with the BGNTL case study – namely that CCS can make the cradle-to-plant-exit CO_{2e} emissions negative for the BGTL process.

Table 4.8 Selected mass and energy flows of cases outlined in of cases outlined in Table 4.7.

Scenario	BGTL	BGTL	BGTL	BGTL
CCS enabled?	Yes	yes	No	No
RSC Steam or IR?	IR	steam	IR	steam
% of output as electricity	23.4	21.5	24.3	26.6
Thermal input (MW HHV)				
Biomass	550	550	550	550
Natural gas	950	950	950	950
Total thermal input	1500	1500	1500	1500
Thermal output (MW HHV)				
Net-Power	170	158	179	191
Total HHV of all liquid fuels	557	579	557	527
Plant thermal efficiency % (HHV)	48.5	49.1	49.1	47.9
Carbon data (tonnes/year)				
Cradle-to-plant-gate CO_{2e} emissions	-1,034,738	-1,034,738	-1,034,738	-1,034,738
Direct CO_{2e} emissions	188,809	199,489	388,967	410,857
Cradle-to-plant-exit CO_{2e} emissions	-845,929	-835,249	295,091	350,770
Plant-exit-to-grave CO_{2e} emissions	882,885	901,534	874,959	831,485
Cradle-to-grave CO_{2e} emissions	36,956	66,285	1,170,050	1,182,255
Carbon to energy output ratios				
$\frac{\text{Cradle-to-plant-exit } CO_{2e} \text{ emissions (grams)}}{\text{GJ of energy output}}$	-40,402	-39,351	13,921	16,963
$\frac{\text{Cradle-to-grave } CO_{2e} \text{ emissions (grams)}}{\text{GJ of energy output}}$	1,765	3,123	55,199	57,173

4.3.5 BGTL sensitivity analysis

Figure 4.7 shows the effect of the natural gas price on each of the BGTL base cases. Natural gas, being the main energy input into the BGTL process, has a very strong negative correlation with increases in price, with price increases of 10-20% resulting in negative profitability of the project.

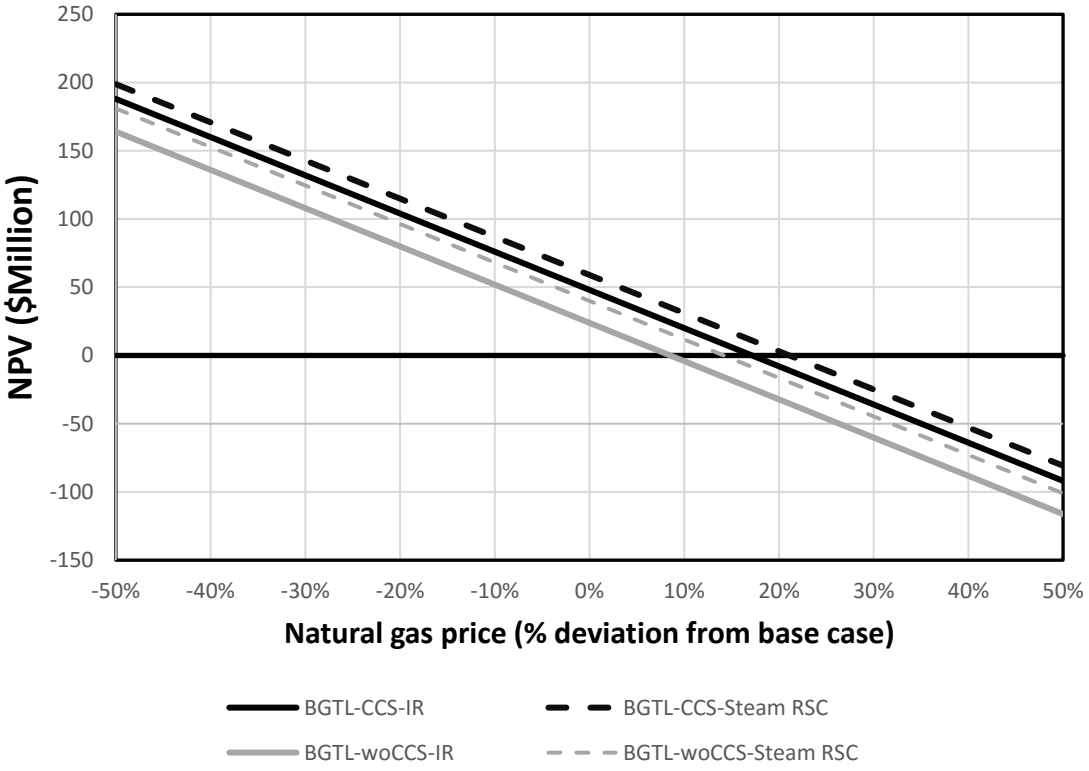

Figure 4.7 Effect of the natural gas price on the NPV of each BGTL base case. All other parameters in this sensitivity analysis were held constant at the base case prices, outlined in Table 4.1.

Figure 4.8 shows the effect of the DME prices on each base case of the BGTL process. Similar to the BGNTL process, the BGTL process relies heavily on the DME price for its profitability, since it is the main fuel produced by the process.

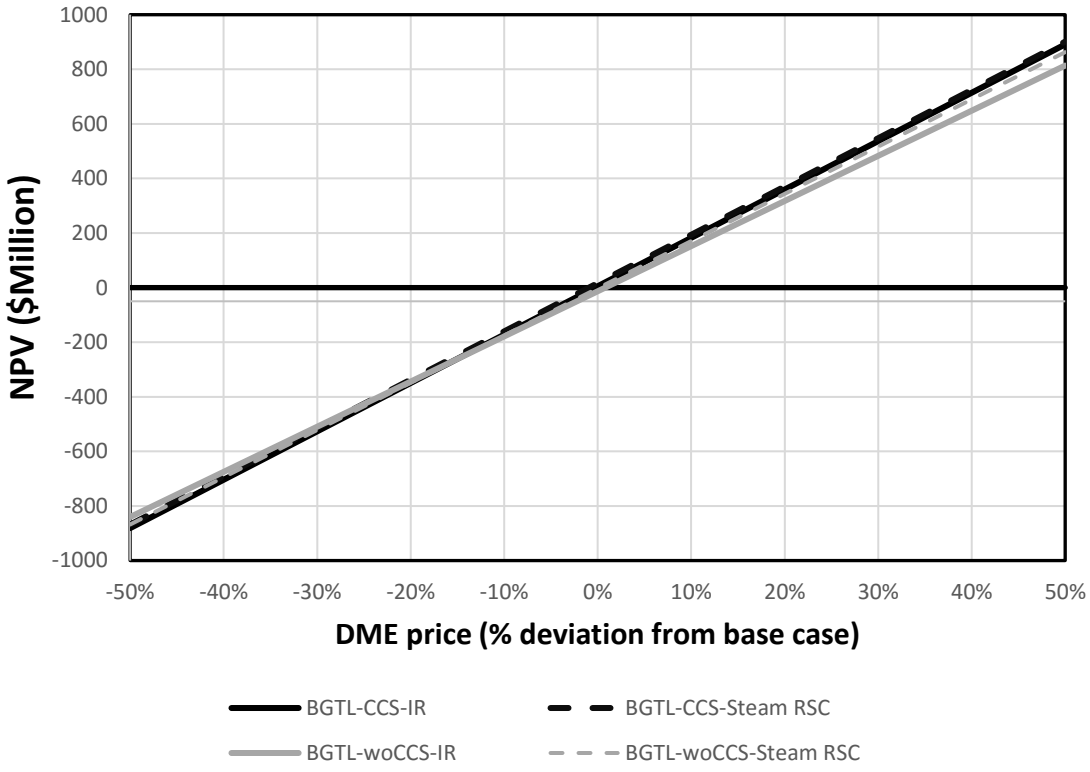

Figure 4.8 Effect of the DME price on the NPV of each BGTL base case. All other parameters in this sensitivity analysis were held constant at the base case prices, outlined in Table 4.1.

Figure 4.9 shows the effect of the CO_2 tax price on each of the BGTL cases. Similar to the BGNTL cases, the cases of BGTL that utilize CCS are able to benefit from the CO_2 tax price with a positive correlation between the CO_2 price and the NPV of the project. Figure 4.9 also shows that when the CO_2 tax falls by 14% ($22/tonne) or 18% ($21/tonne) of the base case CO_2 tax for the steam RSC and the IR case, respectively, it becomes equally profitable to have CCS or non-CCS enabled, making these two prices crossover points.

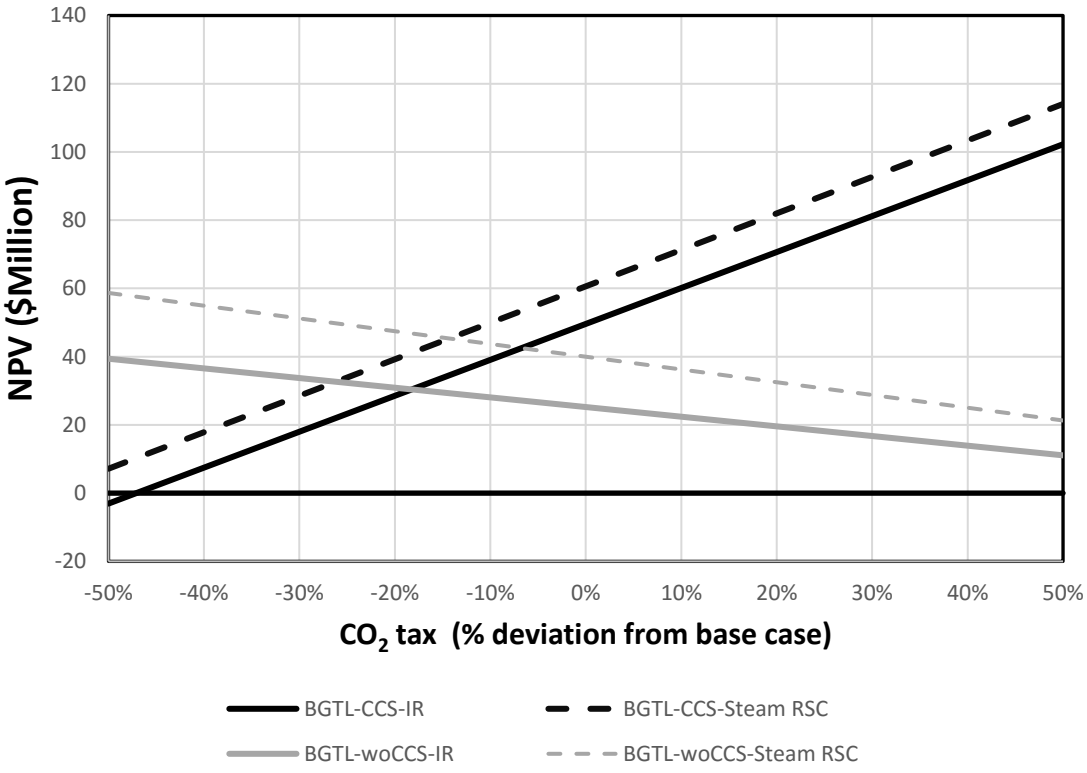

Figure 4.9 Effect of the CO_2 tax price on the NPV of each BGTL base case. All other parameters in this sensitivity analysis were held constant at the base case prices, outlined in Table 4.1.

Figure 4.10 shows the effect of the wood price on the NPV of the BGTL process. Figure 4.10 shows a strong negative correlation with the price of wood. The base case BGTL plants can only handle between a 5-16% wood price increase and still remain profitable.

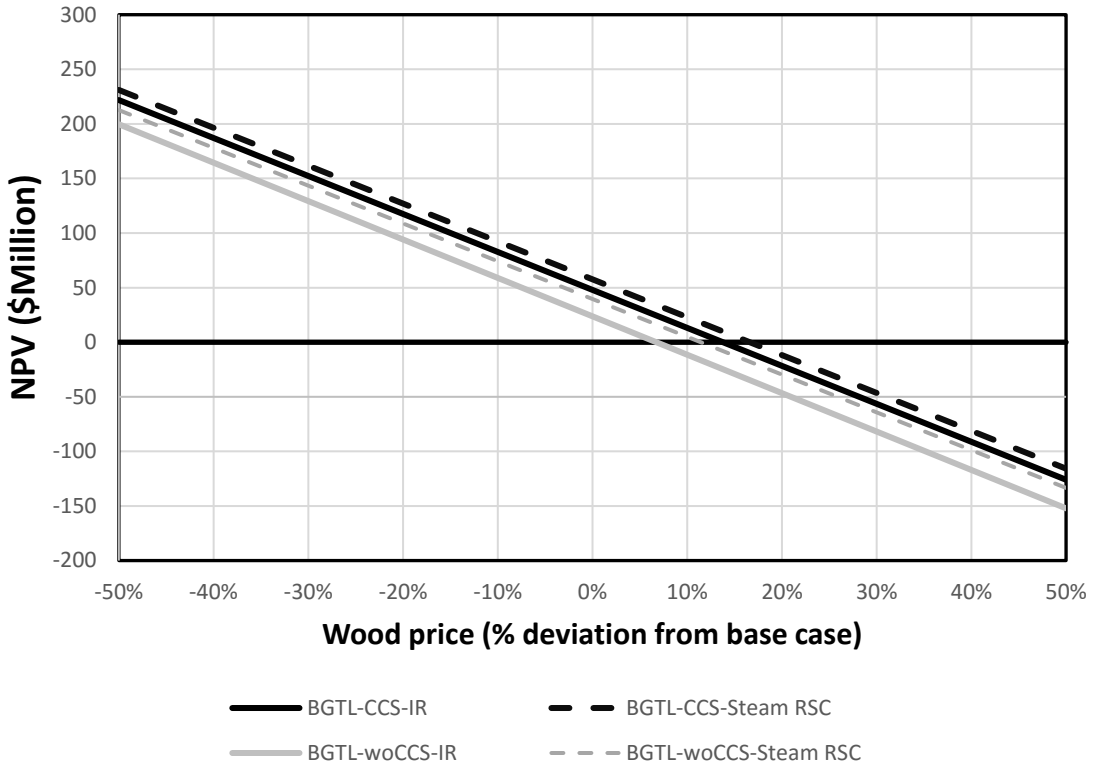

Figure 4.10 Effect of the wood price on the NPV of each BGTL base case. All other parameters in this sensitivity analysis were held constant at the base case prices, outlined in Table 4.1.

Figure 4.11 shows the effect of the electricity price on the profitability of the base case BGTL process. The base case BGTL processes become unprofitable for price drops in electric price of between 5-12%.

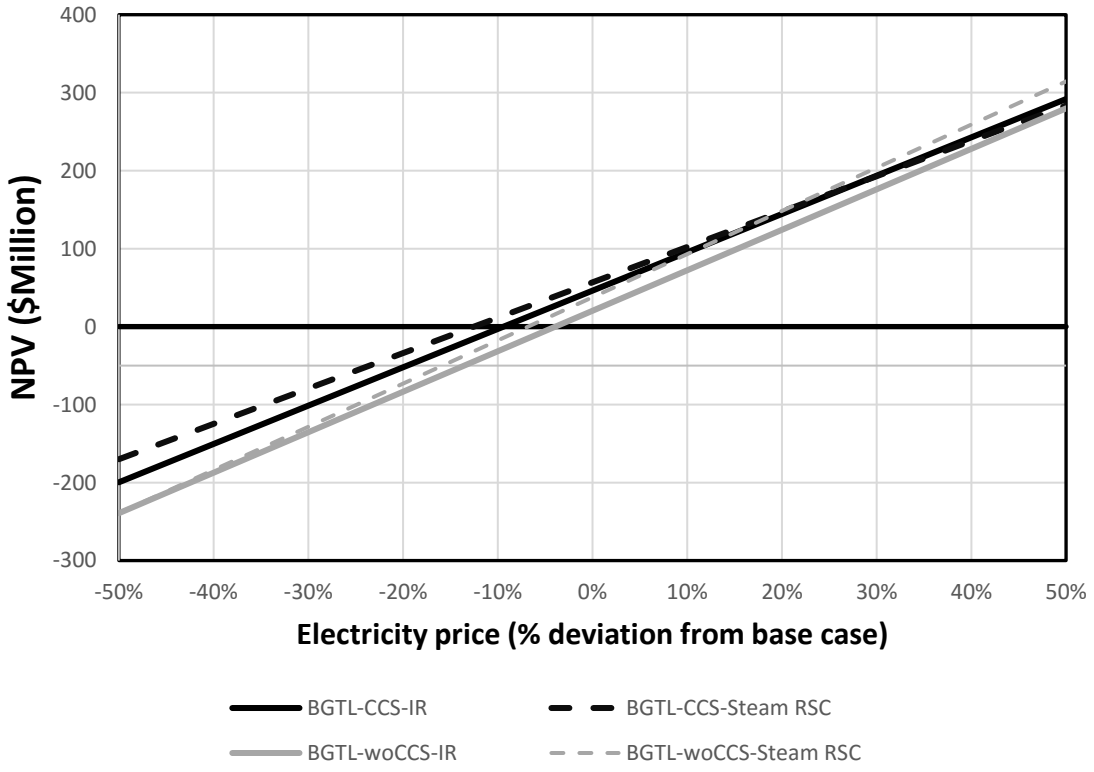

Figure 4.11 Effect of electricity price on the NPV of each BGTL base case. The all other parameters in this sensitivity analysis were held constant at the base case prices, outlined in Table 4.1.

The BGTL process shows good performance and some improvement over the BGNTL process (as seen in the base case studies) – since the BGTL does not purchase hydrogen as part of its fuel stock.

4.4 Optimization

4.4.1 Optimization formulation

The objective of this optimization study is to design a plant that maximizes the economic NPV of the proposed BGNTL process (and the other considered processes). The variables that affect the proposed process are the numerous decisions that occur when designing the base case of the system. This includes which way to send the syngas and how much to recycle in certain areas of the plant. Therefore, the following decision variables, outlined in Table 4.9, were identified for the various cases.

Table 4.9 Optimization decision variables and descriptions

Decision variable	Description
X_1	The fraction of ATR reformed natural gas in the syngas mixing section sent to fuels production.
X_2	The fraction of natural gas syngas derived from the IR that is sent to fuels production. **Note:** If the process case does not consider the use of the IR, the remaining MWth that would be sent to the IR gets added to the total extra power that is considered in decision variable X_8.
X_3	The fraction of biomass-derived syngas that is sent to the WGS for fuels production.
X_4	The fraction of mixed 2.01 H_2/CO syngas that is sent to MeOH and DME (instead of FT).
X_5	The fraction of off-gas sent to power production (instead of getting recycled to the MeOH reactor).
X_6	The fraction of methanol sold (instead of getting sent to DME production).
X_7	The fraction of FT off gas that gets sent to power production (instead of getting recycled).
X_8	The fraction of the remaining MWth (HHV) that is not consumed by the IR or by the gasifier, that is either used as ATR natural gas or thermal energy for hydrogen production via the CuCl cycle. The variable is set up such as: (Remaining MWth)*X_8 = Energy sent to the CuCl cycle and (Remaining MWth)*(1 - X_8) = energy sent as ATR natural gas. **Note:** For cases that do not consider nuclear this is not a decision variable and all the remaining MWth is sent to the ATR as natural gas input.
X_9	The fraction of syngas sent to power production that is sent to the SOFC (instead of the Gas Turbine).

The decision variables that were considered in each case are shown in Table 4.10. In addition, Figure 4.12, Figure 4.13, Figure 4.14, and Figure 4.15 show the decision variables mapped onto their respective flowsheets.

Table 4.10 Decision variables that were applied for each case.

Case	X_1	X_2	X_3	X_4	X_5	X_6	X_7	X_8	X_9
BGNTL-CCS-IR	✓	✓	✓	✓	✓	✓	✓	✓	✓
BGNTL-**wo**CCS-IR	✓	✓	✓	✓	✓	✓	✓	✓	✓
BGNTL-CCS-Steam RSC	✓	–	✓	✓	✓	✓	✓	✓	✓
BGNTL-**wo**CCS-Steam RSC	✓	–	✓	✓	✓	✓	✓	✓	✓
BGTL-CCS-IR	✓	✓	✓	✓	✓	✓	✓	–	✓
BGTL-**wo**CCS-IR	✓	✓	✓	✓	✓	✓	✓	–	✓
BGTL-CCS-Steam RSC	✓	–	✓	✓	✓	✓	✓	–	✓
BGTL-**wo**CCS-Steam RSC	✓	–	✓	✓	✓	✓	✓	–	✓

Syngas mixing shown in Figure 4.12 below has the most decision variables out of any section of the plant. These decision variables include the splits from the ATR (X_1), the biomass syngas (X_3), the IR syngas (X_2), the remaining thermal energy split between ATR natural gas and nuclear energy (X_8) and the fuel split (X_4).

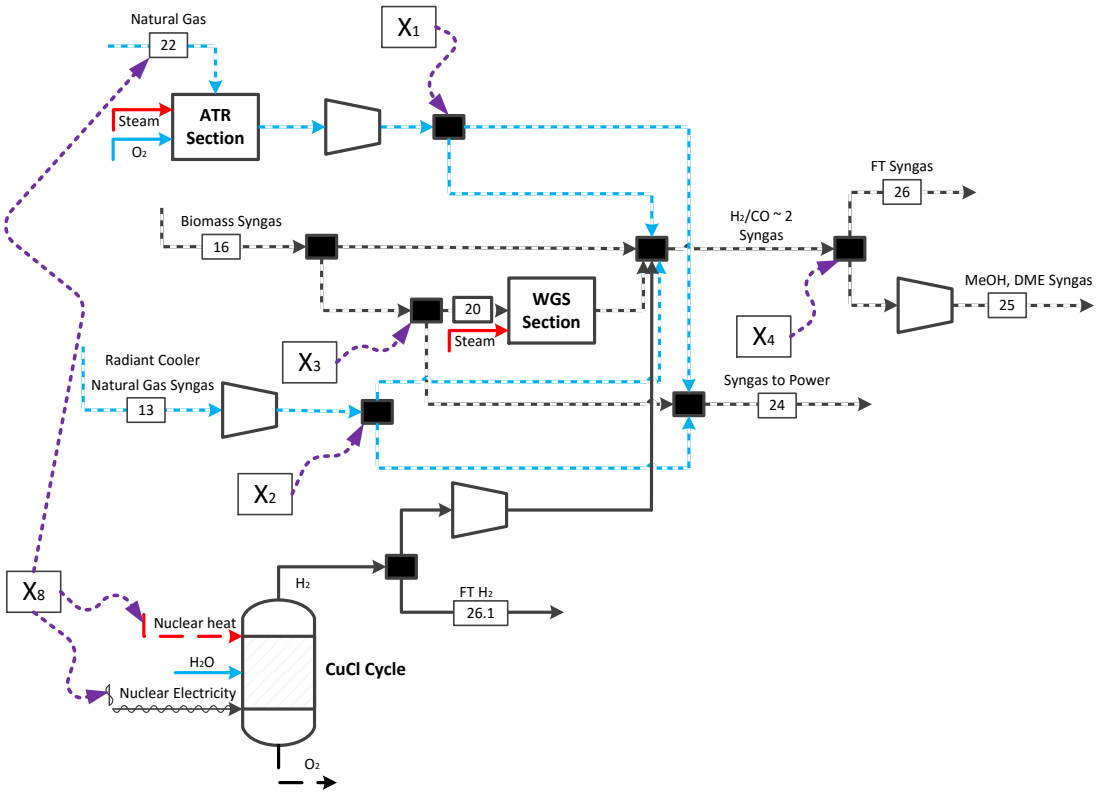

Figure 4.12 Syngas mixing section with decision variable labels (X_1, X_2, X_3, X_4, X_8).

The only decision variable in the FT section, shown in Figure 4.13, is the fraction of syngas that gets sent to power generation or to CO_2 removal, and then sent back to FT (X_7).

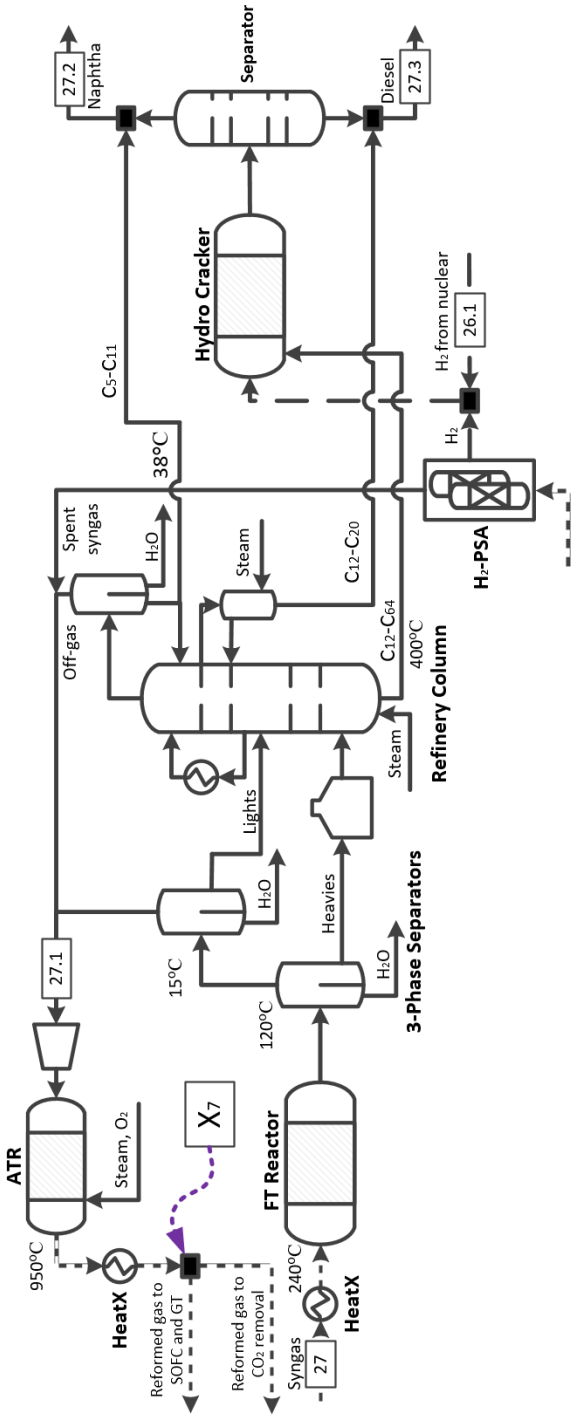

Figure 4.13 FT section with labeled decision variable (X_7).

There are two decision variables in Figure 4.14 – namely the recycle back to the methanol reactor or the sending of unreacted off-gas to power generation (X_5), and the split between the amount of methanol sold and the amount sent to the DME reactor (X_6).

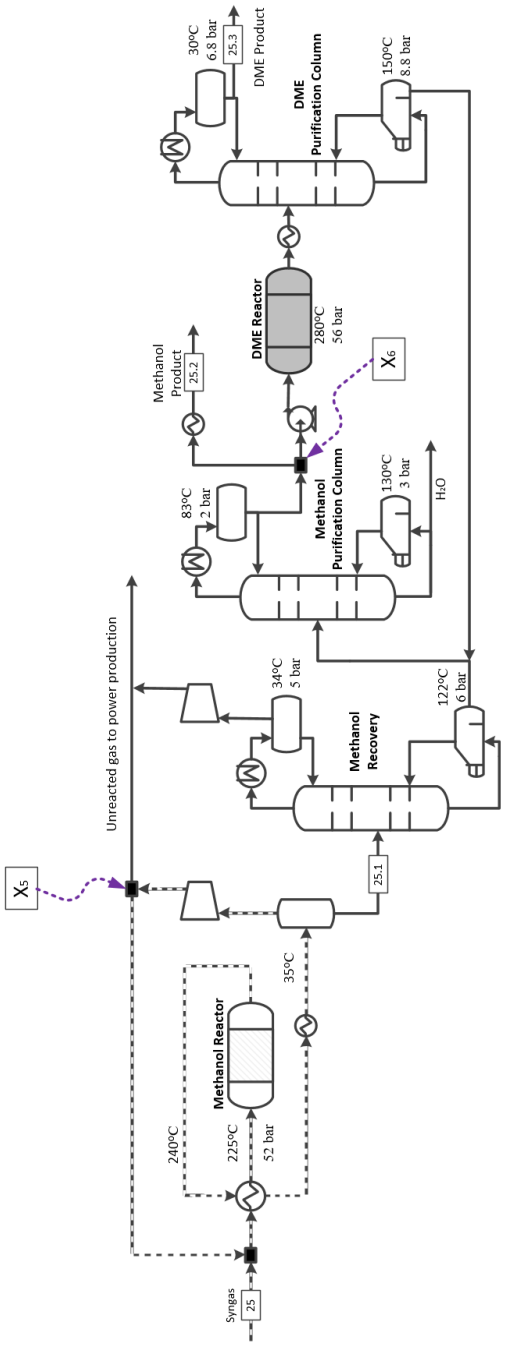

Figure 4.14 Methanol and DME synthesis section with labeled decision variable X_5 and X_6.

The final decision variable is the amount of power syngas and off-gas that gets sent to the SOFC instead of the gas turbine (X_9).

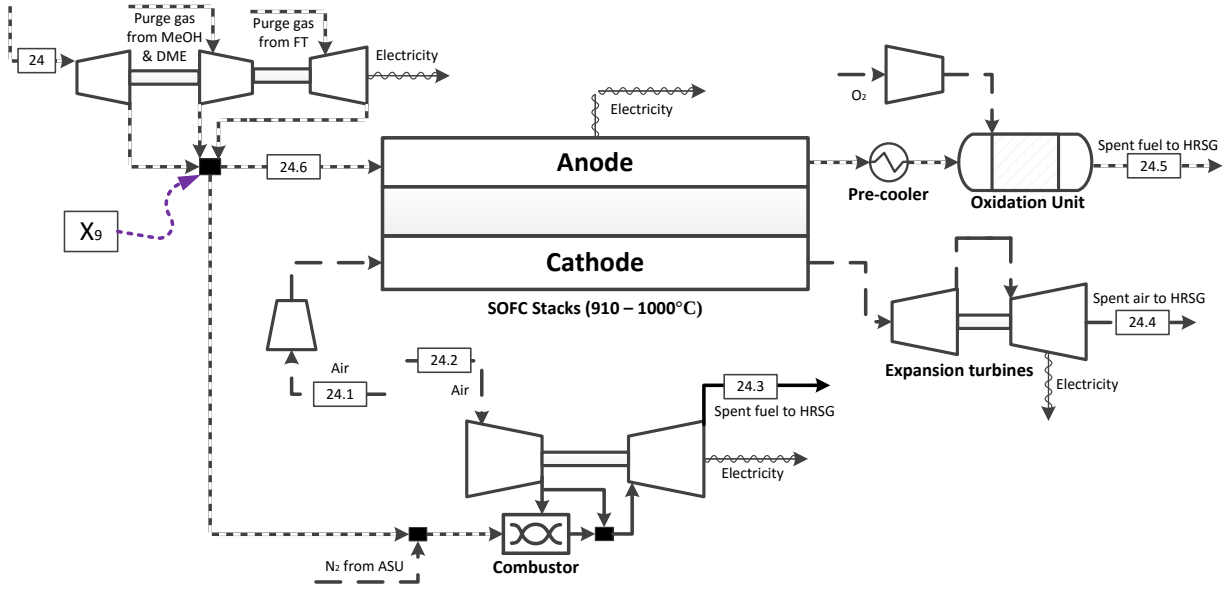

Figure 4.15 Power production section with labeled decision variable X_9.

The objective function and weighting constraints used in this work is the same for each considered case and is shown below as equation set 4.12. This optimization problem was solved using a Particle Swarm Optimization procedure (outlined in the next section), since the objective function and system are non-convex. Weight factors are added to the objective function because the particle swarm optimization (PSO) algorithm cannot handle explicit constraints, and so they have to be added as weighting penalties in the objective function. In equation 4.12, deviation variable β defines the difference between the demand for steam and the available steam. γ is the deviation variable defining the difference

between the demand for hydrogen in the hydrocracker and the available hydrogen produced by the CuCl cycle. ζ is the deviation variable defining the difference between the power demanded by the plant and the power generated.

$$\max_{x_1 \ldots x_n} \text{NPV} - \alpha\beta - \alpha\gamma - \alpha\zeta$$

$$\begin{aligned} \text{s.t} \quad & \text{steam}_{\text{i,dmd}} - \text{steam}_{\text{i,avali}} = \beta \quad \{\text{i} = \text{LP}, \text{MP}, \text{HP}\} \\ & \text{CuCl}_{\text{dmd}} - \text{CuCl}_{\text{avali}} = \gamma \\ & \text{Power}_{\text{dmd}} - \text{Power}_{\text{generated}} = \zeta \\ & \beta, \gamma, \zeta \geq 0 \\ & 0.02 \leq x_{1 \ldots n} \leq 0.98 \end{aligned} \tag{4.12}$$

The reason that the deviation variable β (equation set 4.12) is added to the optimization problem is that in Aspen Plus the steam demand for each pressure level is calculated using a design specification, which can sometimes fail. If this specification fails and the actual available steam is less than the steam demanded, then the deviation variable is triggered (using an `if` statement in Python) and this weighting deviation is added to the objective function as a penalty – this creates non-smoothness in the optimization problem. The same logic was used for the deviation variable γ: if the demanded H_2 gas to the FT section was insufficient, then this deviation is weighted as a penalty in the objective function. Finally, if the power generated by the plant did not sufficiently meet the demand, then the deviation variable ζ is activated and added to the objective function. All of these deviation variables are either positive (active) or zero (inactive), and the weighting factor α was chosen to be

100,000, since the objective function was in $CAD and would sometimes reach over $100 million.

In addition to this, the split fractions of the various decision variables (X_n) are continuous but have upper and lower bounds shown in equation 4.12. The reason these lower bounds were chosen to be [0.02 and 0.98] were for convergence purposes, since Aspen Plus convergence failures would sometimes occur if the bounds were set to 0.99 and 0.01, respectively. In the final implementation, if the variable bounds of 0.02 or 0.98 were reached, the simulation was manually re-run using values of 0 and 1, respectively.

4.4.2 Particle swarm optimization

Particle swarm optimization is a heuristic stochastic optimization approach, which utilizes stochastic and social learning to determine appropriate search directions (Thomas A. Adams & Seider, 2008). Particle swarm optimization is a good approach for this work because the BGNTL and BGTL processes are non-convex processes. Although it cannot guarantee global optimality, it is good at finding local optima, and is in most cases very efficient at doing so.

The optimization procedure was coded in Python, which called Aspen Plus to run the simulation case given a certain set of input decision variables and outputting the realized NPV of that case study. The optimization procedure is a simplified version of the algorithm presented by Adams and Seider (Thomas A. Adams & Seider, 2008) which initializes

particles across the search space randomly and enforces "sticky" bounds. The optimization procedure is as follows outlined in Figure 4.16.

Step 1: Initialize j particles (P_j) in the search space of i dimensions randomly.

$$P_{ji} = (U_i - L_i) \times \text{rand}(0,1) + P_{ji,min}$$

Step 2: Initialize the j particles' velocities (v_j).

$$v_{ji} = 0.1(U_i - L_i) \times \text{rand}(0,1) + P_{ji,min}$$

Step 3: Do N iterations.

I: For each vector P_j assess the objective function at that position.

II: Determine if P_j is the overall best $P_{j,best}$ or personal best $P_{j,personal}$. This information is then saved for the other particles.

III: Update the velocities of each particle P_j.

$$v_j = \omega \times v_j + w_1 \times \text{rand}(0,1) \times \left(P_{j,personal} - P_j\right) + w_2 \times \text{rand}(0,1) \times \left(P_{j,best} - P_j\right)$$

IV: Move the particles.

$$P_j = P_j + v_j$$

V: Check if the velocities make the particle leave the search space bounds. If it does, stick the particle to a bound (U_i or L_i).

For each dimension i:

If $P_{ij} > U_i$:

$P_{ij} = U_i$

Else if $P_{ij} < L_i$:

$P_{ij} = U_i$

End if

VI: Check if the particles have converged to a pre-specified tolerance.

$$d_j = P_j - P_{j,best}$$

If $\max(|d_j|) <$ tol:

$P_{j,best}$ found

Else:

Continue iterating (return to Step 3 **I**)

End if

Nomenclature

P_j is a vector of positions of particle j

P_{ji} is the position of particle j in dimension i

v_j is a vector of velocities for particle j

v_{ji} is the velocities of particle j in dimension i

ω inertia parameter

w_1 personal learning parameter

w_2 social learning parameter

L_i lower bound in dimension i

U_i the upper bound in dimension i

Figure 4.16 PSO algorithm used in this study.

The PSO parameters that were used are summarized in Table 4.11 and were chosen partially based on the work by Adams and Seider (Thomas A. Adams & Seider, 2008).

Table 4.11 PSO parameters used in study.

Parameter	Symbol	Value
Inertia	ω	0.73
Personal	w_1	2.8
Best	w_2	1.3
Max iteration	N	100
Number of particles	P_j	30

4.4.3 Optimization results

4.4.3.1 BGNTL optimization results

A comparison between the base case BGNTL and the optimal design found with the PSO can be seen in Table 4.12. The base case columns have arbitrary values, while the values for the PSO decision variables were rounded to 3 significant digits. The table shows that it is optimal to have CCS with the base case CO_2 tax rate. In addition, it shows that at the optimal values, the cases without CCS have slightly higher thermal (HHV%) efficiencies, since they do not have to pay the power penalty of sequestering the captured CO_2. Furthermore, the optimizer did not select the use of nuclear hydrogen gas for any of the case studies, since it is more expensive than using natural gas. In this study, optimization times in Python were between 2-4 hours for each case (which includes the time spent during Aspen Plus simulations). In addition, the PSO procedure was run several times with different randomized initial particle points for validating the optimal result.

Moreover, it is interesting to see that the non-CCS cases would use the SOFC over the gas turbine, even with its additional cost. This is because the SOFC has much better power conversion and fuel utilization efficiency (i.e when the fuel is oxidized we get a lot of useful heat out of it). The fact that the process does not use the GT is a result of the GT's inability to meet the HPS demands required by the plant. The SOFC stacks are replaced every 10 years and are therefore more expensive to run than a GT; however, the SOFC's gains in efficiency override its costs.

Table 4.12 BGNTL PSO optimization results.

Scenario	BGNTL	**BGNTL**	BGNTL	**BGNTL**	BGNTL	**BGNTL**	BGNTL	**BGNTL**
Base case or optimal case?	Base	**Optimal**	Base	**Optimal**	Base	**Optimal**	Base	**Optimal**
CCS enabled?	yes	yes	yes	yes	no	no	no	no
RSC Steam or IR?	IR	IR	Steam	Steam	IR	IR	Steam	Steam
% of output as electricity	22.7	4.6	23.5	2.4	27.5	5.6	21.6	3.1
Thermal efficiency % (HHV)	48.1	54.3	47.7	54.3	47.9	55.3	46.3	54.9
NPV	**$116,245**	**$1,188,843**	**$25,549**	**$1,209,218**	**$48,803**	**$1,183,414**	**$40,006**	**$1,206,401**
Decision variables								
X_1	0.700	0.980	0.800	0.980	0.650	0.980	0.730	0.980
X_2	0.700	0.980	N/A	N/A	0.650	0.980	N/A	N/A
X_3	0.700	0.980	0.800	0.980	0.650	0.980	0.730	0.980
X_4	0.750	0.980	0.750	0.980	0.700	0.980	0.600	0.980
X_5	0.200	0.137	0.300	0.104	0.100	0.136	0.150	0.101
X_6	0.100	0.020	0.150	0.020	0.150	0.020	0.100	0.020
X_7	0.150	0.980	0.300	0.980	0.800	0.980	0.400	0.980
X_8	0.150	0.020	0.100	0.020	0.080	0.020	0.100	0.020
X_9	0.800	0.980	0.850	0.980	0.500	0.980	0.200	0.980

Figure 4.17 below shows the best known current position of the particles ($P_{j,best}$) movement from the first iteration to the last. Figure 4.17 shows that the process wants to move to a

region of low net-electricity production, but is limited since the plant needs to produce electricity for plant equipment.

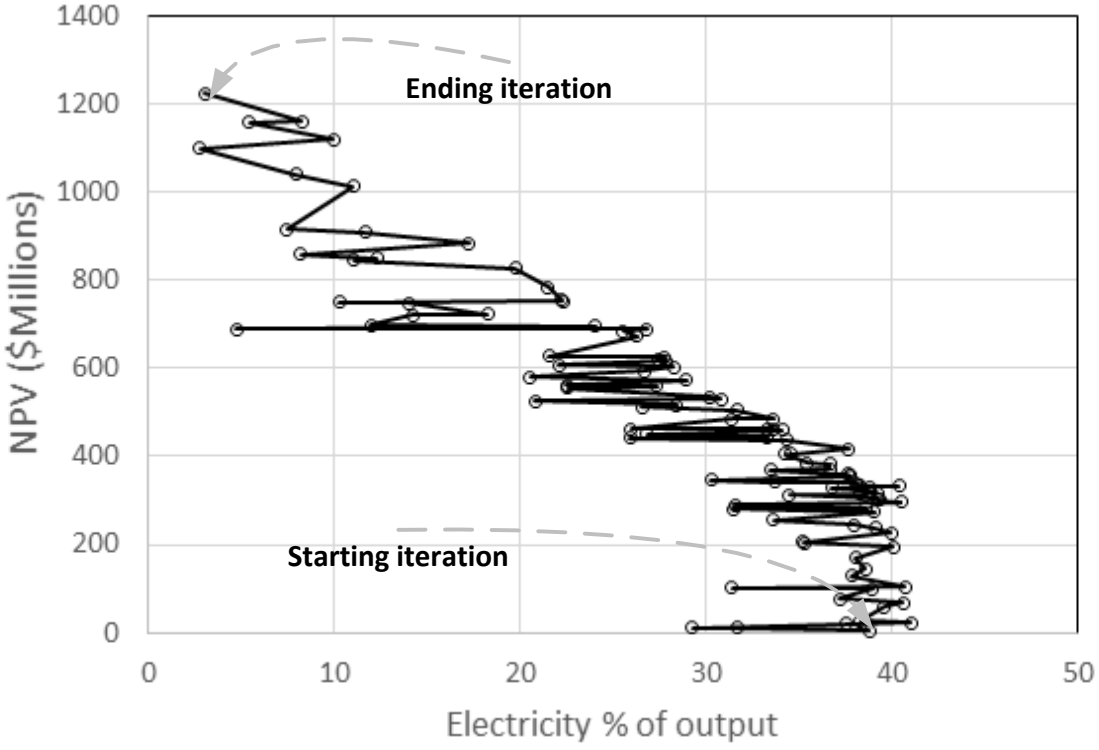

Figure 4.17 The best known current position of the particles of a sample PSO run for the BGNTL, showing the effect of changing electricity % on the NPV of the process.

Figure 4.18 below shows the best known current position of the particles ($P_{j,best}$) movement from the first iteration to the last. Figure 4.18 shows the correlation between the plant thermal efficiency % (HHV) and the NPV of the BGNTL process, as it moves through the optimization. The optimal scenario seems to track towards a high HHV% efficiency.

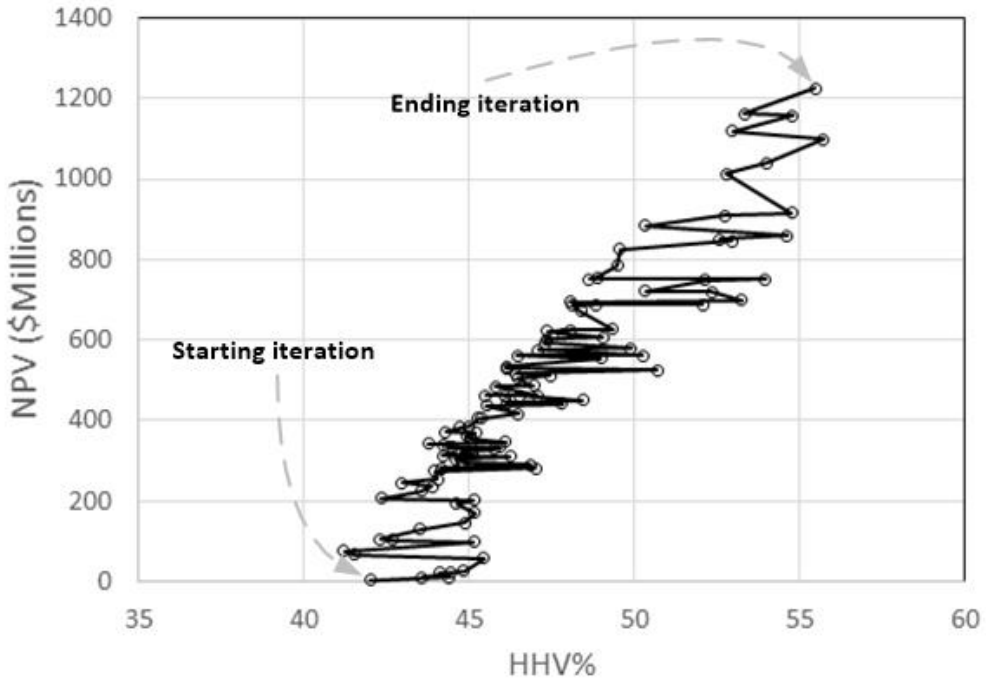

Figure 4.18 The best known current position of the particles of a sample PSO run for the BGNTL, showing the correlation between the BGNTL thermal efficiency % (HHV) and the NPV of the process.

The results seen in Table 4.12 were not used to assess the final optimal design of each plant case. Instead, the simulations were reconstructed with 0.98 assuming 1 and 0.02 assuming 0 – and with certain sections being removed from the process (to omit their capital costs) if they received 0.02 flow. The results of this change to determine the final optimal case can be seen in Table 4.13.

Table 4.13 shows that the optimal case had very large improvements over the base case BGNTL process. In addition, it showed that the addition of the IR was not as beneficial as having a steam RSC with additional natural gas being reformed in the ATR in the syngas mixing section – but only very slightly (about a 0.6% decrease in NPV). Increases in NPV of around 1% were seen when switching to CCS for each case.

Table 4.13 Optimal design for each BGNTL case with alternated flowsheet (all amounts in $CAD).

Scenario	Optimal BGNTL	Optimal BGNTL	Optimal BGNTL	Optimal BGNTL
CCS enabled?	yes	yes	no	no
RSC Steam or IR?	IR	Steam	IR	Steam
% of output as electricity	4.0	2.4	5.0	3.2
Capital cost by section ($1000s)				
Air separation unit	$161,075	$163,060	$159,150	$161,929
Gasifier Island	$137,529	$137,529	$137,529	$137,529
COS removal	$5,643	$5,643	$5,643	$5,643
Acid gas removal	$63,233	$63,233	$63,233	$63,233
SMR upgrade for radiant syngas cooler	$13,753	$0	$13,753	$0
Water gas shift	$7,013	$8,691	$6,736	$8,519
Syngas mixing Autothermal reformer	$12,902	$14,641	$12,673	$14,540
CO_2 removal	$0	$0	$0	$0
CO_2 compression	$14,823	$14,754	$0	$0
FT synthesis, separation, and PSA section	$0	$0	$0	$0
FT autothermal reformer	$0	$0	$0	$0
Methanol synthesis	$174,129	$184,947	$173,684	$185,153
Methanol separation	$5,916	$5,933	$5,914	$5,932
DME synthesis	$25,263	$25,417	$25,242	$25,415
DME separation	$137,402	$138,241	$137,293	$138,230
SOFC stack	$211,203	$189,119	$207,736	$186,333
Steam turbines and condenser	$12,276	$11,622	$11,816	$11,793
Gas compressors	$37,277	$35,423	$36,972	$35,038
Expansion turbine cost	$41,281	$38,214	$40,755	$35,633
Gas turbine	$0	$0	$0	$0
HRSG heat exchangers	$90,125	$87,838	$89,149	$88,024
Cooling tower	$2,423	$2,703	$2,407	$2,516
Indirect Cost	$155,811	$154,039	$152,538	$151,009
Fixed Capital investment	$175,287	$173,294	$171,605	$169,886
Total capital investment	$1,484,364	$1,454,341	$1,453,827	$1,426,354
Cost breakdown at 85% Capacity ($1000s)				
Total labour cost (per year)	$12,144	$12,144	$12,144	$12,144
Total maintenance cost (per year)	$80,632	$79,715	$78,938	$78,147
Operating overhead (per year)	$12,488	$12,374	$12,278	$12,180
Property tax (per year)	$15,581	$15,404	$15,254	$15,101
General expenses (per year)	$78,518	$78,499	$78,892	$78,873
Solvents, water, catalysts, and sequestration costs (per year)	$31,117	$30,990	$16,567	$16,657
Total fuel cost (per year)	$121,238	$122,711	$120,337	$122,165
Sales breakdown at 85% Capacity ($1000s)				
Methanol sales (per year)	$0	$0	$0	$0
DME sales (per year)	$803,356	$810,922	$802,375	$810,816
Gasoline sales (per year)	$0	$0	$0	$0
Diesel Sales (per year)	$0	$0	$0	$0
Electricity sales (per year)	$18,826	$11,053	$23,724	$15,076
CO_2 credit purchases (per year)	$25,846	$25,845	-$937	-$813
Gross earnings (per year)	$427,987	$428,437	$422,924	$422,956
Average annual income tax (per year)	$214,460	$214,462	$212,439	$212,679
Net Present Value	$1,288,384	$1,295,560	$1,274,138	$1,282,488

4.4.3.2 BGTL optimization results

The optimization results for the BGTL process are very similar to the BGNTL process and will not be discussed. The optimal results showed that both the BGTL and BGNTL processes maximized DME production and the BGNTL process eliminated nuclear H_2 use, making it the same as the BGTL in the optimal case. Therefore, the optimal case found in this work was the BGTL process, but will be referred to in the next sections as the optimal BG(N)TL process.

4.4.3.3 Optimal BG(N)TL - DME analysis

In the optimal design scenario seen in Table 4.13, there was also an accompanied minimum DME selling price to keep the project profitable. The minimum selling prices depending on the case are summarized in Table 4.14. Table 4.14 shows that the CCS cases had a lower associated minimum DME price than the non-CCS cases. Work by Salkuyeh and Adams showed that for a coal fed process that generated DME in a similar way, their process had a minimum DME price of $577/tonne – it should also be noted that this work did not account for carbon taxes (Salkuyeh & Adams II, 2015).

Table 4.14 Minimum DME selling prices for each optimal case described in Table 4.13.

Optimal Scenario	BG(N)TL	BG(N)TL	BG(N)TL	BG(N)TL
CCS enabled?	yes	yes	No	No
RSC Steam or IR?	IR	steam	IR	steam
Minimum DME price ($/tonne)	798	800	805	807

In addition to the DME price, DME is compared on a life cycle basis to its replacement fuel, diesel. This allows for easy comparison from an environmental perspective. The life cycle cradle-to-grave emissions for diesel are summarized in Table 4.15.

Table 4.15 Cradle-to-grave life cycle emissions for diesel fuel.

GHG emissions source	grams $CO_{2,e}$ / GJ	Reference
Feedstock Extraction	8,495	(S&T Consultants Inc., 2007)
Feedstock Transportation	935	(S&T Consultants Inc., 2007)
Land use changes, cultivation	2	(S&T Consultants Inc., 2007)
Fuel Production	12,968	(S&T Consultants Inc., 2007)
Gas leaks and flares	2,643	(S&T Consultants Inc., 2007)
Fuel dispensing	138	(S&T Consultants Inc., 2007)
Fuel distribution and storage	575	(S&T Consultants Inc., 2007)
Diesel combustion in vehicle	77,382	("U.S. Energy Information Administration (EIA)," 2016)
Cradle-to-grave emissions for diesel	103,138	

The thermal efficiency (HHV%) and $CO_{2,e}$ data for the optimal BG(N)TL plant is shown in Table 4.16. This data shows that if there is CCS, the optimal BG(N)TL plant that generates only DME can generate it with 96,678 less grams of $CO_{2,e}$ per GJ of energy than conventional diesel. In addition, if no CCS is used in the optimal BG(N)TL plant, then DME can be generated with 52,344 less grams of $CO_{2,e}$ per GJ of energy than conventional diesel. This makes the optimal BG(N)TL process almost half as environmentally damaging in a life cycle analysis than diesel when carbon capture is not used, by producing half as much greenhouse gas emissions. Overall, the life cycle of the optimal BG(N)TL case using CCS has net negative CO_2 emissions, as a result of taking carbon from the air in the form of biomass and sequestering CO_2 into the ground.

Table 4.16 Selected mass and energy flows of cases outlined in Table 4.13.

Optimal scenario	BGNTL/ BGTL	BGNTL/ BGTL	BGNTL/ BGTL	BGNTL/ BGTL
CCS enabled?	yes	yes	No	No
RSC Steam or IR?	IR	steam	IR	steam
% of output as electricity	4.0	2.4	5.0	3.2
Thermal input (MW HHV)				
Biomass	550	550	550	550
Natural gas	950	950	950	950
Nuclear energy	0	0	0	0
Total thermal input	1500	1500	1500	1500
Thermal output (MW HHV)				
Net-Power	33	20	42	27
Total HHV of all liquid fuels	800	807	799	807
Plant thermal efficiency % (HHV)	55.5	55.1	56.1	55.6
Carbon data (tonnes/year)				
Cradle-to-plant-gate CO_{2e} emissions	-1,033,846	-1,033,806	-1,034,568	-1,034,635
Direct CO_{2e} emissions	0	0	1,072,039	1,067,150
Cradle-to-plant-exit CO_{2e} emissions	-1,033,846	-1,033,806	37,471	32,515
Plant-exit-to-grave CO_{2e} emissions	1,176,583	1,187,664	1,175,145	1,187,508
Cradle-to-grave CO_{2e} emissions	142,737	153,858	1,212,616	1,220,023
Carbon to energy output ratios				
$\frac{\text{Cradle-to-plant-exit } CO_{2e} \text{ emissions (grams)}}{\text{GJ of energy output}}$	-43,094	-43,405	1,547	1,354
$\frac{\text{Cradle-to-grave } CO_{2e} \text{ emissions (grams)}}{\text{GJ of energy output}}$	5,950	6,460	50,065	50,794

The carbon efficiency is the percentage of carbon atoms in the feed – this includes the fuels used to generate power for the plant – which end up in the liquid fuels products (Salkuyeh & Adams, 2013). Essentially, it shows how efficient the plant is at utilizing carbon, by dividing the amount of carbon sequestered, emitted, and in the fuels, by the total carbon in the feed. Therefore, a process that focuses on putting carbon in the fuel will have a higher carbon efficiency. Table 4.17 summarizes the following carbon efficiencies in the optimal case. The results show an improvement over the base case results, with improved carbon efficiency. This is because in the optimal case, fuel production of DME is maximized and there is significantly less electricity produced. However, when CCS is enabled, the carbon

efficiency decreases because of the power requirements of the CCS process, decreasing the amount of available syngas to produce fuels. Additionally, Table 4.17 shows that the ATR is slightly more carbon efficient than the IR. This is due to the complexity and increased accuracy of the IR model as compared to the more simplistic ATR.

Table 4.17 Carbon efficiency breakdown of cases outlined in Table 4.13.

Optimal scenario	BG(N)TL	BG(N)TL	BG(N)TL	BG(N)TL
CCS enabled?	yes	yes	No	No
RSC Steam or IR?	IR	steam	IR	steam
% carbon in feed sequestered	47.1	46.7	0	0
% of carbon in feed emitted to the atmosphere	0	0	46.9	46.5
% of carbon in the feed ending up in fuels (carbon efficiency)	52.9	53.3	53.1	53.5

4.4.3.4 Maximizing DME production while optimizing carbon efficiency

In the optimal case, the BGNTL does not utilize nuclear energy, which results in a higher NPV. However, to optimize carbon efficiency, nuclear energy needs to be incorporated, which results in a financial penalty. Table 4.18 below shows the effect of optimizing the carbon efficiency of the optimal BGNTL case that maximizes DME. In other words, the PSO algorithm has all decision variables from the optimal BGNTL case fixed, except for the amount of recycled off-gas (X_5) and the fraction of remaining thermal energy (X_8). These two decision variables are changed to optimize carbon efficiency while making the most DME possible. This shows that with the addition of hydrogen in the optimal case, we will see a reduction in profit of the project, but the carbon efficiency of the plant will increase as less CO_2 is formed. The decrease in NPV is apparent as the cost of hydrogen gas generated by the CuCl cycle is more expensive than natural gas.

Table 4.18 Carbon efficiency breakdown of the four BGNTL cases, which have maximized DME production, while optimizing carbon efficiency.

Scenario: Maximizing DME production and carbon efficiency	BGNTL	BGNTL	BGNTL	BGNTL
CCS enabled?	yes	yes	No	No
RSC Steam or IR?	IR	steam	IR	steam
% carbon in feed sequestered	42.6	37.5	0	0
% of carbon in feed emitted to the atmosphere	0	0	42.2	35.5
% of carbon in the feed ending up in fuels (carbon efficiency)	57.4	62.5	57.8	64.5
Decision variables of interest				
X_5	0.216	0.262	0.214	0.237
X_8	0.521	0.778	0.551	0.804
Thermal input (MW HHV)				
Biomass	550	550	550	550
Natural gas	543	211	520	187
Nuclear energy	407	739	430	763
Total thermal input	1500	1500	1500	1500
Thermal output (MW HHV)				
Net-Power	64	89	71	83
Total HHV of all liquid fuels	674	563	670	570
Plant thermal efficiency % (HHV)	49.2	43.4	49.4	43.5
NPV ($1,000s)	$865,451	$556,467	$849,976	$569,762

When compared with Table 4.17, it can be observed that the carbon efficiency values increase from around 5 – 11%, based on if the IR or RSC steam case is used. The BGNTL cases using steam RSC have higher carbon efficiencies than the IR case. This is because the IR plant has more steam demands, and when X_8 increases (hydrogen production in the CuCl is increased and natural gas sent to the syngas mixing ATR is decreased), less steam is generated in the heat recovery portion of the syngas mixing ATR reformer. This makes the steam demands of the IR a limiting factor of the plant. However, when the RSC is used to make steam, more hydrogen can be used (X_8 can increase more) as the steam demands of the plant are less since there is no SMR RSC and extra steam is generated in the gasifier. As hydrogen production increases from the CuCl cycle and is added to the fuel-destined

syngas, less CO gets turned into CO_2 which is emitted. This means that more carbon ends up in the fuel production, thereby increasing carbon efficiency.

Chapter 5

Conclusions and Recommendations

5.1 Conclusions

The objective of this work was to design and analyze the economic and environmental impacts of a biomass-gas-nuclear-to-liquids polygeneration process for use in Ontario, Canada. The process was scrutinized using a techno-economic analysis approach with environmental considerations.

Chapter 2 provided a literature review into the background of specific unit operations considered in the BGTNL process and the current research in the field of polygeneration processes. The literature review of polygeneration processes showed that research was lacking in the field of polygeneration processes that utilized biomass, natural gas and nuclear.

Chapter 3 discussed the overview of the process structure and each unit operation used in the BGNTL process. The chapter walked through each unit operation with explanation in how it was modeled and its purpose in the overall process structure. The whole process model was implemented in Aspen Plus, but some models were developed outside of this modeling environment. The IR model was developed in gProms and was implemented into Aspen Plus as a reduced order model. In addition, ProMax was used to implement the AGR and CO_2 capturing flowsheets used in the BGNTL process. In addition to the entire process flow sheet being described, sample stream data was provided to show how the streams evolved through the BGNTL polygeneration process.

Chapter 4 provided an in-depth analysis of the base case techno-economic analysis of the BGTNL and BGTL processes that were considered in this work. This section showcases the applicability of the base case process with sensitivity analyses. The applicability of the process to utilize biomass gas and nuclear to make liquid fuels and power with a positive NPV was established. A key finding was that there is a positive trend between CCS in the BGNTL process and NPV with CO_2 tax. As CO_2 taxes increase, the NPV of the process increases because of the negative cradle-to-plant-exit CO_{2e} emissions. From the CO_2 sensitivity analysis, it was observed that a price increase of 5% ($26/tonne) and a decrease of 46% ($14/tonne) in the CO_2 tax were the crossover points of the steam RSC and IR cases, respectively. In other words, for CO_2 tax prices higher than $26/tonne for the steam RSC case, it is better to forego carbon capture. This is also true for the IR case when the CO_2 tax is reduced by 46% ($14/tonne), it is better to forego carbon capture. Chapter 4 also shows the applicability of the process to use biomass gas to make liquid fuels and power, without the use of nuclear. In this case, when the CO_2 tax is reduced by 14% ($22/tonne) from the base case, it becomes better to forego carbon capture in the steam RSC case. This is also true for the IR case when the CO_2 tax is reduced by 18% from the base case ($21/tonne).

Additional sensitivity analyses were then conducted for the BGNTL and the BGTL processes. Similar results were found in each process. In addition to the effect of CO_2 tax, sensitivity analyses were also conducted on other key parameters, such as wood price, DME price, and electricity price. Of these, the most impactful parameter to the process was

the DME price, since it was produced in the largest quantity and was heavily relied on for profitability.

The optimization section in Chapter 4 identified several switching decision variables. A PSO framework was outlined to maximize NPV in consideration of these decision variables. Results of the optimization found that the optimal case made only fuel in the form of DME (that is, the process maximized the amount of DME), used no H_2 gas generated by the CuCl cycle (it was not as profitable to purchase H_2 and O_2 gas from the CuCl plant), and sent all fuel and off-gas to power the SOFC. This was true for each of the 4 BGNTL and BGTL cases. In the optimal case, it was found that having the RSC making steam was slightly better than the IR by about 0.6% NPV, and switching from non-CCS to CCS resulted in a 1% increase in NPV. This result shows that the carbon tax of $25/tonne is very close to a CCS and non-CCS economic crossover point in the optimal scenario.

Interestingly, it was also found that the BGNTL process turned out to be the same as the BGTL process in the optimal form. In other words, after optimization, it was found that it was more profitable not to use nuclear hydrogen. Instead, in the optimal case, the BGNTL uses natural gas to upgrade the syngas' hydrogen content; this is because of the sufficient H_2 to CO ratio in the syngas derived from natural gas, and its lower price.

Minimal DME prices to keep optimal cases profitable were around $798 - $807 for CCS and non-CCS cases, respectively. Prices below these would yield a negative NPV for the optimal BG(N)TL processes.

It was found that the CO_{2e} life cycle impact in the optimal BG(N)TL case of DME production was much less environmentally damaging compared with traditional diesel production. Specifically, in the CCS case, the DME had approximately 100,000 less grams of CO_{2e} / GJ of energy than a traditional diesel production. In the non-CCS case, the impact was half that of the conventional diesel production (approximately 50,000 less grams of CO_{2e} / GJ of energy). However, it should be noted that there is a large amount of uncertainty in these numbers, due to the uncertain location of the BGNTL plant. The location of the BGNTL plant affects the amount of carbon emissions generated from the cradle-to-plant-gate harvesting and transportation of woody biomass from the forest to the plant gate (see Table 4.3). The harvesting and transportation of woody biomass is the largest and most uncertain parameter in determining the CO_{2e} life cycle impact of the plant.

Finally, it was observed that carbon efficiency is significantly improved in cases using the nuclear CuCl cycle to generate hydrogen; however, with a negative economic impact. The most carbon efficient BGNTL cases were those using the RSC to produce steam. On the whole, 5-11% increases in carbon efficiencies were observed over the financially optimal BGNTL case without nuclear energy.

Overall, this research provides promising potential for woody biomass usage in polygeneration processes with the addition of nuclear energy and natural gas.

5.2 Recommendations for future work

There is a significant amount of work still to be considered in this venture of work. Various ideas include:

1. Incorporating different products into the process. The system can produce other products, such as olefins, ethanol, aromatics, and other hydrocarbon fuels.
2. Analyzing a biomass-only case that is profitable, or to find minimum selling prices of the fuels this system could produce. In addition, biomass inputs other than wood could be explored, such as switchgrass and other non-food competitive biomass products.
3. Parallel computing could be exploited with Python, in order to reduce optimization time.
4. The optimization framework could include operating conditions (such as pressures and temperatures) in addition to switching variables. Decisions would then not only be direction of flow, but also selection of temperatures and pressures, for example.
5. Direct DME synthesis could be used instead of an indirect pathway. A single reactor setup could be explored.

6. Instead of having a second ATR in the FT section, the syngas mixing ATR could be used to handle the recycled off-gas from the FT section, in addition to reforming natural gas.

List of References

Adams, T. A., & Barton, P. I. (2010). High-efficiency power production from coal with carbon capture. *AIChE Journal*, *56*(12), 3120–3136. http://doi.org/10.1002/aic.12230

Adams, T. A., & Barton, P. I. (2011a). Combining coal gasification and natural gas reforming for efficient polygeneration. *Fuel Processing Technology*, *92*(3), 639–655. http://doi.org/10.1016/j.fuproc.2010.11.023

Adams, T. A., & Barton, P. I. (2011b). Combining coal gasification, natural gas reforming, and solid oxide fuel cells for efficient polygeneration with CO2 capture and sequestration. *Fuel Processing Technology*, *92*(10), 2105–2115. http://doi.org/10.1016/j.fuproc.2011.06.019

Adams, T. A., & Ghouse, J. H. (2015). Polygeneration of fuels and chemicals. *Current Opinion in Chemical Engineering*, *10*, 87–93. http://doi.org/10.1016/j.coche.2015.09.006

Adams, T. A., Nease, J., Tucker, D., & Barton, P. I. (2013). Energy Conversion with Solid Oxide Fuel Cell Systems: A Review of Concepts and Outlooks for the Short- and Long-Term. *Industrial & Engineering Chemistry Research*, *52*(9), 3089–3111. http://doi.org/10.1021/ie300996r

Adams, T. A., Salkuyeh, Y. K., & Nease, J. (2014). Processes and simulations for solvent-based CO 2 capture and syngas cleanup. In *Reactor and process design in sustainable energy technology* (pp. 163–231). Elsevier Amsterdam.

Adams, T. A., & Seider, W. D. (2008). Practical optimization of complex chemical processes with tight constraints. *Computers & Chemical Engineering*, *32*(9), 2099–2112. http://doi.org/10.1016/j.compchemeng.2008.02.007

Adams II, T. A., & Barton, P. I. (2009). A dynamic two-dimensional heterogeneous model for water gas shift reactors. *International Journal of Hydrogen Energy*, *34*(21), 8877–8891. http://doi.org/10.1016/j.ijhydene.2009.08.045

Adams II, T. A., & Barton, P. I. (2010). High-efficiency power production from natural gas with carbon capture. *Journal of Power Sources*, *195*(7), 1971–1983. http://doi.org/10.1016/j.jpowsour.2009.10.046

Ahrenfeldt, J., Thomsen, T. P., Henriksen, U., & Clausen, L. R. (2013). Biomass gasification cogeneration – A review of state of the art technology and near future perspectives. *Applied Thermal Engineering*, *50*(2), 1407–1417. http://doi.org/10.1016/j.applthermaleng.2011.12.040

Bercic, G., & Levec, J. (1993). Catalytic dehydration of methanol to dimethyl ether. Kinetic investigation and reactor simulation. *Industrial & Engineering Chemistry Research*, *32*(11), 2478–2484. http://doi.org/10.1021/ie00023a006

Burr, B., & Lyddon, L. (2008). A comparison of physical solvents for acid gas removal. In *87th Annual Gas Processors Association Convention, Grapevine, TX, March* (pp. 2–5).

Bussche, K. V., & Froment, G. F. (1996). A steady-state kinetic model for methanol synthesis and the water gas shift reaction on a commercial Cu/ZnO/Al 2 O 3 catalyst. *Journal of Catalysis*, *161*(1), 1–10.

Carbon levy and rebates. (2016). Retrieved July 20, 2016, from /climate-carbon-pricing.aspx

Clausen, L. R., Elmegaard, B., & Houbak, N. (2010). Technoeconomic analysis of a low CO2 emission dimethyl ether (DME) plant based on gasification of torrefied biomass. *Energy*, *35*(12), 4831–4842. http://doi.org/10.1016/j.energy.2010.09.004

Clausen, L. R., Houbak, N., & Elmegaard, B. (2010). Technoeconomic analysis of a methanol plant based on gasification of biomass and electrolysis of water. *Energy*, *35*(5), 2338–2347. http://doi.org/10.1016/j.energy.2010.02.034

Dimethyl Ether Prices - Alibaba.com. (n.d.). Retrieved July 9, 2016, from https://www.alibaba.com/showroom/dimethyl-ether-prices.html

Export Data and Price of mdea Zauba. (n.d.). Retrieved July 10, 2016, from https://www.zauba.com/export-METHYLDIETHANOLAMINE+MDEA-hs-code.html

Ferrandon, M. S., Lewis, M. A., Tatterson, D. F., Nankanic, R. V., Kumarc, M., Wedgewood, L. E., & Nitsche, L. C. (2008). The hybrid Cu–Cl thermochemical cycle. I. Conceptual process design and H2A cost analysis. II. Limiting the formation of CuCl during hydrolysis. In *NHA annual hydrogen conference, Sacramento convention center, CA* (Vol. 10, pp. 3310–3326). Retrieved from https://www.researchgate.net/profile/Magali_Ferrandon/publication/239555289_THE_HYBRID_CU-CL_THERMOCHEMICAL_CYCLE_I_CONCEPTUAL_PROCESS_DESIGN_AND_H2A_COST_ANALYSIS_II_LIMITING_THE_FORMATION_OF_CUCL_DURING_HYDROLYSIS/links/561bd88408ae6d17308b08ec.pdf

Field, R. P., & Brasington, R. (2011). Baseline Flowsheet Model for IGCC with Carbon Capture. *Industrial & Engineering Chemistry Research*, *50*(19), 11306–11312. http://doi.org/10.1021/ie200288u

Ghouse, J. H., & Adams, T. A. (2013). A multi-scale dynamic two-dimensional heterogeneous model for catalytic steam methane reforming reactors. *International Journal of Hydrogen Energy*, *38*(24), 9984–9999. http://doi.org/10.1016/j.ijhydene.2013.05.170

Ghouse, J. H., Seepersad, D., & Adams, T. A. (2015). Modelling, simulation and design of an integrated radiant syngas cooler and steam methane reformer for use with coal gasification. *Fuel Processing Technology*, *138*, 378–389. http://doi.org/10.1016/j.fuproc.2015.05.035

Government of Canada, C. R. A. (2004, January 16). Classes of depreciable property. Retrieved July 10, 2016, from http://www.cra-arc.gc.ca/tx/bsnss/tpcs/slprtnr/rprtng/cptl/dprcbl-eng.html

Government of Canada, C. R. A. (2005, July 1). Corporation tax rates. Retrieved July 10, 2016, from http://www.cra-arc.gc.ca/tx/bsnss/tpcs/crprtns/rts-eng.html

Government of Canada, N. R. C. (n.d.-a). Average Gasoline Retail Prices in Canada. Retrieved July 9, 2016, from http://www2.nrcan.gc.ca/eneene/sources/pripri/prices_bycity_e.cfm

Government of Canada, N. R. C. (n.d.-b). Average Retail Diesel Prices in Canada. Retrieved July 9, 2016, from http://www2.nrcan.gc.ca/eneene/sources/pripri/prices_bycity_e.cfm?PriceYear=0&ProductID=5&LocationID=66,8,39,17#PriceGraph

Government of Ontario. (2016). *Ontario's five year climate change action plan 2016-2020* (p. 86). Retrieved from http://www.applications.ene.gov.on.ca/ccap/products/CCAP_ENGLISH.pdf

Hamelinck, C., Faaij, A., Denuil, H., & Boerrigter, H. (2004). Production of FT transportation fuels from biomass; technical options, process analysis and optimisation, and development potential. *Energy*, *29*(11), 1743–1771. http://doi.org/10.1016/j.energy.2004.01.002

Hewson, D., Oo, A., Albion, K. J., & Keir, A. (2011). *BIOMASS RESIDUALS STUDY FOR OPG REPOWERING PROGRAM* (p. 118). Ontario, Canada: Ontario Power Generation (OPG). Retrieved from http://www.canadiancleanpowercoalition.com/pdf/BM22%20-%20Biomass%20Residuals%20Study%20for%20OPG%20Repowering%20Program.pdf

Historic inflation Canada – historic CPI inflation Canada. (n.d.). Retrieved July 10, 2016, from http://www.inflation.eu/inflation-rates/canada/historic-inflation/cpi-inflation-canada.aspx

How much carbon dioxide is produced by burning gasoline and diesel fuel? - FAQ - U.S. Energy Information Administration (EIA). (2016, May 6). Retrieved July 10, 2016, from http://www.eia.gov/tools/faqs/faq.cfm?id=307&t=11

ICF Consulting Canada. (2012). *Life Cycle Greenhouse Gas Emissions of Natural Gas A LITERATURE REVIEW OF KEY STUDIES COMPARING EMISSIONS FROM NATURAL GAS AND COAL* (Literature review) (p. 8). The Canadian Natural Gas Initiative (CNGI). Retrieved from http://www.capp.ca/~/media/capp/customer-portal/documents/215278.pdf

IESO Backgrounder on BPRIA. (2015). Retrieved from http://www.ieso.ca/Documents/procurement/bruce/IESO-Backgrounder-on-BPRIA-2015-12-02.pdf

Khojasteh Salkuyeh, Y. (2015). *New Polygeneration Processes for Power Generation and Liquid Fuel Production with Zero CO2 Emissions*. Retrieved from https://macsphere.mcmaster.ca/handle/11375/17207

Kreutz, T. G., Larson, E. D., Liu, G., & Williams, R. H. (2008). Fischer-Tropsch fuels from coal and biomass. In *25th Annual International Pittsburgh Coal Conference* (Vol. 29). Retrieved from https://www.princeton.edu/pei/energy/publications/texts/Kreutz-et-al-PCC-2008-10-7-08.pdf

Laosiripojana, N., & Assabumrungrat, S. (2007). Catalytic steam reforming of methane, methanol, and ethanol over Ni/YSZ: The possible use of these fuels in internal reforming SOFC. *Journal of Power Sources*, *163*(2), 943–951. http://doi.org/10.1016/j.jpowsour.2006.10.006

Larson, E. D., Jin, H., & Celik, F. E. (2005). Gasification-based Fuels and Electricity Production From Biomass, Without and With Carbon Capture and Storage. *ResearchGate*. Retrieved from https://www.researchgate.net/publication/267704156_Gasification-based_Fuels_and_Electricity_Production_From_Biomass_Without_and_With_Carbon_Capture_and_Storage

Larson, E. D., & Tingjin, R. (2003). Synthetic fuel production by indirect coal liquefaction. *Energy for Sustainable Development*, *7*(4), 79–102.

Lenzen, M. (2008). Life cycle energy and greenhouse gas emissions of nuclear energy: A review. *Energy Conversion and Management*, *49*(8), 2178–2199. http://doi.org/10.1016/j.enconman.2008.01.033

Levin, D. B., Zhu, H., Beland, M., Cicek, N., & Holbein, B. E. (2007). Potential for hydrogen and methane production from biomass residues in Canada. *Bioresource Technology*, *98*(3), 654–660. http://doi.org/10.1016/j.biortech.2006.02.027

Mackenzie, D. H., Prambil, F. C., Daniels, C. A., & Bullin, J. A. (1987). Design & operation of a selective sweetening plant using MDEA. *Energy Progress*, *7*(1). Retrieved from http://www.gasliquids.com/papers/mdea_sweetening_plant.pdf

Ministry of Energy » Achieving Balance Ontario's Long-Term Energy Plan. (2013). Retrieved June 22, 2016, from http://www.energy.gov.on.ca/en/ltep/achieving-balance-ontarios-long-term-energy-plan/#ministers-message

Naidin, M., Mokry, S., Baig, F., Gospodinov, Y., Zirn, U., Pioro, I., & Naterer, G. (2009). Thermal-Design Options for Pressure-Channel SCWRS With Cogeneration of Hydrogen. *Journal of Engineering for Gas Turbines and Power*, *131*(1), 12901. http://doi.org/10.1115/1.2983016

Naterer, G. F., Dincer, I., & Zamfirescu, C. (2013). *Hydrogen Production from Nuclear Energy*. London: Springer London.

Naterer, G. F., Suppiah, S., Stolberg, L., Lewis, M., Ferrandon, M., Wang, Z., … Avsec, J. (2011). Clean hydrogen production with the Cu–Cl cycle – Progress of international consortium, II: Simulations, thermochemical data and materials. *International Journal of Hydrogen Energy*, *36*(24), 15486–15501. http://doi.org/10.1016/j.ijhydene.2011.08.013

Naterer, G. F., Suppiah, S., Stolberg, L., Lewis, M., Wang, Z., Daggupati, V., … Spekkens, P. (2010). Canada's program on nuclear hydrogen production and the thermochemical Cu–Cl cycle. *International Journal of Hydrogen Energy*, *35*(20), 10905–10926. http://doi.org/10.1016/j.ijhydene.2010.07.087

Natural Gas Rate Updates. (n.d.). Retrieved July 1, 2016, from http://www.ontarioenergyboard.ca/OEB/Consumers/Natural+Gas/Natural+Gas+Rates

Nease, J., & Adams, T. A. (2013). Systems for peaking power with 100% CO2 capture by integration of solid oxide fuel cells with compressed air energy storage. *Journal of Power Sources*, *228*, 281–293. http://doi.org/10.1016/j.jpowsour.2012.11.087

Nease, J., & Adams, T. A. (2014). Coal-fuelled systems for peaking power with 100% CO2 capture through integration of solid oxide fuel cells with compressed air energy storage. *Journal of Power Sources*, *251*, 92–107. http://doi.org/10.1016/j.jpowsour.2013.11.040

Okoli, C., & Adams, T. A. (2014). Design and Economic Analysis of a Thermochemical Lignocellulosic Biomass-to-Butanol Process. *Industrial & Engineering Chemistry Research*, *53*(28), 11427–11441. http://doi.org/10.1021/ie501204r

Outlook to 2035 - energy use to rise by a third | BP Energy Outlook | Energy economics | BP Global. (2016). Retrieved June 9, 2016, from http://www.bp.com/en/global/corporate/energy-economics/energy-outlook-2035/energy-outlook-to-2035.html

Peters, M. S., & Timmerhaus, K. D. (1991). *Plant design and economics for chemical engineers* (4th ed). New York: McGraw-Hill.

Phyllis2 - ECN Phyllis classification. (n.d.). Retrieved June 28, 2016, from https://www.ecn.nl/phyllis2/Browse/Standard/ECN-Phyllis#cedar

Pricing | Methanex Corporation. (2016, July 1). Retrieved July 1, 2016, from https://www.methanex.com/our-business/pricing

Queiroz, J. A., Rodrigues, V. M. S., Matos, H. A., & Martins, F. G. (2012). Modeling of existing cooling towers in ASPEN PLUS using an equilibrium stage method. *Energy Conversion and Management*, *64*, 473–481. http://doi.org/10.1016/j.enconman.2012.03.030

Rosen, M. A. (2010). Advances in hydrogen production by thermochemical water decomposition: A review. *Energy*, *35*(2), 1068–1076. http://doi.org/10.1016/j.energy.2009.06.018

Ruth, M. F., Zinaman, O. R., Antkowiak, M., Boardman, R. D., Cherry, R. S., & Bazilian, M. D. (2014). Nuclear-renewable hybrid energy systems: Opportunities, interconnections, and needs. *Energy Conversion and Management*, *78*, 684–694. http://doi.org/10.1016/j.enconman.2013.11.030

Ryland, D. K., Li, H., & Sadhankar, R. R. (2007). Electrolytic hydrogen generation using CANDU nuclear reactors. *International Journal of Energy Research*, *31*(12), 1142–1155. http://doi.org/10.1002/er.1325

Salkuyeh, Y. K., & Adams, T. A. (2013). Combining coal gasification, natural gas reforming, and external carbonless heat for efficient production of gasoline and diesel with CO2 capture and sequestration. *Energy Conversion and Management*, *74*, 492–504. http://doi.org/10.1016/j.enconman.2013.07.023

Salkuyeh, Y. K., & Adams, T. A. (2014). A new power, methanol, and DME polygeneration process using integrated chemical looping systems. *Energy Conversion and Management*, *88*, 411–425. http://doi.org/10.1016/j.enconman.2014.08.039

Salkuyeh, Y. K., & Adams II, T. A. (2015). Co-Production of Olefins, Fuels, and Electricity from Conventional Pipeline Gas and Shale Gas with Near-Zero CO2 Emissions. Part II: Economic Performance. *Energies*, *8*(5), 3762–3774. http://doi.org/10.3390/en8053762

Seepersad, D., Ghouse, J. H., & Adams, T. A. (2015). Dynamic simulation and control of an integrated gasifier/reformer system. Part I: Agile case design and control. *Chemical Engineering Research and Design*, *100*, 481–496. http://doi.org/10.1016/j.cherd.2015.05.006

Seider, W. D., Seader, J. D., Lewin, D. R., & Widagdo, S. (2008). *Product and Process Design Principles: Synthesis, Analysis and Design* (3 edition). Hoboken, NJ: Wiley.

Smith, R. J. B., Loganathan, M., & Shantha, M. S. (2010). A Review of the Water Gas Shift Reaction Kinetics. *International Journal of Chemical Reactor Engineering*, *8*(1). http://doi.org/10.2202/1542-6580.2238

S&T Consultants Inc. (2007). *The addition of Bio-Butanol to GHGenius and a review of the GHG Emissions from Diesel Engines With Urea SCR* (p. 39). Retrieved from http://www.ghgenius.ca/reports/ButanolGHGenius.pdf

Steynberg, A., & Dry, M. (Eds.). (2004). *Fischer-Tropsch technology*. Amsterdam ; Boston: Elsevier.

Tsvetkov, P. V. (2010). *Nuclear power deployment, operation and sustainability*. Rijeka, Croatia: InTech. Retrieved from http://repository.tamu.edu/handle/1969.1/127923

Van der Drift, A., Boerrigter, H., Coda, B., Cieplik, M. K., Hemmes, K., Van Ree, R., & Veringa, H. J. (2004). Entrained flow gasification of biomass. *Energy Centre of Netherlands*. Retrieved from ftp://ftp.ecn.nl/pub/www/library/report/2004/c04039.pdf

Villanueva Perales, A. L., Reyes Valle, C., Ollero, P., & Gómez-Barea, A. (2011). Technoeconomic assessment of ethanol production via thermochemical conversion of biomass by entrained flow gasification. *Energy*, *36*(7), 4097–4108. http://doi.org/10.1016/j.energy.2011.04.037

Wang, Z. L., Naterer, G. F., Gabriel, K. S., Gravelsins, R., & Daggupati, V. N. (2010). Comparison of sulfur–iodine and copper–chlorine thermochemical hydrogen production cycles. *International Journal of Hydrogen Energy*, *35*(10), 4820–4830. http://doi.org/10.1016/j.ijhydene.2009.09.006

Warudkar, S. S., Cox, K. R., Wong, M. S., & Hirasaki, G. J. (2013). Influence of stripper operating parameters on the performance of amine absorption systems for post-combustion carbon capture: Part I. High pressure strippers. *International Journal of Greenhouse Gas Control*, *16*, 342–350. http://doi.org/10.1016/j.ijggc.2013.01.050

Williams, M. C., Strakey, J. P., & Surdoval, W. A. (2005). U.S. Department of Energy's Solid Oxide Fuel Cells: Technical Advances. *International Journal of Applied Ceramic Technology*, *2*(4), 295–300. http://doi.org/10.1111/j.1744-7402.2005.02031.x

XE: (USD/CAD) US Dollar to Canadian Dollar Rate. (2016, July). Retrieved July 17, 2016, from http://www.xe.com/currencyconverter/convert/?From=USD&To=CAD

Zhang, Y., McKechnie, J., Cormier, D., Lyng, R., Mabee, W., Ogino, A., & MacLean, H. L. (2010). Life Cycle Emissions and Cost of Producing Electricity from Coal, Natural Gas, and Wood Pellets in Ontario, Canada. *Environmental Science & Technology*, *44*(1), 538–544. http://doi.org/10.1021/es902555a